Techniques for Optimisation and Analysis of Composite Structures for Damage Tolerance and Buckling Stiffness

Baker, Neil

Award date:
2012

Awarding institution:
University of Bath

Techniques for Optimisation and Analysis of Composite Structures for Damage Tolerance and Buckling Stiffness

submitted by

Neil Baker

for the degree of Doctor of Philosophy

of the

University of Bath

Department of Mechanical Engineering

June 2012

Summary

This thesis explores methods by which carbon fibre reinforced polymers may be efficiently designed with the inclusion of damage tolerance criteria. An efficient method of modelling the compression after impact (CAI) strength of composite materials is selected, and this forms the basis of analysis performed.

The CAI model is initially used as the objective in an optimisation routine using a simple genetic algorithm. This indicates features of a damage tolerant composite laminate, namely that plies near the surface are less axially stiff in the loading direction than those nearer the laminate midplane, with a lower Poisson's ratio than the full laminate. This delays sublaminate buckling under laminate uniaxial compression, thus restricting delamination propagation. The designs produced by the optimisation are verified experimentally.

In order to improve the computational efficiency of the CAI model a simple surrogate modelling technique for sublaminate buckling is presented. This allows a complete database of results to be produced for a given set of ply angles, in this case standard $0/90/\pm45^\circ$ plies. This is used in the full analysis of a collection of layups produced elsewhere to be fully uncoupled, but without the stipulation of midplane symmetry. The surrogate method is shown to reduce computation time by over 99%, and produce results with an average error of less than 0.1% compared to exhaustive analysis. The analysis of the damage tolerance of fully uncoupled laminates shows that the relaxation of midplane symmetry as a design rule gives the designer far more flexibility in layup, and may allow for more damage tolerant laminates to be selected.

Finally, the CAI model is incorporated into a stiffened panel design optimisation problem as a constraint. Firstly the panel is optimised using the infinite strip analysis tool VICONOPT, with three stiffener geometries. The objective function is minimum mass for a panel subject to compressive and out-of-plane loading, with buckling and strain allowable constraints applied. Damage tolerance constraints are then applied in place of a strain allowable, using a bi-level optimisation approach. This method is shown to allow efficient inclusion of damage tolerance as a constraint in stiffened panel design, although it does not account for interactions in global buckling and local sublaminate buckling which may reduce the strength of the panel. Results indicate that the inclusion of damage tolerance analysis in stiffened panel design shows little benefit for low load panels, but can give significant reductions in mass (up to 30%) for higher load panels.

Acknowledgements

The author wishes to take this opportunity to acknowledge the assistance and support of all staff and fellow postgraduate researchers at the University of Bath associated with this project. In particular, the assistance of Andrew Rhead, whose model upon which this work is based, and David Betts, Timothy Dodwell, Moustafa Kinawy, and Wenli Liu, who all gave of their time generously throughout this work. At the University of Glasgow, Christopher York was an helpful collaborator, providing thoughtful insight and input to this work.

Finally, I would like to thank two members of staff in particular. Giles Hunt, although not formally connected with this work, has always been an eager and interested participant in discussions about this project. Indeed, his input has had a not insignificant influence on the work as it is presented here. Most of all, thanks must go to Richard Butler, whose mentoring and supervision over my eight and a half years at the University of Bath has been the single largest factor in my development as both a researcher and engineer. It has been a pleasure.

Contents

List of Figures

List of Tables

Nomenclature

$\mathbf{A}$	=	In-plane stiffness of laminate
A_{11}	=	Axial stiffness of laminate
$\mathbf{B}$	=	Coupling stiffness of laminate
$\mathbf{D}$	=	Flexural stiffness of laminate
E_{11}	=	Longitudinal elastic modulus of material
E_{22}	=	Transverse elastic modulus of material
E_i	=	Peak energy in impact test (Defined as the energy at maximum impact load)
E_{max}	=	Maximum recorded energy in impact test
E_r	=	Residual energy in impact test (Defined as difference between E_i and E_{max})
E_{xx}	=	Effective elastic modulus of laminate longitudinal direction
E_{yy}	=	Effective elastic modulus of laminate in transverse direction
G_1	=	Energy available in laminate for Mode I propagation
G_{12}	=	Shear modulus of material
$G_{\mathrm{I}C}$	=	Critical Mode I energy of resin
$G_{\mathrm{II}C}$	=	Critical Mode II energy of resin
$G_{\mathrm{III}C}$	=	Critical Mode III energy of resin
G_m	=	Inequality constraints in VICONOPT
G_{xy}	=	Shear modulus of laminate
$\mathbf{M}$	=	Moment vector
M_{mid}	=	Moment at skin mid bay due to out-of-plane pressure loading
M_r	=	Moment at skin-rib interface due to out-of-plane pressure loading
M_x	=	Moment in x-direction
M_y	=	Moment in y-direction
M_{xy}	=	Twisting moment in xy-direction
n	=	Interface number in modified CAI model
n_c	=	Number of inequality constraints in VICONOPT

$\mathbf{N}$	=	Load vector
N_x	=	Running load in x-direction
N_y	=	Running load in y-direction
N_{xy}	=	Shear load in xy-direction
p_{0°	=	Percentage of 0° plies in laminate
p_{90°	=	Percentage of 90° plies in laminate
$p_{\pm 45^\circ}$	=	Percentage of $\pm 45^\circ$ plies in laminate
P	=	Rib reaction load
$\mathbf{Q}$	=	Stiffness matrix
$\bar{\mathbf{Q}}$	=	Transformed stiffness matrix
R	=	Rank of design in genetic algorithm
t	=	Ply thickness
U_1	=	Bending energy in sublaminate
U_2	=	Membrane energy in sublaminate
U_2^*	=	Membrane energy in region into which delamination propagates
W	=	Objective function in VICONOPT
$\mathbf{X}$	=	Design variables vector in VICONOPT
γ_{xy}	=	In-plane shear strain in primary loading axis
$\varepsilon^{\mathbf{0}}$	=	Strain vector
ε^C	=	Critical buckling strain
ε_{th}	=	Threshold propagation strain
ε_x	=	Strain in primary loading axis
ε_y	=	Strain in transverse axis
θ	=	Ply angle
κ	=	Curvature vector
κ_x	=	Curvature in primary loading axis
κ_y	=	Curvature in secondary axis
κ_{xy}	=	Twist
ν_{12}	=	Major Poisson's ratio of material
ν_{21}	=	Minor Poisson's ratio of material
ν_{xy}	=	Major Poisson's ratio of laminate
σ_{th}	=	Threshold propagation mean stress

Glossary

ACO	Ant Colony Optimisation
API	Application Programming Interface
BVID	Barely Visible Impact Damage
CAI	Compression After Impact
CFRP	Carbon Fibre Reinforced Polymer
CONMIN	CONstrained function MINinisation
CPU	Central Processing Unit
CT	Computer Tomography
DIC	Digital Image Correlation
DLL	Dynamic Link Library
DTO	Damage Tolerance Optimised
EASA	European Aviation Safety Agency
FE	Finite Element
FEA	Finite Element Analysis
FOD	Foreign Object Debris
GA	Genetic Algorithm
GFRP	Glass Fibre Reinforced Polymer
GEGA	Generalised Elitist Genetic Algorithm
GLARE	Glass Laminate Aluminium Reinforced Epoxy
GUI	Graphical User Interface
GUID	Globally Unique Identifier
ME	Multiple Elitist
PANOPT	Panel ANalysis and OPTimisation tool
PC	Personal Computer
PSO	Particle Swarm Optimisation
QI	Quasi-Isotropic
SERR	Strain Energy Release Rate
VAT	Variable Angle Tow

VE	Variable Elitist
VICON	VIPASA with CONstraints
VICONOPT	VIPASA with CONstraints and OPTimisation
VID	Visible Impact Damage
VIPASA	Vibration and Instability of Plate Assemblies including Shear and Anisotropy

Image Credits

Introduction

Figure 2-1

Birmbaum, 2007, by F. Böhringer.
Cob wall mud construction, 2007, by Fountains of Bryn Mawr.
Ancient Bam, 2002, 2006, by Ales.kocourek.

Figure 2-2

Kohlenstofffasermatte, 2005, by Hadhuey.

Figure 2-3

Carbon fiber-2, 2009, by Cjp24.

Figure 2-4

F35A Prototyp AA1 2, 2007, by Senior Airman J.D. Reyes.
All Nippon Airways Boeing 787-8 Dreamliner JA801A OKJ, 2011, by Spaceaero2.
Chiddingfold 2010, 2010, by Mass Communication Specialist 1st Class J.L. Kelsey.
McLaren MP4, 2007, by J. Chapman.

Figure 2-9

Impact Damage C-Scan, 2012, by A.T. Rhead.

Author's Publications

N. Baker, R. Butler and C.B. York, "Damage Tolerance of Fully Orthotropic Laminates in Compression", *Composites Science and Technology*, Vol. 72, No. 10, pp. 1083-1089, 2012.

A.T. Rhead, R. Butler and N. Baker, "Analysis and Compression Testing of Laminates Optimised for Damage Tolerance", *Applied Composite Materials*, Vol. 18, No. 1, pp. 85-100, 2011.

A.T. Rhead, R. Butler and N. Baker, "The Influence of Fibre Angle on the Compressive Strength of Delaminated Surface Plies", *18th International Conference on Composite Materials*, ICCM, Jeju, South Korea, 2011.

N. Baker, R. Butler and C.B. York, "Maximizing Compression after Impact Strength of Uncoupled Symmetric and Non-Symmetric Laminates",
52nd AIAA/ASME/ASCE/AHS/ASC Structures, Structural Dynamics, and Materials, AIAA, Denver CO, 2011.

N. Baker and R. Butler, "Compression after Impact Modeling of Damage Tolerant Composite Laminates", *51st AIAA/ASME/ASCE/AHS/ASC Structures, Structural Dynamics, and Materials*, AIAA, Orlando FL, 2010.

A.T. Rhead, R. Butler and N. Baker, "Compression Testing of Laminates Optimised for Damage Tolerance", *17th International Conference on Composite Materials*, ICCM, Edinburgh, UK, 2009.

R. Butler, N. Baker and W. Liu, "Damage Tolerance of Buckling Optimized Variable Angle Tow Panels", *50th AIAA/ASME/ASCE/AHS/ASC Structures, Structural Dynamics, and Materials*, AIAA, Palm Springs CA, 2009.

N. Baker, A.T. Rhead and R. Butler, "Optimisation of Aerospace Laminates for Damage Tolerance", *7th ASMO UK / ISSMO Conference on Engineering Design Optimization*, ASMO-UK, Bath, UK, 2008.

Chapter 1

Scope, Objectives and Thesis Overview

The objective of this work is to extend the use of compression after impact (CAI) modelling methods developed by Butler et al. [9], Rhead et al. [58], and Rhead and Butler [56] to more practical design-based problems. In particular the use of the CAI model as an objective function in an optimisation routine is to be explored, as well as surrogate modelling methods to aid this. This knowledge is then applied to a typical aerospace structural design optimisation problem.

It is not the intention of this thesis to produce new modelling techniques for either damage tolerance or buckling analysis, but instead to investigate methods of efficiently combining pre-existing methods of analysis with the aim of showing the ease with which this can be done, and the benefits it brings.

1.1 Chapter Overview

Chapter 2 frames the work presented here in the wider context of engineering composites, and discusses the dangers of impact damage, as well as current industry methods of incorporating damage tolerance in airworthiness requirements. This leads to Chapter 3, which describes an existing CAI model, and discusses improvements made to the model as a part of this work. This model becomes the basis of damage tolerance analysis for the rest of the work presented in this thesis.

Chapter 4 applies the model discussed in Chapter 3 as the objective function in an optimisation routine. A genetic algorithm is used to direct the search, and optimum

ply stacking sequences are given for damage tolerant laminates, which are tested experimentally. Characteristics of a damage tolerant laminate are discussed, as is the effectiveness of the optimisation routine itself.

Chapter 5 explores the use of surrogate modelling techniques to improve the computational efficiency of the CAI model. Infinite strip buckling analysis is replaced with a surrogate model and an exhaustive database method is used to describe the damage tolerance of all possible sublaminates. This method is then applied in Chapter 6, which uses as an example the design space of non-symmetric and symmetric fully uncoupled laminates up to 21 plies thick. All laminates are analysed using both the original model and the surrogate technique, and results are compared. The damage tolerance of non-symmetric laminates and their applicability to aerospace applications is also discussed.

Finally, Chapter 7 incorporates knowledge gained in the development of the surrogate modelling technique into a composite stiffened panel optimisation problem. Initially stiffened panels are optimised with a nominal strain allowable applied. These panels are then optimised with damage tolerance strain constraints set by CAI analysis, and this is compared to the results without these constraints. The benefits of such a method are discussed, and suggestions for future improvements are made.

Chapter 2

Introduction

2.1 History

The word composite is today often associated with modern carbon-epoxy materials, and the high tech applications in which these are utilised, such as the aerospace and motorsport industries. The principle of combining materials of differing properties to derive beneficial characteristics is not new however, and has been exploited by humans for thousands of years.

As with so many areas of engineering, examples of composite materials can be found in nature long before the first experiments with man-made equivalents. For instance wood comprises cellulose and lignin, the cellulose binding together the stiff lignin strands. This composition gives wood directional properties, being stiffer in the grain direction, something that would later be emulated in carbon composites (see Fig. 2-1. This idea of directional stiffness would not however be explored in early man-made composites. Instead these were combinations of a fibrous material such as straw with a binding matrix of mud, clay or similar used as a building material, such as cob or adobe. Figure 2-1 also shows the construction of a wall from cob, a composite comprising mud and straw, and the world's largest adobe structure, the Arg-é Bam citadel in Bam, Iran, before its destruction in an earthquake in 2003. Adobe is a composite of sand and clay with a fibrous material such as straw or manure.

The combination of two or more materials to create a composite allows for the strengths of the materials used to be best utilised, and disadvantages to be negated. In the case of discontinuous unaligned fibres in a matrix, such as with cob or adobe, the fibres act to increase the stiffness of the material in all directions, increasing load carrying capability. More importantly in this case however is the fibre's role in arresting

Figure 2-1: Natural and early composites. Clockwise from top left: Wood grain in pear tree lumber, Construction of a wall from cob, and Arg-é Bam citadel, Bam, Iran, built from adobe.

crack growth in the matrix, especially so in the case of a brittle matrix like mud. This again allows the material to carry much more load before initialisation of failure.

Composite materials like those described to this point will still act generally as a homogenous material when used in bulk. However, the use of a fibrous material opens the prospect of tailoring properties by controlling the alignment of fibres within the material. Continuous carbon fibres are generally manufactured as either a woven cloth (Fig. 2-2), or as unidirectional fibres (Fig. 2-3). These fibres are suspended in a polymer matrix, and can be manufactured either as a prepreg, where the fibre and matrix are laid up together in tacky plies, or in a wet layup, where fibres are laid down then fluid polymer matrix is drawn into the fibres.

Today unidirectional carbon-epoxy composites are used widely in military aircraft (such as the Lockheed Martin F-35, Fig. 2-4, top left), and have an ever-increasing significance in the primary structures of commercial airliners, such as the Boeing 787 (Fig. 2-4, top right). Even the original man-made composites of mud and straw are seeing a resurgence as a sustainable building material, underlining the strength of composites in all their forms.

2.2 Contemporary Composites

Modern structural composites are manufactured in a number of basic forms. Simplest of all is glass fibre-reinforced polymer (GFRP), more commonly known as fibreglass. Early GFRP material consisted of discontinuous randomly placed fibres within a polymer resin matrix, although later usage involved continuous uni-directional or woven glass fibres. GFRP is used in marine applications, in boats ranging in size from kayaks to naval minesweepers (Fig. 2-4, bottom right). Although better strength-to-weight ratios can be achieved using more modern carbon composites, in aerospace GFRP is still a popular choice for gliders as a good compromise between structural performance and cost.

After decades of widespread use in military aircraft, carbon fibre reinforced polymer (CFRP) is rapidly becoming as significant in commercial aircraft manufacturing. The opportunities in saving weight far outweigh the increased manufacturing costs, and both the recently in-service Boeing 787 and Airbus' new A350 make use of composites for a large percentage of the primary structure. CFRP also enjoys a position as the material of choice in top-tier motorsport, with Formula 1, IndyCar and DTM cars

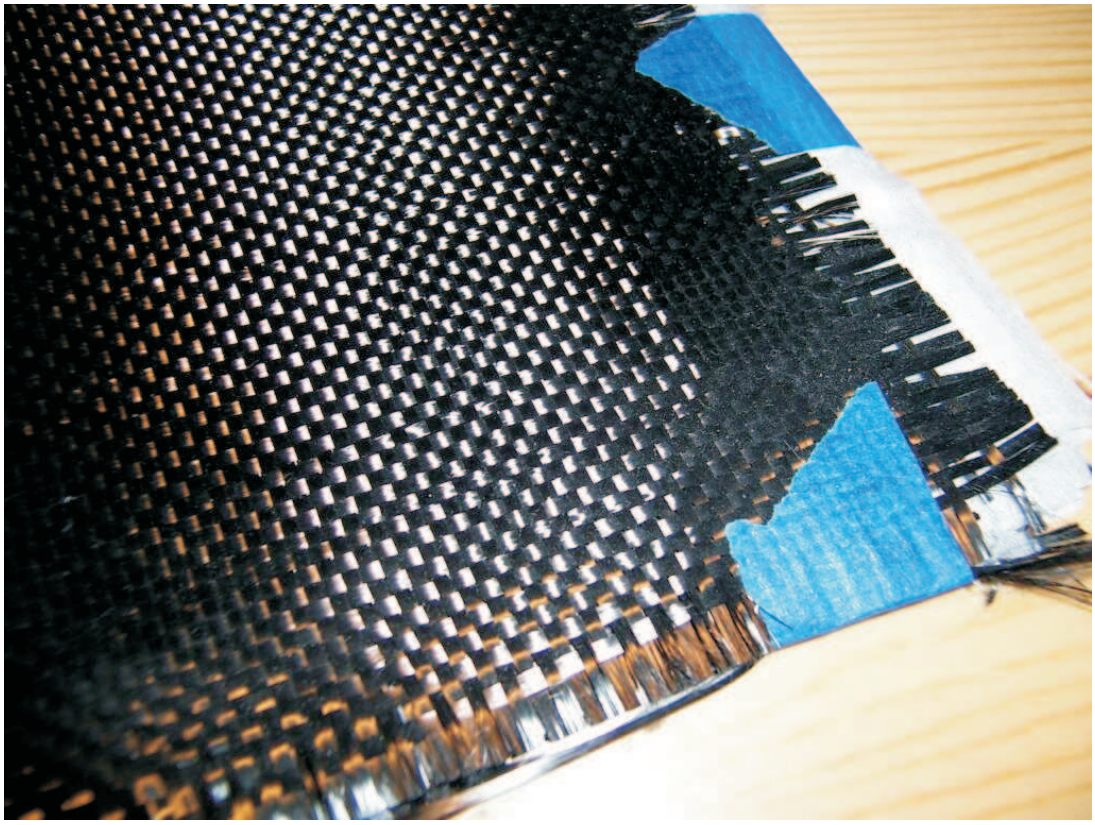

Figure 2-2: Woven composite ply.

Figure 2-3: Unidirectional carbon fibre strands.

Figure 2-4: Modern applications of composite materials. Clockwise from top left: Lockheed Martin F-35 Lightning II, Boeing 787-8, Hunt-Class mine countermeasures vessel, and McLaren MP4/1.

among others relying heavily on composites in their construction. The earliest instance of a carbon fibre composite monocoque in Formula 1 was as far back as 1981, in the McLaren MP4/1 (Fig. 2-4, bottom left).

A number of other composites have been employed in aerospace to a lesser extent, including glass laminate aluminium reinforced epoxy (GLARE) and, with the F-35, carbon nanotubes. As with the cob and adobe of many centuries before, these state-of-the-art products are still simply a combination of materials made to derive beneficial properties from their constituent parts.

2.3 Composite Design

This thesis focuses on those composites most frequently used in aerospace, namely continuous unidirectional CFRP. Conventions for describing these materials will now be presented. Figure 2-5 shows the sign conventions for laminated composite materials. This gives the global terms and directions for describing the orientation of a single ply

within a laminate. The ply stack making up a laminate is described by the angles of each lamina within the layup, generally given with respect to the primary loading axis of the material. For example, a laminate made up of a 0°, 90° and 45° ply would be described as [0/90/45]. Subscripts may also be used to simplify classification. For multiples of the same angle ply a subscript number denotes the number of consecutive plies of the same angle. The subscript 'S' denotes a sequence is symmetric. Figure 2-6 gives examples of these.

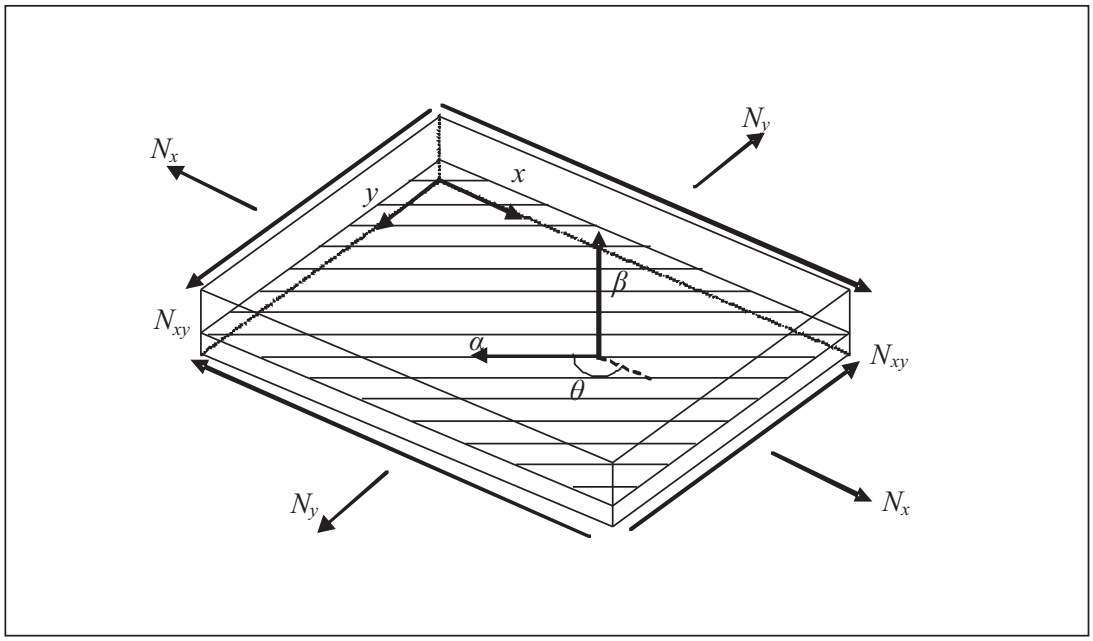

Figure 2-5: Sign conventions in laminated composite materials.

When designing a composite laminate there are a number of considerations, many of which take the form of constraints on the laminate design. Niu [52] described a set of guidelines and practices for manufacturing composites, with a view to improving manufacturability, damage tolerance and strength. One part of this work was a list of characteristics for symmetrical balanced laminates with a view to the above characteristics. Of particular interest are those stated below.

- Use 45° or -45° plies on outer surfaces of the laminate
- Avoid grouping more than six plies of the same orientation
- Avoid grouping 90° plies
- Minimum of 10% plies in each direction

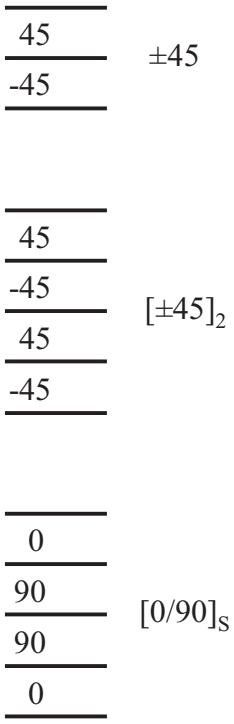

Figure 2-6: Layup notation in laminated composite materials.

The author does not offer a reasoning behind each of these requirements, but for most of these points they can be worked out. Using ±45 plies on the outer surfaces of the laminate helps to increase the damage resistance of the material, as found by Hitchen and Kemp [31]. Further to this, ±45 plies would also increase the laminate buckling strain [19]. Avoiding grouping of plies also helps the damage resistance of the material, as delamination damage tends to occur at the interface between unlike ply angles. If plies are grouped then there are fewer interfaces at which delamination damage can occur, meaning that damage at these interfaces is of a much greater area.

Setting a minimum percentage of plies in each direction is important as it helps to ensure that whatever direction the material is loaded in there are at least a small number of fibres to carry the load. If this were not the case loading would be largely through the resin, which due to low strength and modulus would be liable to fail.

2.4 Benefits of Composites

The increasing use of CFRPs in high performance applications such as aerospace owes itself to the advantages it brings. Primarily it allows for lighter weight structures

as it is less dense than aluminium, and through tailoring of material properties through stacking sequence selection, is also stiffer in its primary load carrying direction. This makes carbon fibre especially attractive in applications where loading is largely in one direction, as is the case for components within an aircraft wing.

Furthermore, the layered orthotropic nature of composites allows for tailoring of the material deformation under load. This can be an advantage in helicopter blades for example, which can be designed to twist when subjected to the centripetal force of rotation.

Although the cost of composites is higher than traditional metallic solutions, the through-life cost savings for a composite aircraft are expected to far outweigh the increase in initial expenditure brought about, and efficiencies in the manufacturing process, including a far lower material waste rates for composites, help to redress the balance.

2.5 Damage in Composites

The laminated nature of modern unidirectional aerospace composites produces excellent in-plane stiffness and strength where desired, but leads to inherent weaknesses out-of-plane. In particular, impacts of seemingly insignificant magnitude can lead to material damage that greatly reduces the ability of a structure to carry load. In aerospace these impact events are broadly separated into two types: low velocity and high velocity impact. As their names suggest, these events are generally split by velocity of impact, and they produce vastly different damage types in the composite material. Impact type damage can also be induced in composites by lightning strike, but this is not considered in this thesis.

2.5.1 High Velocity Impact Damage

High velocity impact of composite structures are generally those an airframe may experience in-flight, be it bird strike, hail, foreign object debris (FOD), or other objects impacting the surface of the aircraft at high speed. These impacts produce visible surface damage, often compromising both the fibres and resin matrix of the material, and in some instances even leading to full penetration of the structure. These impact events are readily detected, either visually or audibly during flight, or in ground inspection. This ease of detection means that such violent events are considered less of an issue in composite aircraft design than the less spectacular low velocity impacts. The work of

researchers such as Flanagan et al. [26] and Kim et al. [40] has explored high velocity impact. The characteristic penetration of high velocity impact can be clearly seen in experiments such as those by Kim et al., as shown in Fig. 2-7.

2.5.2 Low Velocity Impact Damage

In contrast to high velocity impact, low velocity impact damage is often not readily detectable within a composite airframe. This type of damage can be caused by a number of scenarios, both in manufacturing and in service. The most obvious danger with regards to low velocity impact is tool drop; however such damage may also be caused by runway debris on take-off and landing. Low velocity impact damage differs in nature from high velocity in that it primarily consists of inter-ply debonding, known as delamination damage. This is not visible from the surface of the material, and only leaves a small indentation in the impacted surface. Of particular concern to composite aircraft designers is that damage classified as 'barely visible impact damage' (BVID). This damage is defined by dent depth after impact, and delamination diameter. This lower bound diameter is set based on detectability of the damage using non-destructive evaluation techniques in service, and is generally around 35 mm (Fig. 2-8 [28]). An upper bound limit on impact energy is also applied, under the assumption that higher energy impacts would be detectable at the time of the impact event itself.

Various techniques exist that allow non-destructive evaluation of impact damage. The most common of these is ultrasonic C-scanning, which uses the reflection of sound waves from disbonded surfaces within the material to visualise the position of delaminations within impact damaged composites. Another method available is computer tomography (CT), which uses an X-ray system to scan material for defects. From this raw data sections or 3D views can be taken to visualise the damage. Figure 2-9 shows a CT section through an impacted composite laminate. The delaminations can be clearly seen within the material, with interply cracks and crack jumps between ply interfaces. It should be noted that despite the number of delaminations within this sample, very little damage can be seen at the surface, bar a small crack on the lower face.

2.6 Understanding Low Velocity Impact Damage

Although this work will not be directly concerned with prediction of impact damage in composites, it is still important to understand the mechanisms under which it occurs, and its nature. Experimental analysis and analytical modelling of impact events form

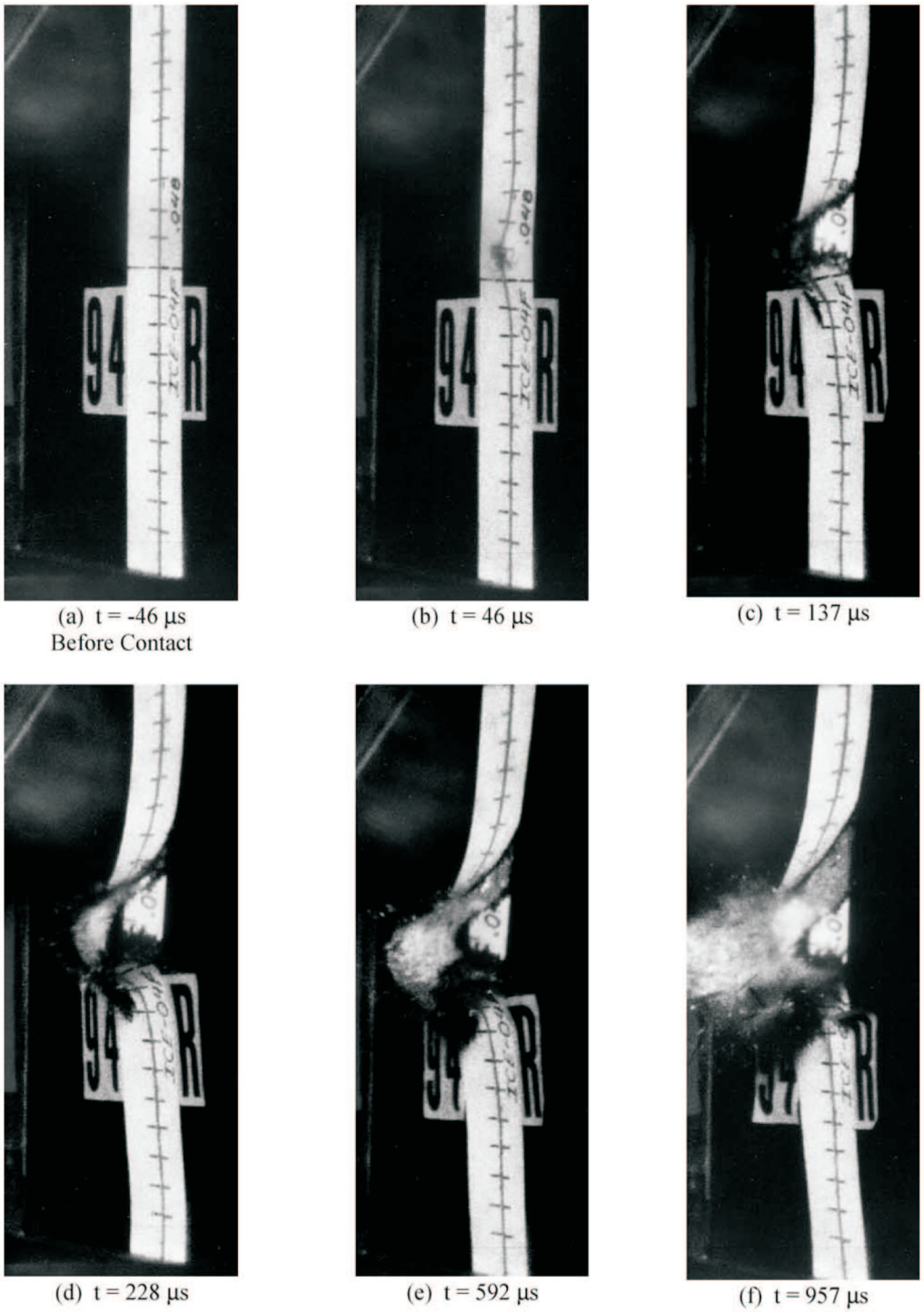

Figure 2-7: High veolcity ice impact on a woven carbon epoxy composite. Backside view of 42.7 mm SHI impacting 1.22 mm thick panel at 106 m/s (199 J); Test 94. From [40].

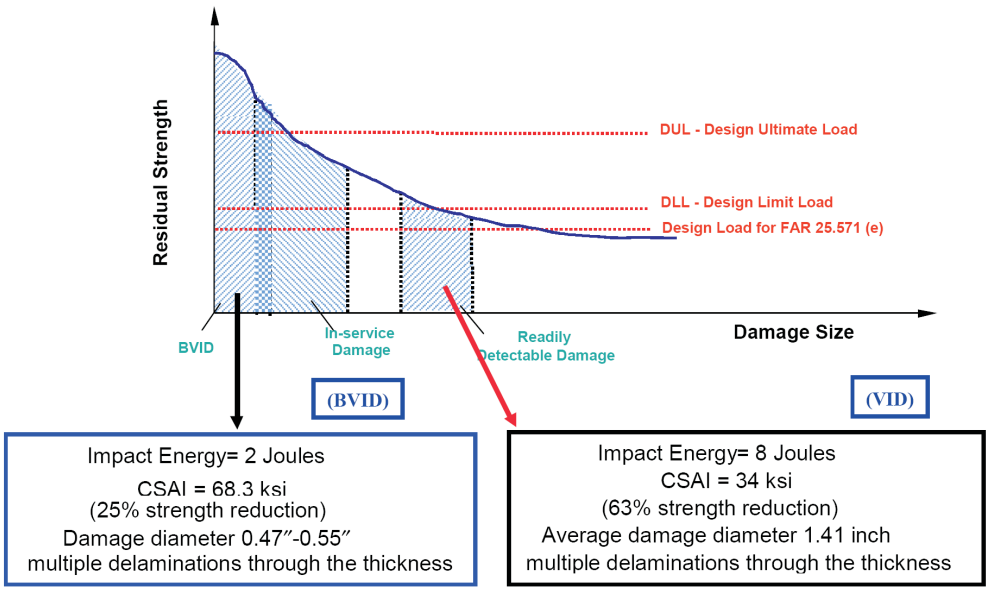

Figure 2-8: Compressive strength after impact versus damage size and design ultimate and limit load values. From [28].

a large part of research into the effects of damage on a composite structure, and a selection of this research will be used here to describe low velocity impact damage.

Hitchen and Kemp [31] performed an experimental analysis on the effect of stacking sequence on impact damage in composites. Six laminate designs were produced, each with a different stacking sequence, but with the same number of plies in each orientation. The panels were subjected to 7 J impacts, followed by analysis of the impact damage produced. A de-ply method was performed on some of the samples in order to measure the total delaminated area caused by the impact. Correlation was found between the number of dissimilar interfaces in the layup and the peak energy E_i required to initiate delamination within the material. It was also found that layups with 45° plies outermost required a higher peak energy to initiate delamination. The peak energy of the laminates was found to have little or no correlation with the maximum energy recorded during the impact event.

Figure 2-10 shows the impact results for one of the samples tested. A relationship is formed between the residual energy in the impact E_r and the total delaminated area in the panel. Residual energy is defined as the difference between the peak energy E_i , that is the energy at peak impact load, and the maximum energy measured in the test E_{max}.

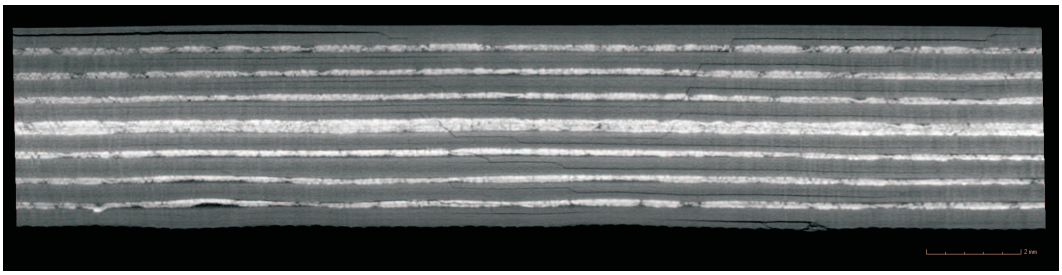

Figure 2-9: CT scan of BVID within a composite laminate. White and grey layers indicate plies of different angles within the material, and black lines between and within these layers indicate delamination damage.

Correlation is drawn between the various layups, with a linear relationship appearing between residual energy and total delaminated area. This relationship corresponds to the strain energy release rate for the delamination, and was found to lie between the experimental values for $G_{\mathrm{I}C}$ and $G_{\mathrm{II}C}$ for the material used.

Once the impact damage had been analysed, compression after impact (CAI) tests were performed. No correlation was found between CAI strength and total delaminated area, or the orientation of outermost plies. There was however found a relationship between CAI strength and area of the largest delamination, with the authors stating that CAI strength was independent of both the shape and through-thickness position of this largest delamination.

Impact damage in composites brings about a wide range of areas of potential research, including modelling of the impact event, modelling of the strength of the material once it has delamination damage, including propagation modelling and prediction of residual strength and stiffness, and the detection of such damage on an aircraft. The work in this thesis is centred on the use of strength modelling methods to inform an optimisation process, with the end goal of producing more damage tolerant composite designs.

2.7 Aviation Regulation

As impact is well established as a contributor to reducing the strength of a composite material it has been necessary for this to be accounted for in the design and testing of commercial aircraft. The aviation industry is heavily regulated, especially with respect to safety. In order to perform research that is relevant to industry it is important to understand the rules that govern the impact resistance and tolerance of composite structures in aircraft.

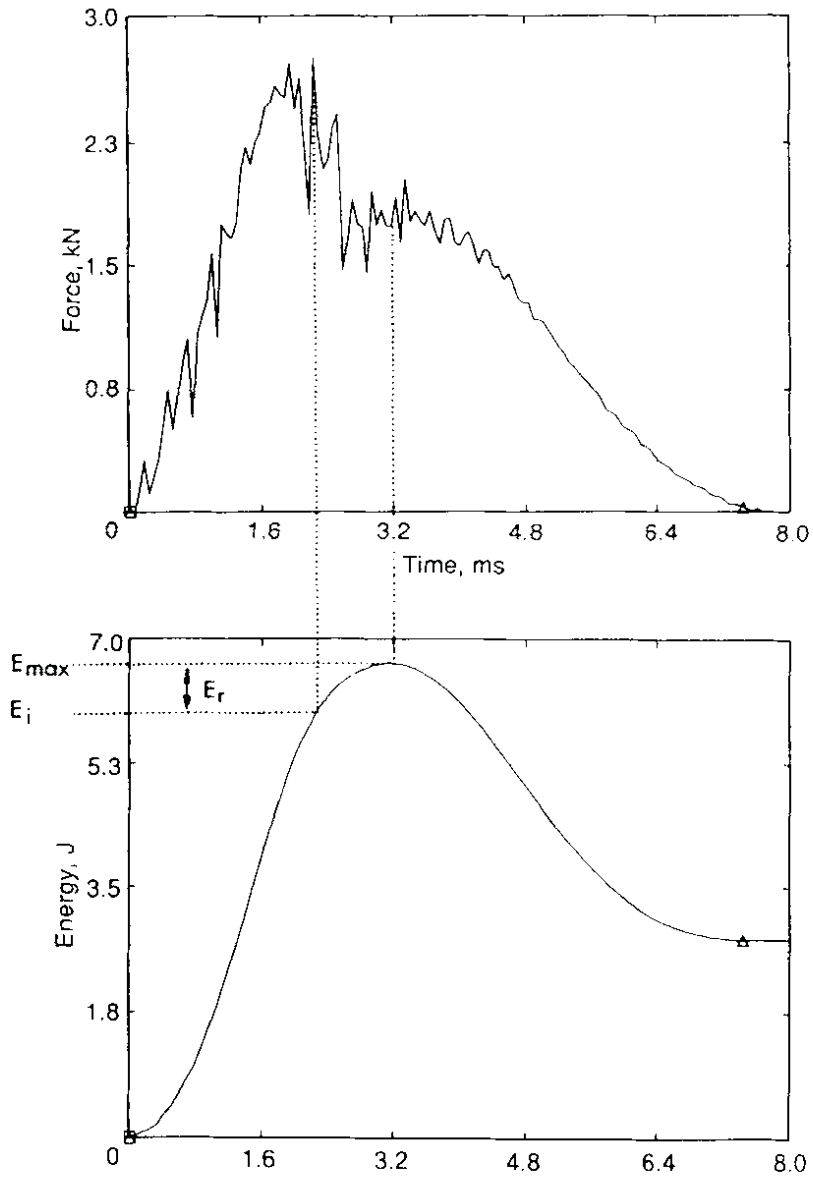

Figure 2-10: A typical force versus time curve and corresponding energy versus time curve for panel 5 from Hitchen and Kemp [31]. The difference in impact energy between the point of peak load and peak energy E_r gives an indication of the energy absorbed through delamination growth in the material.

The European Aviation Safety Agency (EASA) controls certification of aircraft in Europe, and as such publishes airworthiness requirements for all aircraft from light civilian aircraft to the largest commercial airliners. CS-25 [23] provides the requirements which a large aeroplane must meet in order to be certified by EASA. CS-25.571 a) states:

> *"An evaluation of the strength, detail design, and fabrication must show that catastrophic failure due to fatigue, corrosion, or accidental damage, will be avoided throughout the operational life of the aeroplane".*

This gives a general guide as to the requirements, and CS-25 Book 2 [24] gives acceptable means of compliance for this statement. CS-25 Book 2 Subpart D gives guidelines relating to damage tolerance compliance including that *"Impact damage is generally accommodated by limiting the design strain level"* (D4.5). This means that the final objective of work into damage tolerance in composites is to raise the design strain level of the structure, which is limited by damage tolerance of the material. The proof of structure under static loading is covered by D5.8, stating:

> *"It should be shown that impact damage that can be realistically expected from manufacturing and service, but not more than the established threshold of detectability for the selected inspection procedure, will not reduce the structural strength below ultimate load capability. This can be shown by analysis supported by test evidence, or by tests at the coupon, element or subcomponent level".*

The established threshold of detectability will be based to some extent on the boundary at which barely visible impact damage (BVID) becomes visible impact damage (VID). Essentially this means that composite structures need to be able to carry ultimate load with BVID present, but not VID. CS-25 Book 2 also gives guidance in establishing the threshold of detectability, that it should be consistent with the inspection techniques that will be employed on the aircraft in service. Inspection intervals also need to be set, especially with respect to knowledge of impact damage growth under fatigue loading. Section D6 addresses the proof of structure under fatigue. Fail-safe design is covered by D6.2.1:

> *"Structural details, elements, and subcomponents of critical structural areas should be tested under repeated loads to define the sensitivity of the structure to damage growth. This testing can form the basis for validating a nogrowth*

approach to the damage tolerance requirements. ... The repeated load testing should include damage levels (including impact damage) typical of those that may occur during fabrication, assembly, and in service, consistent with the inspection techniques employed."

Further to this, the growth rate of damage under fatigue loading needs to be quantified. D6.2.2:

"The extent of initially detectable damage should be established and be consistent with the inspection techniques employed during manufacture and in service. Flaw/damage growth data should be obtained by repeated load cycling of intrinsic flaws or mechanically introduced damage."

Combining the knowledge of the sensitivity of the structure to damage growth and the rate of growth of damage under fatigue loads allows for inspection routines to be set. D6.2.4 says:

"An inspection programme should be developed consisting of frequency, extent, and methods of inspection for inclusion in the maintenance plan. Inspection intervals should be established such that the damage will be detected between the time it initially becomes detectable and the time at which the extent of damage reaches the limits for required residual strength capability."

This shows the complexity involved in determining what damage to allow within the structure; in fact it can be seen that maintenance intervals become part of the optimisation of the design of the structure. Guidance is also given for safe-life design, in D6.3:

"Component, subcomponent and/or element tests may be used to evaluate the fatigue response of structure with impact damage levels typical of those that may occur during fabrication, assembly, and in service, consistent with the inspection procedures employed. ... It should be demonstrated during the fatigue tests that the stiffness properties have not changed beyond acceptable levels."

In contrast to the provision of inspection intervals in the fail-safe design guidance, the safe-life guidance does not require the growth or no-growth characteristics of damage in the structure to be quantified, instead just that the stiffness of the structure should not change through the fatigue tests.

The samples of regulations and guidelines discussed here show the multitude of considerations that have to be made by designers of aircraft structures, especially composite structures. As this work will look at static strength of impact damaged composites the fatigue regulations are not directly applicable, but future work may include fatigue modelling, hence its inclusion here.

2.8 Conclusion

Composite materials have the potential to give considerable weight savings for commercial aircraft when compared to traditional metal structures, but to fully realise this potential a number of issues must be addressed. This thesis will focus on compression after impact strength of composites, and techniques to allow use of analytical methods for compression after impact strength prediction as drivers for composite structural design.

Chapter 3

Compression after Impact Model

3.1 Introduction

Composite laminates are strong in-plane, but prone to damage when subjected to impact loading. This damage can often be difficult to detect, and can have a significant effect on the compressive strength of a composite component. For this reason allowances need to be made for impact damage in the design of composites.

The modelling of compression after impact (CAI) strength of composites can be split broadly into two areas of interest. Numerical approaches such as finite element analysis (FEA) are generally of a high fidelity, and can currently describe with great detail the progressive failure of an impact damaged composite laminate under compression, as well as other loading conditions [13, 72]. The drawback of these methods is that they tend to be computationally expensive, and whilst they are a very useful analysis tool they are less strong as a tool to aid composite design. In this case analytical methods are more appropriate, for whilst they do not possess the fidelity of FEA modelling, they can produce solutions far more quickly, and as such lend themselves to areas in which the ability to do many analyses in short time is beneficial, such as design optimisation.

Early work in analytical modelling the CAI strength of composite laminates was presented by Chai et al. [15]. Although this 1D model did not capture the complexity of delamination growth in composites completely enough to be validated against experimental results, it was able to predict a number of interesting phenomena in propagation. The analytical model used a thin film assumption, with curvature assumed not to be induced in the base substrate by buckling of the sublaminate. A second model allowed for bending and buckling in the base, but required some numerical analysis to

solve. The models were able to predict different types of propagation, including stable propagation, unstable propagation, and unstable propagation followed by crack arrest.

January of 1985 saw the Journal of Composite Materials publish a number of articles presenting methods pertaining to the modelling and analysis of delaminated composite materials under compressive loading. Shivakumar and Whitcomb [65] presented an investigation into the buckling of sublaminates in a quasi-isotropic laminate. Sublaminates were assumed to be thin compared to the base substrate, so the base was assumed not to deform out-of-plane. Buckling results were produced using both FEA and a Rayleigh-Ritz formulation. The study drew a number of important conclusions that bear great relevance even today. Firstly, a sublaminate within a laminate under uniaxial loading is subject to a biaxial stress state, with Poisson's ratio mismatch and in-plane shear coupling leading to longitudinal, transverse, and shear loads in the sublaminate. Also of interest was the observation that delamination propagation will occur in the direction that yields the lowest sublaminate buckling strain. The work also highlighted the possibility of sublaminates buckling under tensile load due to Poisson's ratio mismatches between the sublaminate and base laminate inducing transverse compression in the delaminated region.

In the same volume Chai and Babcock [14] presented an extension to two-dimensions of the 1D model previously presented by Chai et al. [15]. The 2D analytical model was based on a Rayleigh-Ritz formulation, with delamination growth modelled using an energy balance criterion and assuming self-similar growth. This allows predictions of crack growth stability and direction, with these characteristics found to be influenced by the material anisotropy relative to the primary loading axis.

In 1986 Whitcomb [76] performed a parametric analysis of delamination propagation in a plate with a through-width near-surface delamination. A thin film assumption was applied, with the delaminated region assumed to be thin compared to laminate thickness, so curvature of the full laminate due to sublaminate buckling was neglected. The study found that the energy available for Mode I propagation G_{I} is very sensitive to delamination geometry (length and depth) and the initial imperfection due to the delamination. The importance of mode-mixity and the requirement for a verified mixed-mode growth criterion were also highlighted, with the ratio of Mode I strain energy G_{I} to Mode II strain energy G_{II} needing to be quantified. Figure 3-1 shows each of these crack propagation modes.

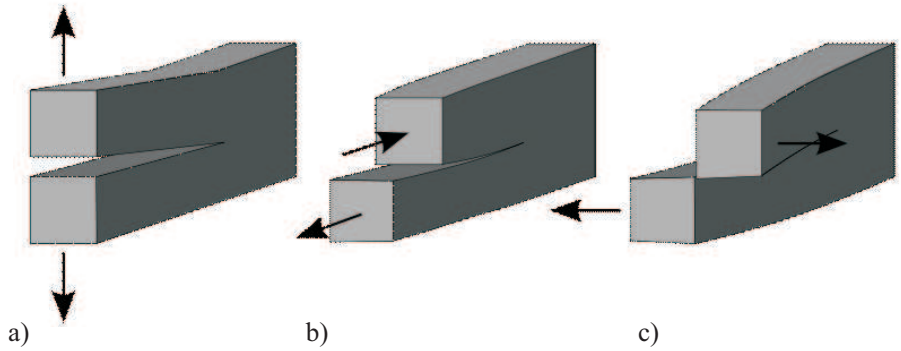

Figure 3-1: Crack propagation modes. a) shows Mode I, b) Mode II, and c) Mode III.

Garg [27] sought to demystify delamination propagation in composites in his 1988 Engineering Fracture Mechanics review article. This work brought together work in the field of composite delaminations to date, and drew the most significant conclusions from the field together. Those of note included the detrimental effect of delaminations on compressive strength, and the root cause of delaminations being poor interlaminar toughness. Garg also points to the lack of visibility of delaminations caused by low velocity impact at the material surface.

Whitcomb and Shivakumar [77] continued their contribution to the field of composite fracture mechanics in 1989, performing strain energy release rate analysis on plates with postbuckled delaminations. This work expanded on their work of 1985 by calculating the strain energy around the delamination front using a virtual crack closing technique. This improvement over previous techniques allows for analysis of delaminations where strain energy release rate varies around the delamination boundary, such as square or rectangular delaminations. The work also found that delamination growth is dependent on delamination aspect ratio, applied strain, and overall delamination geometry.

Early work into analytical modelling of multiple delaminations in a composite material was presented by Suemasu [68]. The delaminations modelled were through-width and equally spaced through-thickness. Rayleigh-Ritz was used as the basis for modelling, with Timoshenko shear effects included due to the low shear stiffness in the delaminated region. Results of the model were compared to experimental results. It was found that the localised reduction in bending stiffness within the delaminated region significantly reduced the buckling load of the overall laminate. This highlights the dangers of delaminations within a composite structure, and the effect they may have on global buckling modes.

Madenci and Westmann [46] explored the mathematics of growth of delaminations in layered materials both pre- and post-buckling. An analytical formulation was presented for axisymmetric and uniaxial loading cases. The results presented, being of a delamination in a homogeneous material, were not meant to accurately predict the behaviour of a damaged composite material, but to provide a benchmark to be used by other studies.

Nilsson et al. [51] presented work comparing experimental results of a delaminated composite under compression with those from finite element (FE) based analysis. The work focussed on prediction of growth of an arbitrary delamination using FE. The method included contact, and automatic mesh generation to allow modelling of crack evolution. These results were compared to experimental testing of a composite laminate with an artificial delamination included. Incremental testing and use of non-destructive C-Scan and X-Ray techniques allowed the authors to compare propagation in the experiment to that predicted by the FE model. The FE method was shown to capture buckling, propagation initiation and shape, as well as stability of propagation, well.

The stability of delamination damage propagation under compressive load was also examined by Kardomateas and Pelegri [38]. Much of the work into delamination growth to this point relies on a thin film assumption, with the base substrate remaining flat during initial loading, buckling, and post-buckling, but initially Kardomateas [37], then Kardomateas and Pelegri produced a closed-form solution that did not require such assumptions. This model was used to define combinations of delamination geometry and applied strain that lead to unstable delamination propagation. The results confirmed that thin film modelling of propagation may not be conservative in its prediction of propagation stability when curvature is induced in the base substrate.

Xiong et al. [82] formulated a prediction method for CAI strength based upon classic composite failure criteria such as Tsai-Wu [73]. This method makes the assumption that sublaminate buckling occurs at the largest delamination in the impacted material, and Rayleigh-Ritz is used to calculate the buckling stress of this sublaminate. This is used to produce a set of reduced moduli for the delaminated sublaminate, which are applied to full plate calculations. Rayleigh-Ritz is used again, with the complex variable method used to take account of the delaminated region. Failure is predicted using an appropriate failure criterion, as described by Whitney and Nuismer [78]. This method is validated using compression tests on quasi-isotropic laminates subjected to impacts at a range of energies. The prediction method agrees well with the experimental

results, although it should be noted that the damage produced in some of the samples was smaller than that defined as BVID [28], and that the failure prediction method required empirical data that was material layup and damage morphology dependent.

Nyman et al. [53] compared two modelling techniques for residual strength of impacted composites to experimental results. The two models were a soft inclusion model for the delaminated region, and an analytical delamination buckling model. The key conclusions of the work were that a simple soft inclusion model provides non-conservative results for residual strength, and that a delamination buckle modelling approach gives excellent agreement with experimental and FE results.

Katerelos et al. [39] performed extensive fatigue tests on impacted composite samples, and then compared these results to a simple analytical model. This modelling technique differed in that it predicts the direction of delamination growth analytically given experimentally derived data on the delamination shape. The model was shown to predict the direction of delamination propagation, and the weakest interface within the laminate.

Riccio and Gigliotti [60] presented a numerical approach to damage tolerance in the preliminary design phase. The approach is based on finite element analysis in ANSYS, but requiring only a limited number of linear buckling analyses with the intention of reducing computation time. The method was applied to two delamination cases, a through-width rectangular delamination, and an enclosed delamination in a square plate. The results of the model are good for delaminations down to approximately 15% laminate thickness, and the authors suggest that its combination of accuracy and efficiency (relative to other FE methods) make it suitable for preliminary design analysis. This numerical technique has benefits over analytical methods discussed here as it is able to predict delamination growth characteristics, rather than just initiation of damage growth.

The basis of all CAI analysis performed in this work is an analytical local sublaminate buckling-induced delamination propagation model, initially proposed by Butler et al. [9], refined by Rhead et al. [58], and extended to static problems by Rhead and Butler [56]. Due to its integral role in this work, it shall be fully discussed here.

3.2 CAI Model

The model is formulated as an efficient method of estimating the CAI strength of a delaminated composite laminate under uniaxial compression. Prediction of propagation strains is energy based, and buckling analysis is performed using the exact finite strip buckling and vibration analysis tool VICONOPT [80, 81]. Modelling of the impact event is beyond the scope of this model, so delamination characteristics are treated as an input to the model.

3.2.1 VICONOPT Buckling Analysis

VICONOPT (VIPASA with CONstraints and OPTimisation) is a computer program combining the computer codes VIPASA (Vibration and Instability of Plate Assemblies including Shear and Anisotropy), VICON (VIPASA with CONstraints), and the mathematical programming optimiser CONMIN (CONstrained function MINimisation). VICONOPT can perform analysis or optimum design of prismatic structures for buckling or vibration, subjected to any combination of invariant in-plane stresses. When applied to this work, VICON is used as a buckling analysis tool for sublaminates within the CAI model.

Buckling analysis in VICONOPT takes place in two phases. Phase one determines the pre-buckling load distribution in the plate, based on uniform end shortening. In the case that out-of-plane loading is specified in the problem extra loading due to bending moments is also included here. These results can be used in the application of material strength criteria, although this work for the most part focuses on the stability of the sublaminate and so it is only utilised in structural design cases, described later in Chapter 7.

The second phase of analysis predicts buckling for the structure over a range of wavelengths calculated using user-specified parameters, maintaining continuity in the buckling pattern across the intersection of connected plates. This involves calculation of plate stiffnesses, followed by setting up of the stiffness and constraint matrices. This is then solved as an eigenvalue analysis of the system at zero frequency. This analysis is repeated at all calculated half-wavelengths. Figure 3-2 details this procedure. A fuller description of this methodology can be found in work by Williams et al. [80].

VICONOPT is chosen to analyse the buckling of sublaminates in the CAI model for a number of reasons. Primarily, its computational efficiency in comparison to finite

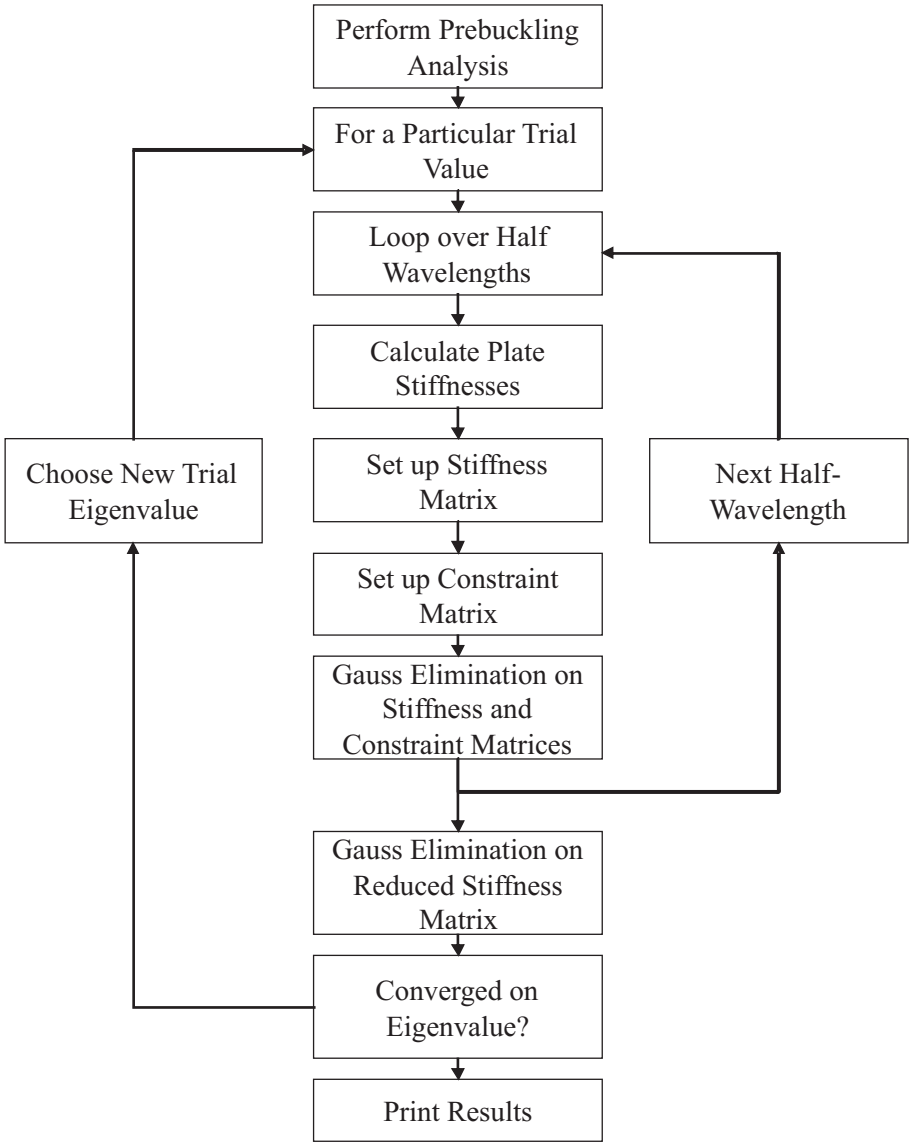

Figure 3-2: VICONOPT Analysis Procedure.

element type analysis, whilst preserving the complexity of the problem being modelled, is the greatest reason. VICONOPT analysis of a single delamination may take only a fraction of a second, opening the possibility of the CAI model being called repeatedly as part of an optimisation routine. It is particularly important that in this analysis VICONOPT is able to analyse non-symmetric and coupled laminates, as delaminations can produce such sublaminates. VICONOPT accounts for laminates with fully populated **A**,**B**, and **D** matrices, as described by Anderson and Kennedy [1].

The model assumes that delamination growth is initiated in either the loading direction or in the transverse direction, and that it is driven by local buckling of a thin delaminated region, henceforth referred to as the sublaminate. It is also assumed that the base substrate remains flat before sublaminate buckling, in the locally post-buckled regime and at propagation (see Fig. 3-3). Strain energy released as a result of delamination growth in the longitudinal or transverse direction is assumed to produce Mode I fracture of the resin material. In reality, the propagation is more complex than is assumed, since growth is mixed mode [76] and may initiate in the transverse direction [14], particularly when there is interaction between buckling of the thin sublaminate and out-of-plane deformation of the laminate. However, the method has been shown to produce accurate lower bound predictions of threshold strain for a range of experimental test laminates [57]. Hence it is used here as a very efficient method for predicting the CAI strength of composite laminates.

3.2.2 Derivation of Delamination Propagation Energy

The CAI model compares the energy within the thin sublaminate before and after a propagation event has occurred, and equates this to the critical Mode I strain energy release rate (SERR) for the resin. Energy is defined in terms of applied strain ε_x, sublaminate buckling strain ε_x^C and laminate axial stiffness A_{11}. Buckling of the sublaminate is analysed using the infinite strip buckling program VICONOPT [80, 81], with sublaminate loads calculated from classical laminated plate theory, assuming strain compatibility at the boundary between the flat, uniaxially-loaded laminate and the delaminated region. It is assumed that load is applied as end shortening, along the sublaminate neutral plane; hence loading is purely in-plane. As a result of strain compatibility at the delamination boundary, transverse and shear loads may be induced in the sublaminate due to, respectively, mismatches between the Poisson's ratio of the full laminate and the sublaminate, and sublaminate extension-shear coupling [65]. Delaminations are modelled as circular, using six equal width strips. The influence of boundary conditions and the number of nodes used in the VICONOPT buckling model

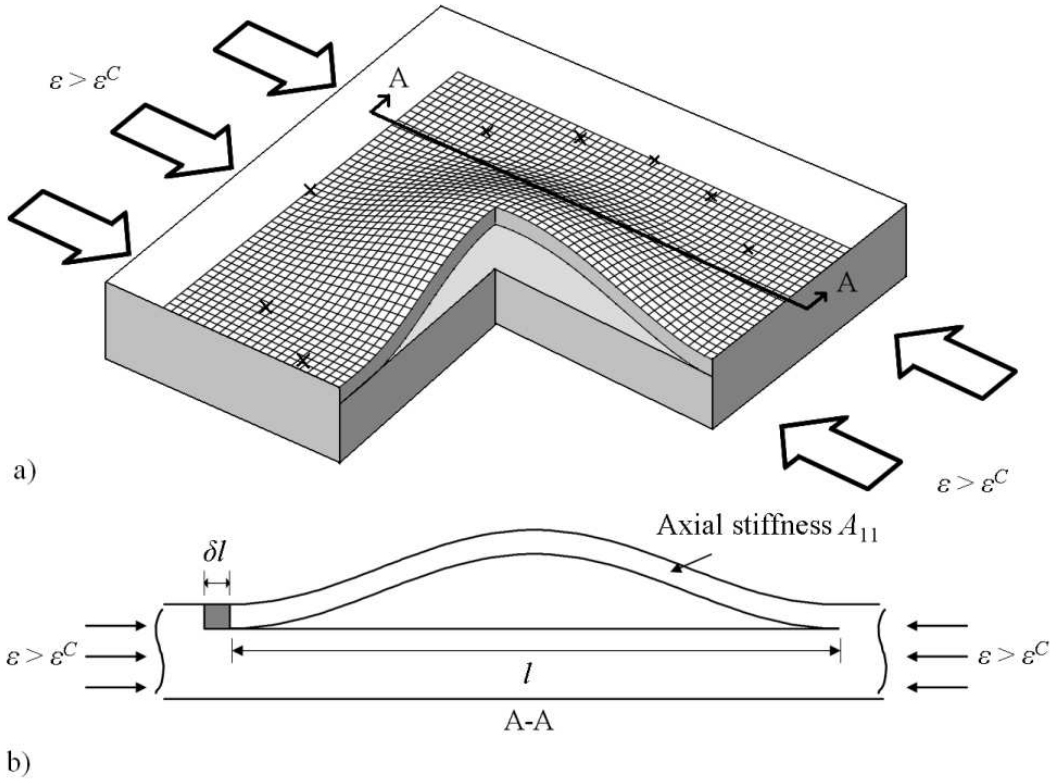

Figure 3-3: Cutaway of sublaminate buckling above delamination, showing a) the buckled thin film over a flat substrate, and b) section A-A displaying region δl into which the delamination propagates.

have previously been explored [58]. Bending energy stored in the buckled sublaminate is equated to the applied in-plane energy [71], leading to Eq. 3.1 for bending energy.

$$U_1(l) = A_{11} l(\varepsilon_x - \varepsilon_x^C)\varepsilon_x^C \tag{3.1}$$

Comparing the energy before and after a propagation event of δl,

$$U_1(l) - U_1(l + \delta l) = A_{11}(\varepsilon_x - \varepsilon_x^C)(\varepsilon_x^C l - \varepsilon_(x, A)^C (l + \delta l)) \tag{3.2}$$

where a subscript A denotes a buckling strain after propagation. To allow this equation to be solved with change in buckling strain after propagation, the buckling strain of a strut is considered. The buckling strain of a strut is of the form

$$\varepsilon^C = \frac{K}{l^2} \tag{3.3}$$

Equations 3.3 and 3.2 imply

$$U_1(l) - U_1(l+\delta l) = A_{11}(\varepsilon_x - \varepsilon_x^C)\left(\frac{K}{l^2} - \frac{K}{(l+\delta l)^2}\right) \tag{3.4}$$

As δl is infinitesimally small, binomial theorem may be used to approximate $(l+\delta l)^{-1}$, with second order terms and higher ignored. Hence

$$U_1(l) - U_1(l+\delta l) = A_{11}(\varepsilon_x - \varepsilon_x^C)\varepsilon_x^C \delta l \tag{3.5}$$

Membrane energy can be approximated as:

$$U_2(l) = \frac{A_{11}}{2} l(\varepsilon_x^C)^2 \tag{3.6}$$

Finally, membrane energy is also released from the region into which the delamination propagates. If propagation extends the delamination by δl in Fig. 3-3 b), then this energy is described as in Eq. 3.7.

$$U_2^* = \frac{A_{11}}{2}\int_0^{\delta l} \varepsilon_x^2 dx \tag{3.7}$$

The bending and membrane energy can be calculated immediately after a propagation of δl by replacing l with $l+\delta l$ in Eqs. 3.1 & 3.6. Equations 3.1, 3.6 & 3.7 can then be combined to determine the energy available for propagation at a given applied strain, as shown in Eq. 3.8.

$$G = \lim_{\delta l \to 0}\left\{U_1(l) - U_1(l+\delta l) + U_2(l) - U_2(l+\delta l) + U_2^*\right\}\frac{1}{\delta l} \tag{3.8}$$

Hence

$$G = \frac{A_{11}}{2}(\varepsilon_x - \varepsilon_x^C)(\varepsilon_x + 3\varepsilon_x^C) \tag{3.9}$$

Note that this is the expression derived by Chai et al. [15] for one-dimensional propagation, except that here it covers a composite sublaminate of axial stiffness A_{11} and two-dimensional sublaminate buckling. In this case it is assumed the sublaminate has no post-buckled stiffness. This assumption gives a lower bound solution, and is more fully discussed elsewhere [58]. Equation 3.9 is then rearranged in terms of applied strain ε_x. By setting G to the critical Mode I SERR of the resin material G_{IC}, the threshold propagation strain $\varepsilon_{th,x}$ may be approximated. This yields Eq. 3.10, describing threshold propagation strain of interface i ($\varepsilon_{th,x,i}$) in terms of local buckling strain $\varepsilon_{x,i}^C$, the axial stiffness of the buckled sublaminate $A_{11,i}$, and the critical Mode I SERR of the resin material G_{IC}. This equation is applied at each delamination individually,

assuming an otherwise undamaged laminate, as also assumed by Hwang and Liu [33]. In this work Eq. 3.10 is applied at each individual ply interface up to a quarter of the laminate thickness, i.e. to $n = N/4$.

$$\varepsilon_{th,x,i} = -\varepsilon^C_{x,i}\left(1 - \sqrt{4 + \frac{2G_{IC}}{A_{11,i}(\varepsilon^C_{x,i})^2}}\right), i = 1, 2, \ldots n \tag{3.10}$$

Equation 3.10 is not applied below 25% of total laminate thickness as at this depth the thin film assumption is invalid.

3.2.3 Sublaminate Analysis

The energy-based propagation strain derived in Section 3.2.2 takes sublaminate buckling strain as an input, and is independent of the method by which this is calculated. This may be produced through finite element analysis, or taken from experimental analysis in order to validate the derivation independently of the buckling prediction. Generally however, the exact finite strip analysis program VICONOPT [80, 81] is used due to favourable correlation with higher fidelity finite element modelling [11], and the speed of analysis it allows, which is of great importance with a view to integration of the model into an optimisation routine.

The model is based on a thin film approximation, that is buckling of a near-surface delamination does not result in out-of-plane deformation of the base laminate, or the laminate around the delamination. Buckling analysis of the delaminated sublaminate is performed using VICONOPT. Loads on the sublaminate are calculated assuming that a uniform end shortening strain is applied to the full laminate in the primary load direction, and that the plate is free to strain transversely due to Poisson's ratio effects. The analysis is intended for symmetric laminates, so no in-plane/out-of-plane coupling is included in the deformation of the full laminate. This assumption also precludes the model to thin film problems, where sublaminate buckling does not induce global out-of-plane deformation. Using classical laminated plate theory, the in-plane loads induced in the sublaminate through the full laminate under a uniform end shortening ε_x are given by Eq. 3.11.

$$\begin{Bmatrix} N_x \\ N_y \\ N_{xy} \end{Bmatrix} = \begin{bmatrix} A_{11} & A_{12} & A_{16} \\ A_{12} & A_{22} & A_{26} \\ A_{16} & A_{26} & A_{66} \end{bmatrix} \begin{Bmatrix} \varepsilon_x \\ \varepsilon_y \\ \gamma_{xy} \end{Bmatrix} + \begin{bmatrix} B_{11} & B_{12} & B_{16} \\ B_{12} & B_{22} & B_{26} \\ B_{16} & B_{26} & B_{66} \end{bmatrix} \begin{Bmatrix} \kappa_x \\ \kappa_y \\ \kappa_{xy} \end{Bmatrix} \tag{3.11}$$

Assuming no in-plane shear or out-of-plane deformation in the laminate, and that the

laminate is free to strain transversely, Eq. 3.11 becomes

$$\begin{Bmatrix} N_x \\ N_y \\ N_{xy} \end{Bmatrix} = \begin{bmatrix} A_{11} & A_{12} & A_{16} \\ A_{12} & A_{22} & A_{26} \\ A_{16} & A_{26} & A_{66} \end{bmatrix} \begin{Bmatrix} \varepsilon_x \\ -\varepsilon_x \nu_{xy} \\ 0 \end{Bmatrix} \tag{3.12}$$

where ν_{xy} is the Poisson's ratio of the full laminate. In Eqs. 3.11 & 3.12 the axial stiffness values A_{mn} refer to the in-plane stiffness properties of the sublaminate.

The sublaminates modelled using Eq. 3.12 may not be symmetric, and may exhibit all types of coupling. It is assumed that loading of the sublaminate is through uniform end shortening, and hence loads are applied at the sublaminate neutral axis and most in-plane/out-of-plane coupling is removed. Loading through the neutral axis will not however minimise extension-twist coupling, as dictated by the B_{16} and B_{26} values in Eq. 3.13 below.

$$\begin{Bmatrix} M_x \\ M_y \\ M_{xy} \end{Bmatrix} = \begin{bmatrix} B_{11} & B_{12} & B_{16} \\ B_{12} & B_{22} & B_{26} \\ B_{16} & B_{26} & B_{66} \end{bmatrix} \begin{Bmatrix} \varepsilon_x \\ \varepsilon_y \\ \gamma_{xy} \end{Bmatrix} + \begin{bmatrix} D_{11} & D_{12} & D_{16} \\ D_{12} & D_{22} & D_{26} \\ D_{16} & D_{26} & D_{66} \end{bmatrix} \begin{Bmatrix} \kappa_x \\ \kappa_y \\ \kappa_{xy} \end{Bmatrix} \tag{3.13}$$

Again applying conditions of free transverse strain and no in-plane shear or out-of-plane deformation, Eq. 3.13 becomes

$$\begin{Bmatrix} M_x \\ M_y \\ M_{xy} \end{Bmatrix} = \begin{bmatrix} 0 & 0 & B_{16} \\ 0 & 0 & B_{26} \\ B_{16} & B_{26} & 0 \end{bmatrix} \begin{Bmatrix} \varepsilon_x \\ -\varepsilon_x \nu_{xy} \\ 0 \end{Bmatrix} \tag{3.14}$$

It can be seen that with the reduced B matrix due to neutral axis loading, only M_{xy} out-of-plane loading is induced in the sublaminate. These terms cannot be included in VICONOPT, and are generally small, so are ignored.

3.2.4 Damage Modelling

Due to the prismatic nature of the analysis VICONOPT performs, the delaminated sublaminate is modelled in a series of triangular and trapezoid strips that approximate the shape of the delamination. In the absence of an effective, efficient method of modelling delaminations caused by low velocity impact a circular delamination that fully encompasses the delamination damage is used as an approximation [56]. Figure 3-4 shows a typical delaminated circle as modelled in VICONOPT.

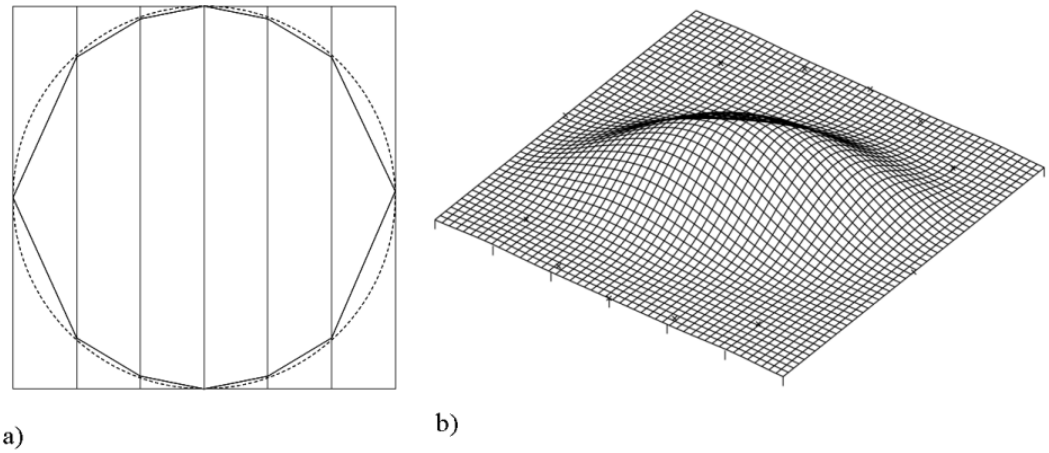

Figure 3-4: Discretisation of sublaminate in VICONOPT, showing a) approximation of circular delamination with triangular and trapezoid strips, and b) typical mode shape of buckled sublaminate predicted by VICONOPT.

In the work of Rhead et al. [56] the width of strips across the delamination remains constant. Previous studies have explored the effect of the number of strips modelled on the solution VICONOPT gives [58], showing that six strips allows a sufficient level of accuracy for this type of analysis.

Typically a single VICONOPT sublaminate buckling analysis takes in the region of 0.25 seconds, depending on the properties of the plate being modelled. As VICONOPT is a serial FORTRAN code it does not make use of the multiple cores in modern desktop PCs; however the nature of the CAI analysis is such that all of the buckling analyses required for a single laminate can be run concurrently, greatly improving the average time per analysis.

3.2.5 Stability of Propagation

As well as allowing prediction of the propagation strain for a given delamination within a composite material, the CAI model can also be interpreted to give predictions on the stability of the propagation that takes place. The prediction of stability of propagation depends on the assumption that as the delamination area increases, the buckling strain of the delaminated region decreases. Figure 3-5 shows the relationship between buckling strain and delamination diameter for a circular delamination.

Figure 3-5 shows a reduction in buckling strain with growth in a circular delamination in all directions; however growth may be in a single direction, dictated by the directional

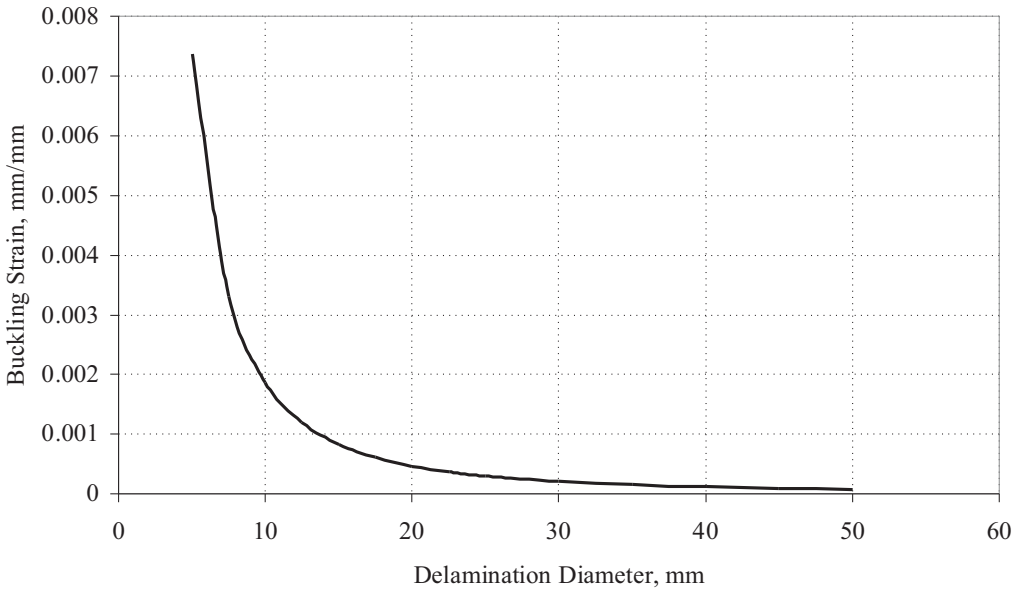

Figure 3-5: Relationship between delamination diameter and buckling strain of a [45/0] sublaminate in a quasi-isotropic laminate.

stiffness and loading of the buckled sublaminate [65]. In some cases directional growth may in fact increase buckling strain. An example of this may be seen in the buckling load of a simply-supported rectangular plate. Figure 3-6 shows the cusping curves of change in buckling load of a simply supported plate with respect to its aspect ratio, as presented in ESDU 80023a [22]. This response to a change in aspect ratio of the plate being buckled is due to the increased energy required when the longitudinal and transverse buckling wavelengths are not divisible. This means buckling factors minimise at integer values of aspect ratio for a homogenous material, and reach a peak at some point between these integers. For orthotropic materials these points of minimum buckling load are scaled by the ratio of bending stiffnesses in x and y. A similar effect would be seen in a circular delamination changing in aspect ratio, as would be the case if the delamination propagated in one direction.

The change in buckling strain of the delaminated region caused by propagation will directly influence whether that propagation is stable or unstable. By plotting threshold strain against buckling strain using Eq. 3.10 the stability of growth can be explored. Figure 3-7 shows such a plot. The relationship between threshold strain and buckling strain is quadratic, so there lies a minimum threshold strain at a given buckling strain, which can be derived from Eq. 3.10 to give Eq. 3.15.

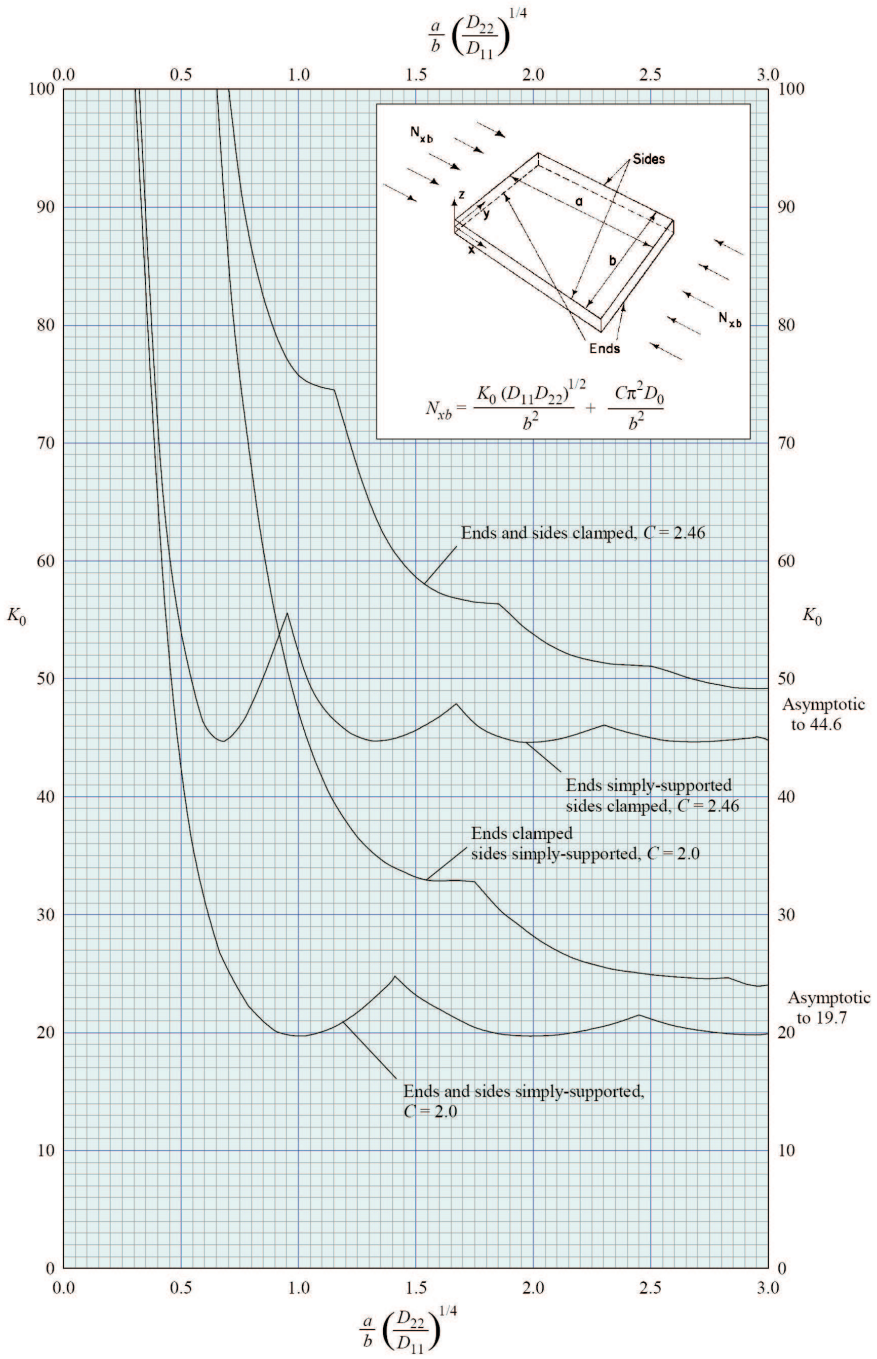

Figure 3-6: Compression buckling of orthotropic plates with varying aspect ratio under uniaxial load. Combinations of clamped and simply-supported edge conditions. Taken from ESDU 80023a [22].

$$\varepsilon_{th,x,i} = \sqrt{\frac{2G_{IC}}{6A_{11,i}}} \tag{3.15}$$

If the sublaminate buckling strain is lower than this buckling strain, and propagation reduces the sublaminate buckling strain, then propagation will be stable. This is because the change in buckling strain increases the critical threshold strain of the sublaminate, and assuming end shortening strain is held constant during the propagation event, there is no longer sufficient energy in the system to continue the delamination growth. If propagation causes an increase in buckling strain, then in this region of the curve the propagation is unstable, as threshold strain reduces with the change in buckling strain. To the right of the point of minimum threshold strain the reverse is true with respect to stability of propagation.

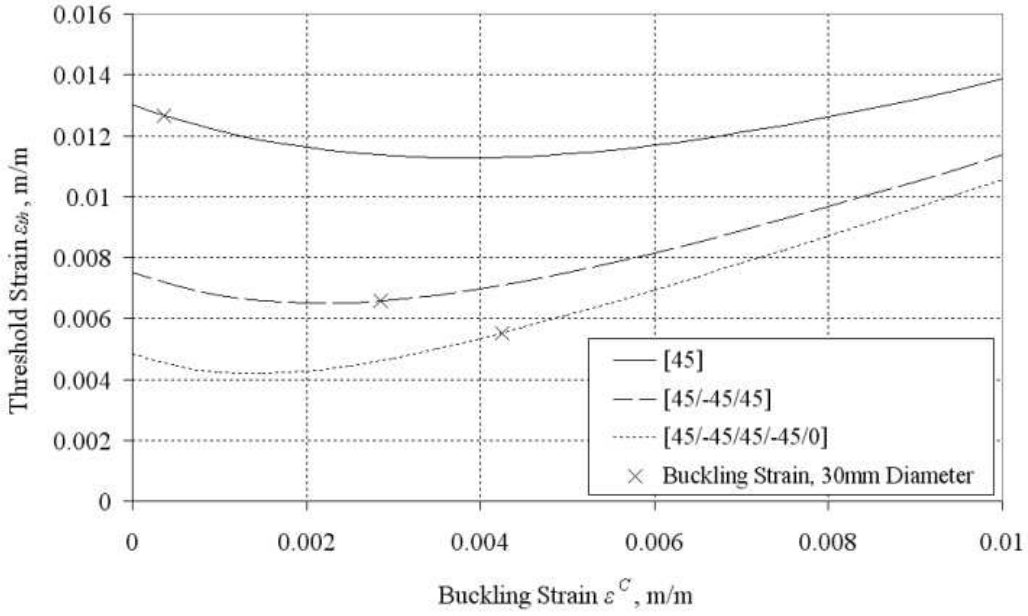

Figure 3-7: Relationship between buckling strain and threshold strain for selected sublaminates in a $[(\pm 45)_2/0_3/\text{-}45/0_3/45/0_3/(\mp 45)_2]_T$ laminate.

The buckling strain response to delamination growth is not a linear effect; Fig. 3-6 shows the potential effect of propagation in a single direction. The complexity of this relationship makes it difficult to predict stability beyond initial propagation using this method; however if a method of modelling the direction and shape of propagation efficiently were found then it would be possible to model this stability.

3.3 Adaptations of the Model

3.3.1 Extension to Transverse Propagation Analysis

The energy formulation described in Section 3.2.2 was modified to account for transverse propagation by Butler et al. [11]. This modified model approximates energy available for propagation in terms of Mode I energy.

In the physical problem, propagation around the delamination front is mixed mode [70], and this leads to some difficulties in modelling delamination growth. For an accurate prediction a model is needed to estimate the proportion of energy released in Modes I, II and III, (using methods of quantifying mode mixity), and also requires as an input an accurate value for the material critical values for SERR in Modes I, II and III cracking. Experimental techniques to find Mode I values are well established [18], but tests for Mode II and III SERR are not as simple [42, 85]. If a generalised method can be derived that does not require estimations of Mode II and Mode III critical values, then its solutions will be dependent on material parameters for which there is less uncertainty.

The modified model, as with the original, isolates Mode I propagation by assuming all energy in the postbuckled system is held either in bending energy in the buckled sublaminate, or membrane energy outside the delamination perimeter. The assumption that energy within the buckled sublaminate is entirely bending derived equates to an assumption of radial compression at the delamination boundary. This energy is then assumed to be released as if from a delaminated strut. In reality, the two-dimensionality of the sublaminate, and the transverse and shear loads that are induced within it, mean that the Mode I contribution is less than modelled; however ignoring the two-dimensional effects seems to have little influence on the predictions made by the model with reference to experimental and FEA results [11].

Derivation of this transverse energy follows a similar method as described in Section 3.2.2, resulting in the following equation:

$$\varepsilon_{th,x,i} = -\varepsilon^C_{x,i}\left(1 - \sqrt{4 + \frac{2G_{IC}}{A_{mm,i}(\varepsilon^C_{x,i})^2}}\right), i = 1, 2, \ldots n \tag{3.16}$$

where $A_{mm,i}$ is the axial stiffness of sublaminate i, and m is selected depending on the relative stiffnesses of the sublaminate in the longitudinal and transverse directions. If the sublaminate is stiffer in the longitudinal direction then $m = 1$, otherwise $m = 2$.

In the case where $m = 1$, Eq. 3.16 reduces to Eq. 3.10. Otherwise, Eq. 3.16 describes an equivalent system in which pre-buckling strain is assumed to act in the longitudinal x-direction, and post-buckling strain is applied in the transverse y-direction. It is this assumption that gives Mode I equivalent energy release in the transverse propagation model.

3.3.2 Free Edge Impact Damage

The benefit of the general formulation of the CAI model is that it can be adapted to model differing damage types. With the buckling analysis being independent of the energy-based analysis it is possible to use higher or lower fidelity methods of buckling analysis as required, or to change the delamination type being modelled.

One such adaptation of the CAI model is to free edge damage [59]. In contrast to a face impact, a free edge impact creates delaminations that are not fully enclosed. Although delamination is still the predominant damage caused by such an impact, it is more susceptible to fibre and intra-ply matrix damage than a composite subjected to a face impact [59].

There are two impact events that may lead to a delamination at a free edge, shown in Fig. 3-8. The first is an out-of-plane impact near to a free edge (Fig. 3-8 a). The second is an in-plane impact at a free edge (Fig. 3-8 b). This impact leads to more fibre and intra-ply matrix damage than the out-of-plane free edge impact.

In the case of free edge impact the propagation formulation remains the same, and Eq. 3.10 is still applied. The difference lies in the calculation of the sublaminate buckling strain, which is modified to represent the free edge damage instead of an enclosed delamination. Figure 3-9 shows the discretisation of an elliptical free edge sublaminate used.

Although the distribution of nodes around the plate boundary for an enclosed delamination was shown to have a negligible effect on the predicted bucking strain of such a sublaminate, the same is not found to be true of the free edge delaminations, particularly when the delamination is non-circular. Therefore, when modelling free edge delaminations, nodes are placed so as to be equidistant from each other around the restrained delamination boundary. This can be seen in Fig. 3-9.

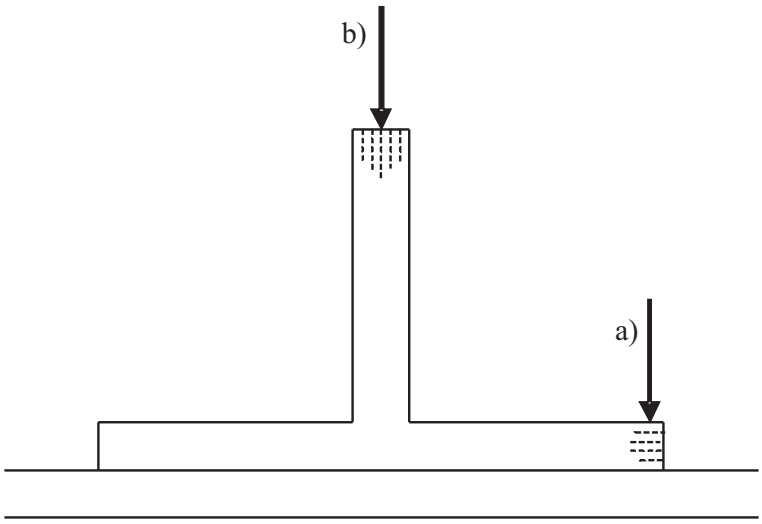

Figure 3-8: Free edge impact types, showing a) out-of-plane impact near a free edge and b) in-plane impact at a free edge. Dashed lines indicate delaminations within each laminate.

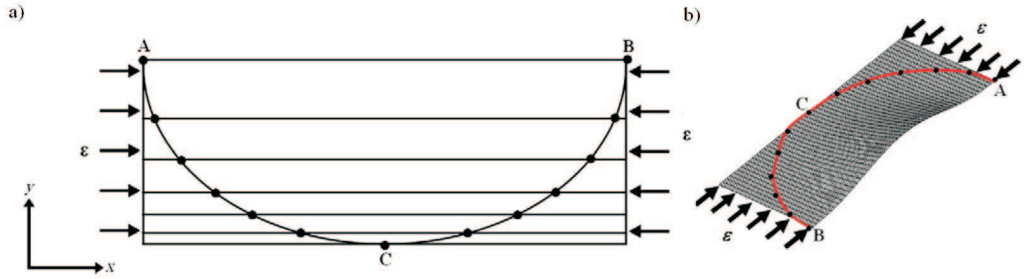

Figure 3-9: Free edge delamination modelling, showing a) discretisation in VICONOPT and b) typical buckling mode shape. Taken from Rhead et al. [59].

Due to the free edge present within the buckling model, the calculation of the sublaminate loads needs to be modified. The sublaminate loads calculated for the enclosed delamination in Section 3.2.3 assume compatibility around the entire boundary of the delamination, which is not the case for the free-edge case. The loading of this sublaminate is more complicated, but to simplify the problem upper and lower bound assumptions are made on the loading.

Sublaminate loads are once again calculated using classical laminated plate theory, but with two differing assumptions. The first is that there is zero transverse strain (Eq. 3.17), the second is zero transverse load (Eq. 3.18).

$$\begin{Bmatrix} N_x \\ N_y \\ N_{xy} \end{Bmatrix} = \begin{bmatrix} A_{11} & A_{12} & A_{16} \\ A_{12} & A_{22} & A_{26} \\ A_{16} & A_{26} & A_{66} \end{bmatrix} \begin{Bmatrix} \varepsilon_x \\ 0 \\ 0 \end{Bmatrix} \tag{3.17}$$

$$\begin{Bmatrix} N_x \\ N_y \\ N_{xy} \end{Bmatrix} = \begin{bmatrix} A_{11} & A_{12} & A_{16} \\ 0 & 0 & 0 \\ A_{16} & A_{26} & A_{66} \end{bmatrix} \begin{Bmatrix} \varepsilon_x \\ -\varepsilon_x \nu_{xy} \\ 0 \end{Bmatrix} \tag{3.18}$$

The free edge model shows good correlation when the failure mode of the impact damaged component is captured by the model [59], but due to the secondary fibre and matrix damage caused by such an impact other failure modes have been shown to dominate. In these cases the results of the CAI free edge impact model is non-conservative as a sole measure of compression after impact strength.

3.3.3 Damage Tolerance of Variable Angle Tow Laminates

The ability to tailor material stiffnesses in-plane is one of the major advantages of aerospace composite materials. When using straight fibres however this stiffness cannot vary with in-plane position in the material. This can be achieved by changing the fibre path in-plane, such as is the case with variable angle tows (VAT). By varying the angle of a tow across a plate its stiffness can be altered, which can lead to increases in buckling performance. Figure 3-10 shows a typical VAT path for a buckling optimised simply-supported plate.

Figure 3-10 indicates the tendency of a buckling optimised fibre path for a simply supported plate to place steep ply angles at the transversely supported edges, and shallower angles in the middle of the plate. This design gives buckling-resistant layups in the unsupported mid-region of the plate, and high axial stiffness load carrying fibres near the supported edge, where bending stiffness has less of an impact on the buckling load of the plate.

Such ply steering can lead to significant increases in laminate buckling performance [34, 69] but may have a detrimental effect on damage tolerance. As the layup of the material is effectively changing with position in-plane, the threshold strain for a delamination within the laminate will not only depend on its position through-thickness, but also its position (x,y) within the panel. Butler et al. [10] explored the damage tolerance of a prismatic buckling optimised composite panel, and showed that damage tolerance must be accounted for in these panels due to their increased critical strains.

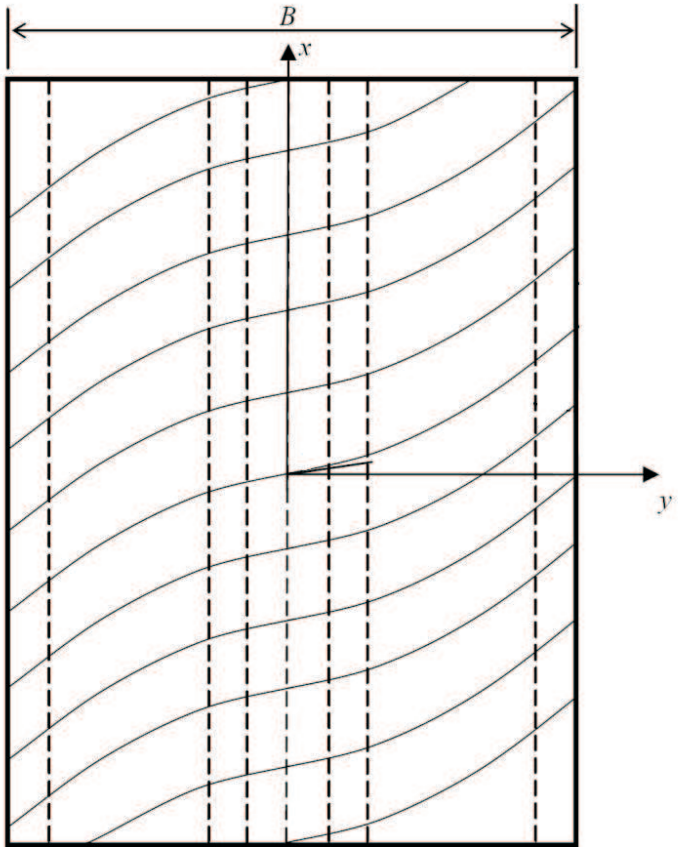

Figure 3-10: Typical buckling optimised prismatic VAT panel configuration. Based on laminate of layup $[\pm\theta]_S$. Taken from Butler et al. [10].

In the work of Butler et al. [10] a number of simplifying assumptions were made. Rather than modelling the change in fibre angle across a delamination, a straight fibre approximation was used in this region. As the fibre angle changes across the plate a number of CAI analyses were performed in different transverse locations to find the position at which damage tolerance is critical. For each of these locations the layup of the entire laminate through-thickness was assumed constant, amounting to an assumption that the plate was free to strain transversely, and that each location transversely is able to strain according to its own Poisson's ratio. When the VAT panel is analysed in isolation this would be the case but when taken as part of the wider structure interaction with other components, in particular the ribs, this assumption may not be valid, especially if the damage is in close proximity to a constrained edge.

Theoretical investigations performed into the damage tolerance of VAT panels [10] concluded that a typical simply-supported buckling optimised VAT panel was less damage tolerant to impacts mid-bay, and that the higher the loading of the plate, the more critical damage tolerance becomes. This second point can also be made of the damage tolerance of straight fibre composite laminates.

3.4 Limitations of the Model

The CAI model described here is intended to be an efficient method of estimating the CAI strength of a delaminated composite material. As such a number of assumptions and simplifications are made to ensure computation time is kept to a minimum. These mean that certain modes of failure are not well captured, especially those where out-of-plane deformation of the wider structure interacts with the local buckling of a delaminated region.

3.4.1 Analysis of Non-symmetric Laminates

One of the key assumptions of the model is that the base substrate remains undeformed out-of-plane throughout the loading regime, from pre-buckling right through to delamination propagation. This thin film assumption is valid for thin sublaminates in a symmetric laminate, but may not be suitable in some other applications, where coupling in the composite laminate may lead to out-of-plane deformations when uniaxial load is applied. One instance in which this would be the case is in helicopter blades, which often display an extension-twist coupling for aerodynamic reasons.

3.4.2 Interactive Buckling in a Composite Structure

As described above, out-of-plane deformation is not accounted for in the CAI model, but this deformation may not only occur as a pre-buckling coupling driven effect. When within a composite structure, local buckling of a delamination may interact with global buckling, the effects of which may significantly reduce the failure strength of the structure. This interaction is a far more challenging modelling task than can be undertaken with this CAI model, and is further complicated by the dependance of the interaction on the position of the delamination within the global structure. For that reason interaction is not considered in this thesis, but is highlighted as a consideration for future work.

3.5 Computational Implementation

The functionality of the CAI model has previously been implemented into a Windows based program [4]; however this was designed purely for control through a user interface for single laminate analysis. To allow integration of the CAI model into a computational algorithm a number of small modules need to be developed to automate each process within the CAI model analysis routine. This includes interfacing with the buckling analysis tool VICONOPT, and the ability to run the analysis either through a graphical user interface (GUI), or as a function call in an optimisation routine. For this work the program is redesigned to allow integration with other programs, such as optimisation routines, and to take advantage of the multiple processors present in modern desktop PCs.

3.5.1 Computational Implementation of the CAI Model

To allow computational automation of the CAI model, the energy analysis is written into a .dll (dynamic link library). This code mostly deals with the mathematics described in Sections 3.2.2 and 3.3.1, using inputs either from a controlling optimisation routine, or inputs specified in a GUI.

VICONOPT buckling analysis also needs to be automated, so a VICONOPT application programming interface (API) is developed to allow VICONOPT analysis to be called from another piece of computer code.

3.5.2 VICONOPT API

The VICONOPT FORTRAN code has been compiled to run on a number of operating systems; for this work the Win32 version of the program is used. In this state VICONOPT runs as a console application, with inputs being taken from a user specified input file, the location of which is provided by the user through the console interface. Outputs are written to a similar output file in the same location as the input. Automation of this entire process is vital to allow full integration of VICONOPT into any other computer code, so an API wrapper is developed.

The VICONOPT API is written in C♯ [48], and comprises three main components: writing of input files, control of the VICONOPT application, and reading of results from output files. All of this functionality is built into a single class, and compiled as a .NET dll for integration into any .NET-based program. As VICONOPT is a legacy FORTRAN application it has no ability to utilise multiple processing cores. In the

past this was not an issue, but with modern PCs utilising multiple processing cores this means that a single VICONOPT application is not making full use of the processing power available in a multicore CPU. For this reason the VICONOPT API is written in such a way as to allow multiple instances of VICONOPT to run simultaneously. As VICONOPT controls inputs and outputs through text files each instance of the program needs to be run in a separate folder to avoid overwriting of files created in the calculation process. Figure 3-11 shows the process for multiple VICONOPT analyses.

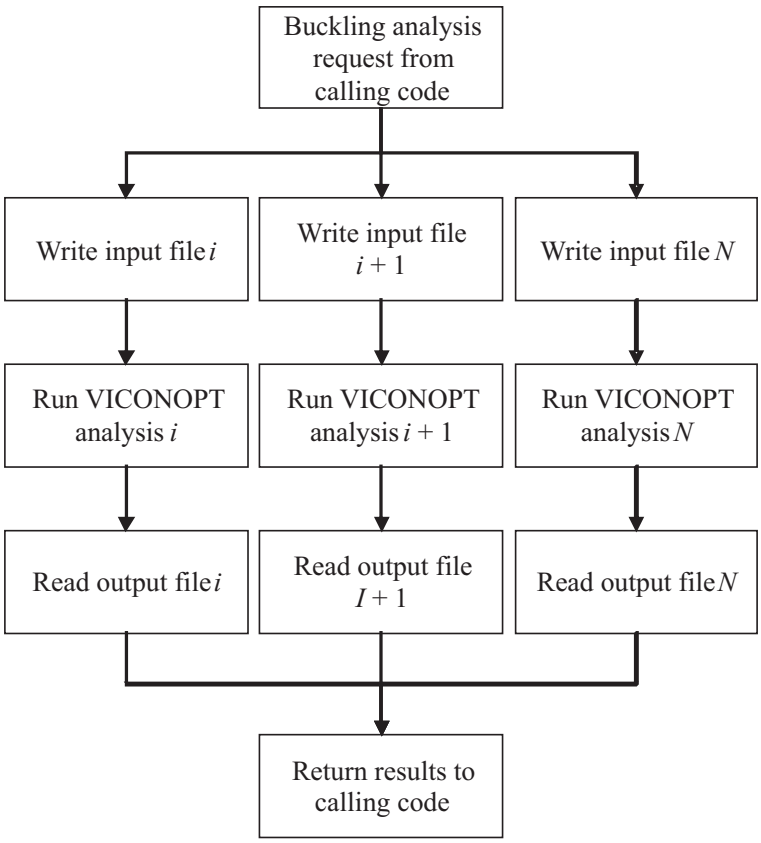

Figure 3-11: Flow chart for parallel VICONOPT buckling analysis in CAI model.

In a typical run of the CAI model the calling code requests a number of VICONOPT runs, sending information about the sublaminates being analysed and the loads applied to the VICONOPT API. The required VICONOPT instances are created, and the sublaminate analyses are performed in parallel. Results are then returned to the calling code. This method of parallelising computer code is known as multi-threading, and is becoming increasingly important as desktop PCs derive more computing power from larger numbers of processing cores rather than higher clock speeds or operations per

cycle.

3.5.3 CAI Analysis

To aid use of the model to analyse the damage tolerance of individual, user specified laminates, a GUI was created to allow users to perform quick analysis of a given laminate. Once again this interface was developed in Microsoft Visual Studio, using the C♯ language. As well as performing analysis using the CAI model, it also provides material, layup, and damage database functions for the user, allowing quick repeated analysis of the same layups with differing damage morphology for example. Figure 3-12 shows the CAI Analysis interface.

C♯ is an object-oriented programming language, so the program is split into a number of classes, each of which holds parameters and methods required for a particular part of the analysis process. This object-oriented approach is well suited to the modelling of physical systems [61], with objects created for each material, layup and so on. As an example here, the class handling layups will be described.

3.5.4 CompositeLayup Class

Generally, a class in an object-oriented programming language will hold parameters (values or objects that describe the class), methods (functions that perform calculations within the class) and constructors (methods that run when a new object is created). Accessors may also be used as a way to restrict the user's ability to access and edit parameters within the class. These will be described in turn with respect to the CompositeLayup class.

Parameters

The parameters for the CompositeLayup class must describe the materials used in the laminate, the layup and thickness of the plies, and the resulting stiffnesses of the laminate. Arrays are used to hold material, angle and thickness information, with each position in these arrays corresponding to a ply in the laminate. The class also holds details of the layup that help with its classification in the layup database, such as a name, description, and dates of creation and modification. Table 3.1 shows the parameters used in the CompositeLayup class.

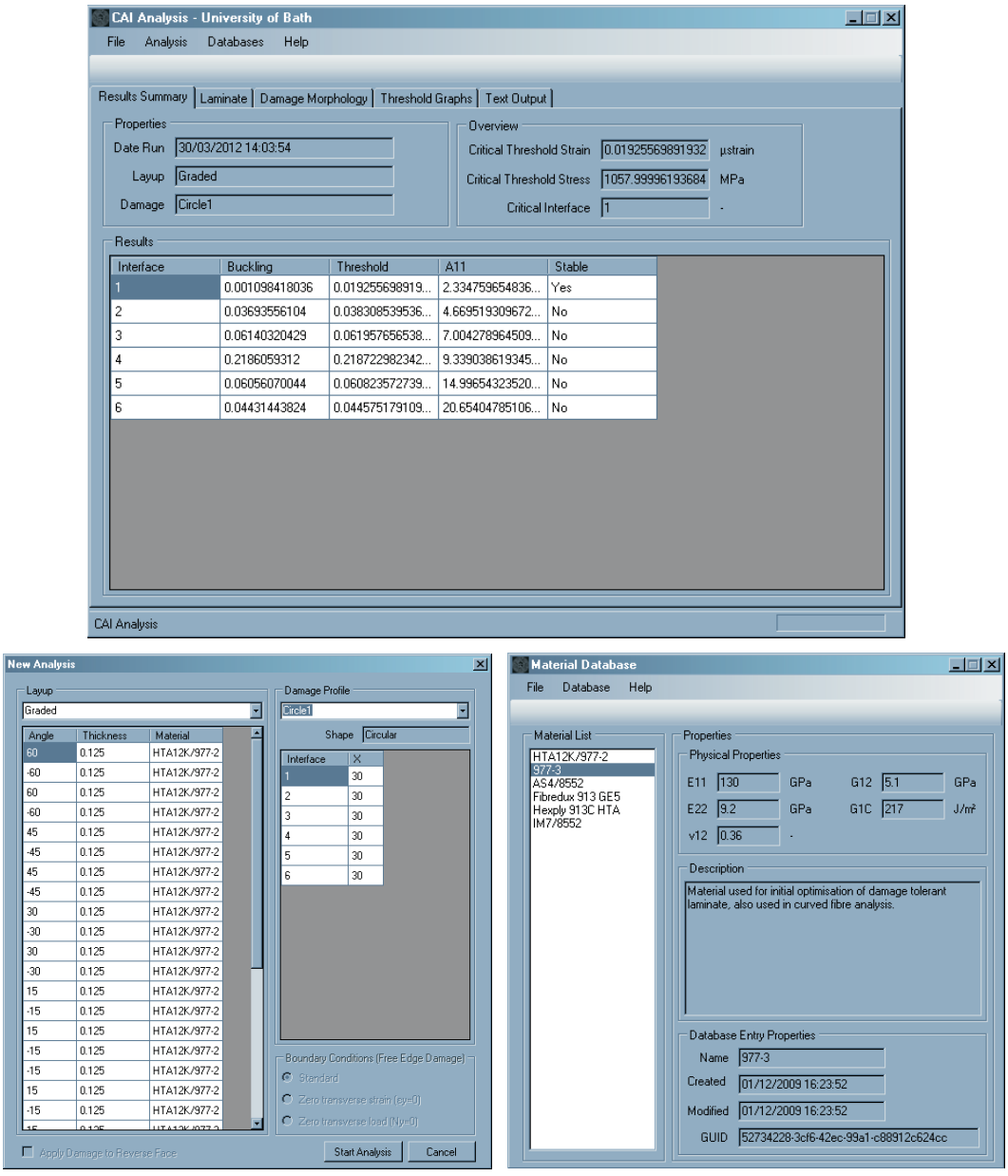

Figure 3-12: User Interface for CAI Analysis Program.

Name	Type	Description
`name`	`string`	Name of the layup, used to identify layup to user in database
`description`	`string`	Description of layup set by user
`anglesUsed`	`double[]`	Array of all ply angles used in the laminate
`thicknessUsed`	`double[]`	Array of all ply thicknesses used in the laminate
`materialsUsed`	`Guid[]`	Array of GUIDs for all materials used in the laminate. Materials can then be retrieved from the material database by their GUID
`angleLayup`	`int[]`	Layup of the laminate given in ply angles referenced from the `anglesUsed` array
`thicknessLayup`	`int[]`	Thicknesses of each ply, referenced from `thicknessUsed` array
`materialLayup`	`int[]`	Materials of each ply, referenced from `materialsUsed` array
`dateCreated`	`DateTime`	Date on which layup was created
`dateModified`	`DateTime`	Date on which layup was last modified
`identifier`	`Guid`	GUID identifier for layup in database
`length`	`int`	Number of plies in the layup
`aMatrix`	`double[,]`	**A** matrix calculated for the layup
`bMatrix`	`double[,]`	**B** matrix calculated for the layup
`dMatrix`	`double[,]`	**D** matrix calculated for the layup
`qMatrix`	`double[][,]`	**Q** matrix calculated for each ply
`qBarMatrix`	`double[][,]`	$\bar{\mathbf{Q}}$ matrix calculated for each ply
`extendedCalcualtionPerformed`	`bool`	Bool value to check whether **A**, **B**, and **D** matrices, modulus and Poisson's ratio calculations have been performed

Table 3.1: Parameters in the CompositeLayup class.

Constructors

Constructors are methods that run when an object of a class is constructed. In the case of the `CompositeLayup` class this constructor takes arguments to set the parameters for the layup. Arguments are validated to ensure there are no errors, with exceptions thrown if, for example, the arrays specifying ply thicknesses and angles are not of the same length, or if the values in these arrays reference a thickness or ply angle address not found in the `thicknessUsed` or `anglesUsed` arrays.

Methods

The methods for the `CompositeLayup` class perform the calculations for laminate stiffness matrices, and also calculate the laminate effective modulus and Poisson's ratio.

```
public CompositeLayup Sublaminate(int Length)
```

This method allows the user to split the layup, producing a sublaminate from the top surface, with the number of plies specified by the argument `Length`.

```
public CompositeLayup Sublaminate(int StartPoint, int Length)
```

This overload for the `Sublaminate` method allows the user to produce a sublaminate starting from the ply `StartPoint`, with the number of plies specified by the argument `Length`.

```
private double CalcPoissonsRatio()
```

Calculation of the laminate Poisson's ratio is handled by this method. As a `private` method it cannot be called from outside the `CompositeLayup` class, but is instead called by the `get` accessor `Nuxy`. The calculation performed in this method gives an approximation of Poisson's ratio for a symmetric or non-symmetric laminate. In the case of the latter, the full **A**, **B**, and **D** matrices is solved with unit N_x load, and calculating the ratio of ε_x to ε_y. This derivation is shown in Appendix A.

```
private void CalcDerivedValues()
```

When analysis beyond calculation of **A**, **B**, and **D** matrices is required, such as in the calculation of effective modulus or Poisson's ratio, the `CalcDerivedValues` method calculates various inverted and multiplied matrices based on the **A**, **B**, and **D** matrices. These calculations are not performed on creation of a `CompositeLayup` as they are computationally expensive and not always required by the user.

```
public void CalcLaminateProperties()
```

This method is called to calculate **A**, **B**, and **D** matrix values, including calculation of the **Q** and $\bar{\mathbf{Q}}$ matrices for each ply.

```
private double CalcEffectiveModulusxx()
```

This method calculates the effective modulus of the laminate in the x direction. This calculation is derived for symmetric and non-symmetric laminates, and is shown in Appendix A.

Accessors

To reduce the possibility of another piece of code inadvertently changing one of the parameters in the `CompositeLayup` class all parameters are set to `private`, and reading and editing of these parameters is controlled through accessors, `get` and `set`. Any parameters that the user may require access to are given a `get` accessor, such as laminate **A**, **B**, and **D** matrices. In the case of the `CompositeLayup` class editing of most parameters will likely change other parameters too, so `set` accessors are only applied to parameters such as `Description`. A `get` accessor is also used to retrieve laminate effective modulus and Poisson's ratio data; using these accessors calls the `CalcEffectiveModulusxx()` and `CalcPoissonsRatio()` methods respectively.

3.6 Conclusion

The CAI model described here, as initially proposed by Butler et al. [9], refined by Rhead et al. [58], and extended to static problems by Rhead and Butler [56], is an efficient method of modelling the compression after impact strength of composite laminates under uniaxial compression, with acceptable correlation with experimental results. A computer framework has been developed to automate the analysis process, and allow the model to be used within a wider optimisation routine. Further, a GUI has been developed to allow quick analysis of single composite laminates.

The next chapter will apply this CAI model as the objective in an optimisation routine as a method of determining the features of a damage tolerant composite laminate.

Chapter 4

Optimisation of Composite Laminates for Damage Tolerance

4.1 Introduction

Using a suitably efficient method of analysing the compression after impact (CAI) strength of composite laminates, it is possible to direct a search of a relevant laminate design space to explore characteristics of damage tolerant composite layups. The definition of this design space is key, as the orthotropic nature of laminated fibrous material is such that general stacking of plies will often result in coupling behaviour that is undesirable in most practical applications of the material, especially where they are replacing homogenous materials such as aluminium in airframes. Conversely, if the design space selected is not broad enough then certain damage tolerant characteristics may not be achievable within its scope. Furthermore, the selection of a suitable method of directing the search of the design space is also important, with a number of issues arising that will be described in this chapter. The following work looks to define a design space that allows for the features of a damage tolerant laminate to be explored, and then optimise within this design space using a suitable search method.

The methodology and results in this chapter were presented at the 51st AIAA/ASME/ASCE/AHS/ASC Structures, Structural Dynamics and Materials Conference in Orlando FL [5].

4.2 The Laminate Design Space

In its most general form, a composite laminate constructed from unidirectional lamina has a design space that is discrete with respect to the number of plies it contains, but continuous with respect to the angle variable of each of these plies. If the number of plies in the laminate is fixed then the problem can be treated as a continuous optimisation problem in an n-dimension design space, where n is the number of plies. For these problems a gradient-based optimisation method may be used, with derivatives calculated numerically depending on the objective for which the laminate is being optimised. The use of such a method may not however be able to reliably obtain a global optimum solution within this design space.

The issue with such unconstrained design spaces is the likelihood of solutions exhibiting undesired coupling responses. Of the coupling possible in a composite laminate, only bend-twist coupling is generally tolerated (but minimised) in engineering applications, unless another coupling is specifically desired, for example extension-twist coupling in helicopter rotor blades. To remove these coupling responses laminates are forced to be balanced and symmetric. Forcing symmetry ensures that there is no in-plane/out-of-plane coupling present, whilst balancing (an equal number of angle plies in the positive and negative directions) removes extension-shear coupling. It should be noted that the stipulation of a layup being balanced and symmetric to remove in-plane/out-of-plane coupling is a sufficient, but not necessary, condition. Chapter 6 explores laminate coupling, including laminates that are not symmetric, but are still uncoupled.

Another consideration for the design space is the parameter for which the composite laminate is to be optimised. In a real world design situation weight or cost tend to be the final design drivers, and as such would be seen as the objective function in the optimisation routine. In this case, phenomena such as buckling and damage tolerance would be included in the problem as constraints, limiting the feasible region of the design space. To allow for weight to be optimised the number of plies in the laminate would need to be changed during the routine, meaning the problem can no longer be seen as the optimisation of an n ply laminate as an n-dimension design space, as adding or dropping plies would change the design space. For this reason the optimisation process needs to be able to handle adding or dropping plies from the design. This can either be included directly in the definition of the design space, or solved by using a bilevel optimisation technique. Chapter 7 presents a bilevel technique for optimising composite panels for minimum mass, given damage tolerance and buckling constraints.

4.2.1 Lamination Parameters

A further concern in industrial applications of composites is manufacturability. Ply angles are not usually treated as continuous in a design routine as a large percentage of the potential design space can be reached with a relatively small number of ply angles. This phenomenon can be shown with the use of lamination parameters, such as described by Tsai and Hahn [74].

Lamination parameters can be used to express the **A**, **B** and **D** matrices of the plate constituent equations in terms of material invariants and 12 lamination parameters. These can help to reduce the number of variables in an optimisation problem, and can also aid in visualising a laminate design space. For example Setoodeh et al. [64] used the lamination parameters design space to optimise variable-stiffness laminates. This work found that designs optimised using lamination parameters exhibited superior compliance in comparison to those optimised using fibre angle parametrisation. Bloomfield et al. [8] have used lamination parameters to describe the feasible design space for laminates made up from a given array of ply angles.

As well as helping with visualisation of the laminate design space, perhaps more importantly lamination parameters give a number of convex subspaces by which the laminate is described. This is of benefit when compared to simply defining the layup by its ply angles as it produces a much easier design space in which to optimise. By comparison, the design space for ply angle defined laminates is complex and will contain many highly localised optima.

Unfortunately this benefit of lamination parameters with respect to optimisation cannot be realised for damage tolerance optimisation problems. Lamination parameters are a bulk measure of the properties of a composite laminate, and as such cannot be used to characterise behaviours heavily dependent on the ply-by-ply layup of the material. As a result the percentage of the lamination parameter design space covered by any given combination of ply angles does not necessarily reflect the coverage based on a parameter such as damage tolerance. This means that to draw conclusions on characteristics of damage tolerant laminates, a larger design space may be needed.

4.3 Optimisation Methods

The optimisation of a discrete problem brings about issues that do not arise with more conventional continuous problems. Continuous problems that can be differentiated

allow the use of gradient-based methods, and for design spaces with few local optima these methods are extremely efficient at finding optimal solutions. Even in the case that a continuous problem is not differentiable gradients may still be calculated numerically, and the methods are still relatively efficient.

Traditional numerical methods for optimisation, such as Dantzig's simplex algorithm [50], are well suited to continuous and linear problems with a distinct solution, but are difficult to adapt to highly non-linear discrete problems, as many composite problems are. Early work into the optimisation of composite laminates applied these mathematical methods to the problem. Schmit and Farshi [62, 63] formulated the problem as a continuous one, using the method of inscribed hyperspheres to linearise constraints. This was then solved using a standard simplex algorithm. The solution then has to be discretised in order to adhere to manufacturable ply thicknesses and angles, thereby possibly producing a non-optimal solution. In order to fully capture the problem of composite laminate optimisation its discrete nature needs to be addressed. The advent of evolutionary optimisation algorithms gave a way of optimising a composite laminate, without treating it as a continuous problem. Genetic algorithms (GAs) were quickly identified as good candidates for the optimisation of composite laminates, as they are well suited to searching a discrete design space.

Discrete optimisation problems may be handled in two main ways. The first is to discretise the solutions from a continuous optimisation method. Although this allows the use of continuous methods, gradient-based search methods are more difficult to apply as the discrete design space will not easily give gradients, either by analytical or numerical differentiation. The alternative to discretisation of a continuous solution is to use a search algorithm that is inherently discrete. These methods are metaheuristic, and include ant colony optimisation (ACO) and the GA. These methods analyse solutions within a discrete design space as a digital representation of its variables, without any other knowledge than the fitness of each design.

There are a wide range of publications on metaheuristic optimisation methods, such as GAs [20, 54, 67], particle swarm optimisation (PSO) [16] and ACOs [20]. These outline the methodology behind each of the algorithms, computational implementation, and techniques to tune and improve convergence and solution quality and confidence. The texts referenced here will give a good overview for each of these methods.

Le Riche and Haftka [41] used a genetic algorithm along with lamination parameters to optimise a laminate stacking sequence for maximum buckling load. Strain and con-

tiguity constraints were applied, and results were compared to those of a branch-bound method. The article concluded that although the genetic algorithm was computationally expensive in terms of objective function calls, it becomes relatively more efficient the larger the design space becomes. A further benefit of the GA is its ability to find multiple optima in a single optimisation run. The authors also note that the computation time for the GA could be significantly improved by parallelisation, as the algorithm lends itself well to parallel computing.

Nagendra et al. [49] proposed a number of improvements to a standard GA in order to improve reliability and reduce computational time for composite stiffened panel problems. Changes were made to a standard GA using crossover, mutation and permutation. To these standard genetic operators were added deletion and addition operators, and two new swap operators. Results showed that the new operators gave lower mass solutions, and a larger number of near optimum solutions. The importance of well selected probabilities for genetic operators was also stressed, with the demonstration of a 60% reduction in reliability with a poorly chosen probability of ply deletion.

Wiggenraad et al. [79] examined optimisation of a stiffened composite panel with buckling and damage tolerance constraints. PANOPT was used to optimise the panel for three design cases, these being undamaged, a stiffener de-bond, and a cut stiffener. The solution was found to tend towards a design with a more compliant skin and thicker, stiffer stringers compared to a panel optimised with only buckling constraints. Also discussed were the implications of modelling damage in a finite strip analysis program, with the conclusion that the limitations of finite strip do not prevent the modelling of worst case damage, in this case debonding of a stiffener between two ribs. This means that results gained from finite strip are applicable to certification of panels with regards to performance following this type of damage. It was concluded that the inclusion of damage tolerance constraints on the design of a stiffened composite panel, in this case, produced a weight penalty of only 5%. It was also stated that inclusion of further damage constraints, in particular impact damage, would cause further weight penalties.

Soremekun et al. [66] compared the effectiveness of a standard genetic algorithm to that of a generalised elitist genetic algorithm (GEGA) when applied to two problems, one with multiple global optima, and another with a single global optimum surrounded by a large number of points with fitnesses close to that of the optimum solution. Three types of GEGA were tested, a multiple elitist selection (ME1) where a pre-defined

number of the best parent designs were transferred to the next generation, a multiple elitist selection (ME2) where a pre-defined number of the best of the combined parent and children designs were transferred to the next generation, and a variable elitist selection (VE), which acts as ME2, but with the number of elite designs transferred from one generation to the next being variable during the optimisation process. VE allows for the algorithm to interrogate a large design space quickly in early generations, and then focus in on global optima found in later generations. It was found that for problems with multiple global optima both multiple elitist and variable elitist, with a low number of preserved designs each generation, were found to out-perform the standard GA, with more optima found at a lower computational cost per optimum. For the problem with one global optimum surrounded by many points with a close fitness value it was found that VE gave the best performance, with computation costs comparable to that of a standard elitist genetic algorithm without the problems of premature convergence.

PSO is another evolutionary algorithm that can be applied to the optimisation of composite laminates, and Hassan et al. [29] performed a study comparing the performance of PSO to that of GA for a number of design optimisation problems, including three benchmark tests, and two tests representative of real-life problems. The PSO method used is applied to discrete problems by way of rounding variable values found to the nearest integer when dealing with any discrete variables. The GA tested implements selection, crossover and mutation, and both methods use the same population size and convergence criteria. Results showed that PSO is as effective as GA in producing high quality solutions, but requires less computational effort. The reduction in computational effort is problem dependant however, with the smallest reduction coming from constrained, non-linear problems with discrete variables. This is a category into which the optimisation of composites often falls, meaning the benefits of PSO, although still attainable, are to some extent diminished when dealing with composite laminates.

4.4 Genetic Algorithm

Following investigation of the optimisation techniques available it was decided that the GA was best suited to the problem presented. GAs have been successfully applied to a wide range of composite optimisation problems, and are generally favoured in this area for being a discrete method, removing the need for the discretisation of solutions that would be required with other optimisation techniques. The GA takes as its inspiration

the theory of evolution and natural selection, or 'survival of the fittest'. The algorithm mimics this by working in generations, where the 'parents' from a previous generation are used as the basis for the 'children' that will make up the next. The best solutions from the previous generation are more likely to be chosen as parents through a weighting system, thereby ensuring that more of the good traits of the previous generation are carried forward to the next than the bad traits. A 'mutation' operator is also generally employed in GAs as a means of ensuring that no traits are ever lost permanently in the course of an optimisation. This gives a low probability chance that a trait within a design will be randomly changed in each design each generation. Figure 4-1 shows the general form a typical GA will take.

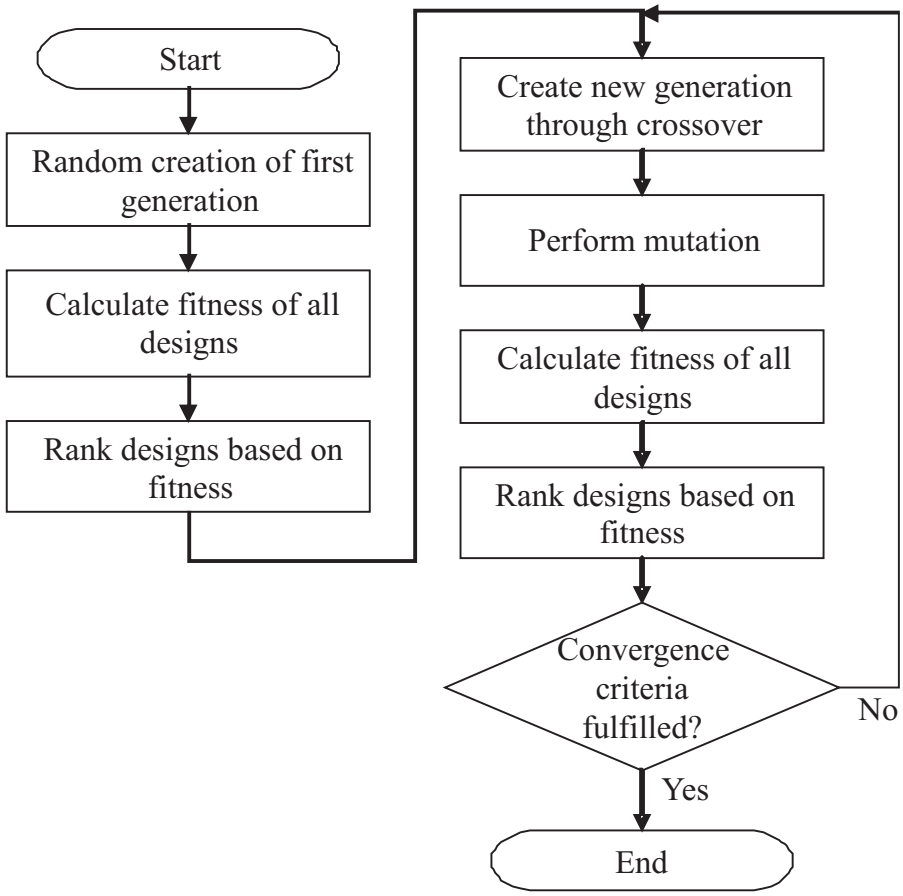

Figure 4-1: Block diagram for general Genetic Algorithm.

4.4.1 Encoding of Designs

As previously stated, the GA is a discrete optimisation method. This is derived from the way in which the solutions are encoded within the algorithm. This is known as

genotype-phenotype mapping. Figure 4-2 shows a generic design used in a GA.

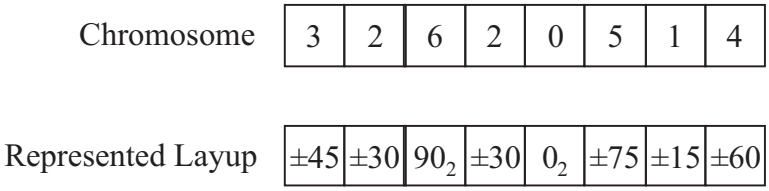

Figure 4-2: Encoding of designs in a Genetic Algorithm. Table 4.1 shows the encoding used in the Genetic Algorithm.

As can be seen in Fig. 4-2, each design is made up of an array of integers. These integers are allowed to take a set number of values, in the simplest form they are treated as bits, allowing values of '0' or '1' only (binary encoding). In the case of optimising a composite laminate it is convenient for each of these integers to represent a single ply or pair of plies in the laminate, with the number of values each can take being limited by the number of ply angles that are manufacturable. Table 4.1 shows the encoding used in this work. This method of encoding is known as discrete non-binary encoding, as opposed to the aforementioned binary encoding, as each integer can in this case take multiple values.

GA Code	0	1	2	3	4	5	6
Ply Angle (degree)	0_2	±15	±30	±45	±60	±75	90_2

Table 4.1: Encoding of ply angles in a Genetic Algorithm.

4.4.2 Ranking and Weighting of Designs

Each of the designs within the population must be assessed according to the specified objective function, the result of which allows designs to be ranked by fitness. In cases where regions of the design space are infeasible penalty functions may be applied to the objective function, weighted by how much the design violates constraints. The strength of this penalty function should be tuned for a particular problem; too weak and it will not exclude infeasible designs from the final results, too strong and feasible designs near the constraint boundary may not be reached.

Simple ranking of the designs within a generation is not enough when selecting which designs will be used to seed the next generation; a method of setting the probability of selection is also required. For this a weighting method is used. Equation 4.1 calculates the probability that a given design will be selected:

$$\mathbb{P}(\text{selection}) = \frac{2(N_{\text{designs}} - R + 1)}{N_{\text{designs}}(N_{\text{designs}} + 1)} \tag{4.1}$$

where R is the rank of the design. The weighting produced by this is shown in Fig. 4-3.

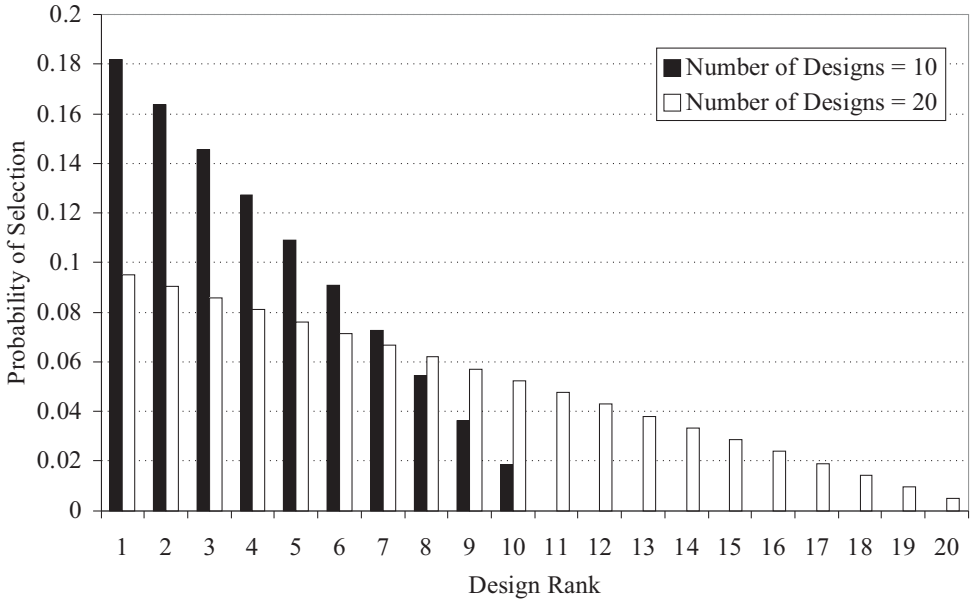

Figure 4-3: Probability of selection of candidate design based on fitness function rank for design spaces of 10 and 20 candidates.

This weighting linearises the change in probability of selection with design ranking, giving the best designs a higher probability of selection as parents for the next generation.

4.4.3 Crossover Operator

The crossover operator is the primary method by which new designs are produced in a GA. Two parents are selected by the weighted selection process in which better designs are more likely to be picked. In the case of single-point crossover a random point in the chromosome is chosen as the crossover point, and the two parents are split at this point and joined to produce a child, as shown in Fig. 4-4. This operation is repeated until a new generation of designs has been produced. As the parental selection process is weighted towards better designs the next generation carries forward the good design traits of the previous one, and removes those designs with poor traits. By this action the quality of the population improves generation by generation.

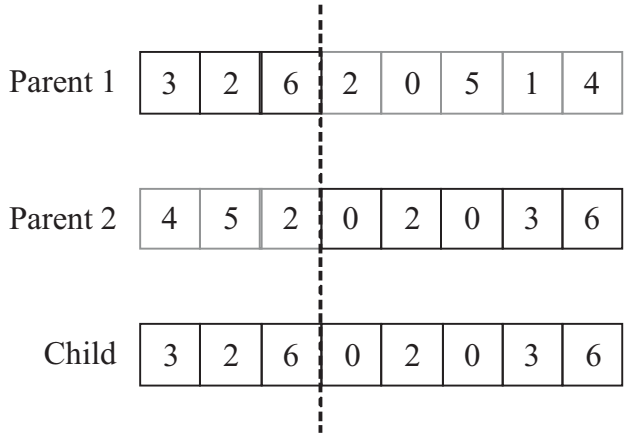

Figure 4-4: Single-point crossover in a Genetic Algorithm.

4.4.4 Mutation Operator

In some rare cases a good design trait can be lost from the gene pool through crossover, or simply does not appear in the initial population. The mutation operator is designed to overcome this problem by randomly changing a single gene in a design, allowing lost traits to return to the gene pool (see Fig. 4-5).

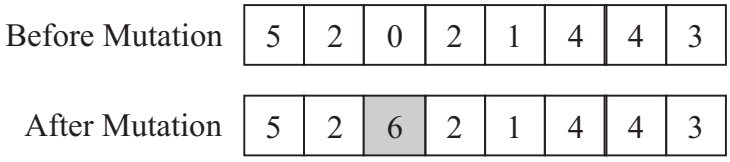

Figure 4-5: Mutation in a Genetic Algorithm.

During the creation of a new child design the choice is generally made between crossover or mutation, with mutation taking place at low probability. If mutation is chosen, then genes can be picked stochastically to mutate. This is a simple task in the case of a binary encoded problem, as the bit chosen to mutate can be switched, but in a discrete non-binary problem there are a number of alleles for the gene to mutate to. It is a matter of tuning of the GA as to whether the new allele is simply again a stochastic choice, or if it may be more effective to target the new choice. In cases where there is some relation between the possible alleles it may be preferable to choose the new allele from those in close proximity to the old one within the design space.

4.4.5 Elitism

Most GAs employ some sort of elitism to ensure that the best designs of a generation are not lost. This usually means the direct transportation of the best designs of a generation to the next in order to preserve them. In some cases multi-elitism is used by which a number of the best designs are moved to the next generation unaltered. More refined solutions involve variable elitism, whereby the number of elite designs moved from one generation to the next is varied depending on the total number of generations performed. Methods such as this can reduce the convergence time of a GA. The GA presented in this work is multi-elitist, as convergence times encountered do not warrant the application of a variable-elitist algorithm.

4.4.6 Convergence Criteria

There are a range of methods by which to decide upon the termination of a GA routine. The simplest is to run the GA for a set number of generations; however this gives no indication as to whether an optimum or even near optimum solution has been found, and is generally an inefficient use of computing time. More effective is the practice of measuring the fitness of the population through the generations, and how this changes. This can either be done by calculating an average fitness of the total population, or by comparing the fitness of the best design generation by generation. In the case of a population average fitness the convergence criterion would be set as less than m percent improvement in n generations, where m and n would be set based upon the problem being modelled. When using the fitness of the best design in the population the convergence criterion is simply set as n number of generations without improvement of the best design. Figure 4-6 shows a sample convergence plot for a GA. In this case it can be seen that the fitness of the best design in a generation always increases with passing generations, as the best design from the previous generation is retained in this elitist algorithm, but the average fitness does not necessarily improve.

4.5 Example Optimisation Process

4.5.1 Genetic Algorithm Parameters

Much of the optimisation work done in the composites field is performed using GAs. This metaheuristic search algorithm is well suited to composite optimisation due to its inherently discrete nature matching that of a vast majority of composite optimisation problems. In this case a simple GA was used, including multi-elitism (2 designs retained per generation), single-point crossover (probability of 0.8) and mutation (probability

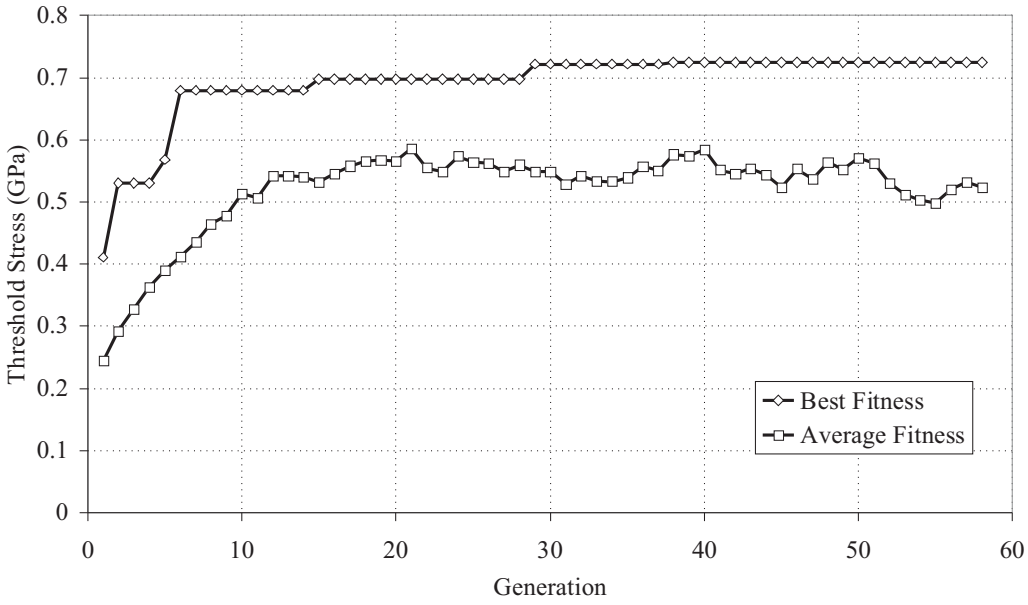

Figure 4-6: Typical convergence plot for a genetic algorithm optimisation routine.

of 0.05). The population size was 100, and the fitness function was the threshold stress of the laminate. Convergence was measured as a function of the number of generations passed without improvement of the best design. The fitness of each design was given to be the critical threshold stress of the laminate, calculated using the CAI model described in Chapter 3. In the absence of a suitable damage modelling method a single damage morphology was assumed for all laminates. The reliance of current aircraft regulations on damage size and detectability rather than impact energy levels [23, 24] makes this a reasonable approach to take, as long as the chosen damage morphology is an appropriate worst case approximation.

4.5.2 Problem Definition

For simplicity, the optimisation problem was defined as maximising the CAI strength (defined by the critical propagation threshold stress) of a 32-ply symmetric composite laminate constructed using HTA12K/977-2 pre-preg material (properties in Table 4.2), allowing plies in plus-minus pairs of angles between 0° and 90°, in 15° intervals. Delamination damage in the laminate was assumed to be of constant diameter, set at $d_i = 32$ mm, based on damage observed in other 4 mm thick composite plates with BVID [58, 56]. As GAs are not guaranteed to converge to an optimum solution the routine was repeated a number of times, producing a range of candidate layups. No

other constraints were applied to the optimisation so the designs produced may not be practical; for example they may contain large blocks of equal angle plies. However, these laminates indicate the characteristics of a damage tolerant composite laminate. Table 4.3 details the best of the layups found using the GA (GA_1 - GA_3), and compares them to a quasi-isotropic (QI) control laminate. The stated propagation stress values are those predicted by the CAI model in each case, taking into account the effective axial modulus E_{xx} of the laminate.

Material	E_{11}, GPa	E_{22}, GPa	G_{12}, GPa	ν_{xy}	t, mm	G_{IC}, J/m^2
HTA12K/977-2 [45]	147	8.5	4.9	0.30	0.125	478
IM7/8552 [12]	171	9.08	5.29	0.32	0.125	278

Table 4.2: Material Properties.

Laminate	Layup	E_{xx}, GPa	ν_{xy}	Predicted Propagation Stress σ_{th}, MPa
QI	$[45/0/\text{-}45/90]_{4S}$	55.9	0.308	263
GA_1	$[\pm 75_3/90_2/0_2/\pm 45/0_4]_S$	75.8	0.093	962
GA_2	$[90_4/\pm 60/\pm 75/\pm 45/0_6]_S$	65.2	0.148	902
GA_3	$[\pm 75/90_6/\pm 15/\pm 30/0_4]_S$	67.9	0.100	887
EXH (24 ply)	$[\pm 60/\pm 45/\pm 30/\pm 15_3]_S$	76.7	0.675	564
DTO	$[\pm 60_2/\pm 45_2/\pm 30_2/\pm 15_2]_S$	54.9	0.622	1064

Table 4.3: Predicted propagation stress and optimised laminate layups. Results given are for a constant through-thickness damage diameter of 32 mm.

4.5.3 Exhaustive Search

As a supplement to the genetic algorithm an exhaustive search was performed over a smaller design space. The laminate was limited to 24 plies, made up of plus-minus angle-ply pairs in a symmetric layup. The efficiency of the CAI model allowed for the 117,649 (7^6, i.e. 7 possible angles in 6 through-thickness locations) permutations to be solved in around 20 hours using a desktop PC. The search produced a stress-optimised damage tolerant laminate, shown in Table 4.3 (EXH 24 ply). The exhaustive search produces a lower threshold stress than the GA because of the reduction in the number of plies in the laminate, reducing the ability to balance the requirements of overall laminate stiffness, Poisson's ratio mismatch between the full laminate and sublaminates, and axial stiffness of outer plies.

4.5.4 Optimisation Results

The results from the GA optimisation and exhaustive search were applied to an intuitive search of the 32 ply design space. The results back up previous observations that damage tolerant laminates have plies with low axial stiffness at their outer faces, and axially stiffer plies towards the middle of the laminate. Similar results of low axial stiffness outer plies were seen in the work of Czabaj et al. [17], wherein damage tolerance of different QI layups were compared for sandwich structures, and those with low axial stiffness plies outermost performed best in CAI tests. The configurations selected by the GA combine damage tolerant plies at shallow depths where the laminate is susceptible to failure due to localised buckling with less damage tolerant, but better load carrying plies at depths where localised buckling will not occur. These designs do however suffer from reduced overall longitudinal bending stiffness as shown in Table 4.4, and may also be susceptible to lateral propagation, as described in work by Butler et al. [11].

Laminate	D_{11}, kNmm	D_{12}, kNmm	D_{22}, kNmm	D_{33}, kNmm	$N_{xb,Lim}$, N/mm
QI	0.354	0.110	0.288	0.122	0.332
GA_1	0.139	0.048	0.625	0.061	0.229
GA_2	0.109	0.055	0.642	0.067	0.224
GA_3	0.122	0.036	0.667	0.049	0.206
EXH (24 ply)	0.117	0.062	0.122	0.067	0.156
DTO	0.192	0.157	0.356	0.169	0.373

Table 4.4: Flexural stiffness and buckling load for a simply-supported, high aspect ratio plate for damage tolerance optimised laminates.

The intuitive search leads to a 32-ply symmetric laminate of plus-minus ply pairs that exhibited predicted threshold stress far in excess of that previously achieved [55, 56, 58]. This layup is detailed in Table 4.3 (DTO). Note that the high stress values for this design are unrealistic since failure would in practice occur by some other mechanism. The results of the CAI model applied at the outermost 8 interfaces of the quasi-isotropic (QI) and DTO layups are shown in Figs. 4-7 and 4-8. Damage diameters in these plots are based upon experimental data presented later.

The QI layup displays typical results for both buckling and threshold strains. The buckling strain of the sublaminates increases with increasing sublaminate thickness, with threshold strain minimising at the 5^{th} interface (0.625 mm deep). At this interface buckling strain is predicted to occur at 0.003 mm/mm, with a threshold strain of 0.00485 mm/mm. The behaviour of the DTO laminate is unlike that of the QI layup,

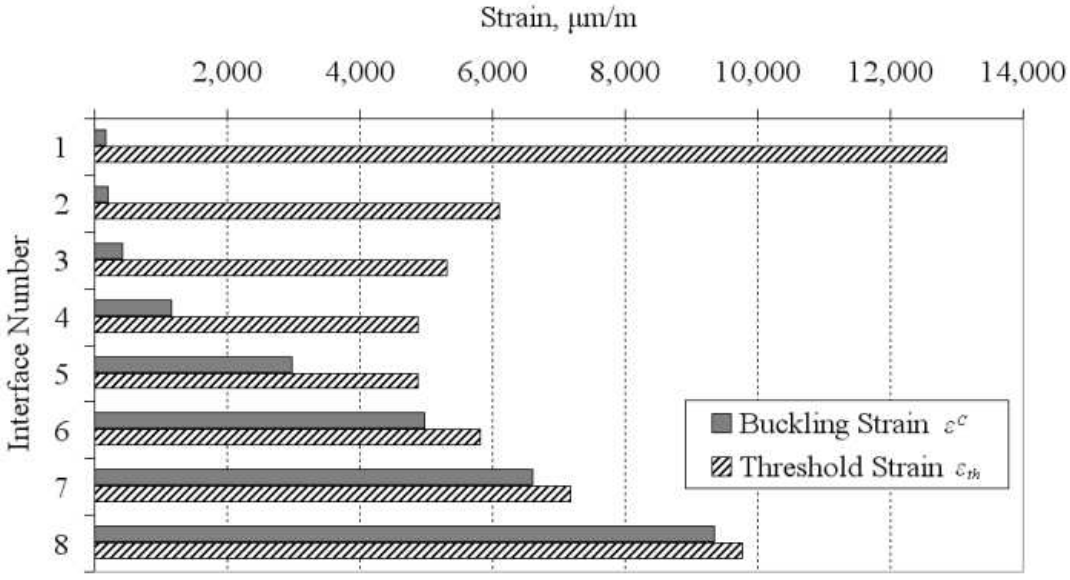

Figure 4-7: CAI model results for quasi-isotropic (QI) control laminate, $d_{1-8} = 30$mm, material HTA12K/977-2.

with buckling and threshold strains maximising at interface 4. Other than the first ply sublaminate, all buckling strains are far in excess of realistic strains for composites, the lowest of these being around 0.02 mm/mm.

Characteristics of a Damage Tolerant Laminate

All of the layups detailed in Table 4.3 show characteristics that may be attributed to giving the laminates improved damage tolerance when compared to more typical quasi-homogenous layups. The first characteristic to note is the distribution of stiffness through the thickness of each of the laminates. In all cases, the fibres near the surface of the laminate are less axially stiff in the loading directions than those near the laminate midplane. The threshold strain equation associated with the CAI model used (Eq. 3.10) predicts that the lower the axial stiffness of the sublaminate, the higher the sublaminate propagation strain. This is because the less stiff sublaminate accrues strain energy at a lower rate than a stiffer laminate, and so requires a higher applied strain to reach the critical strain energy release rate.

A second characteristic to be discussed is the Poisson's ratio of the laminates. Table 4.3 shows that the GA optimised laminates have a very low Poisson's ratio as a result

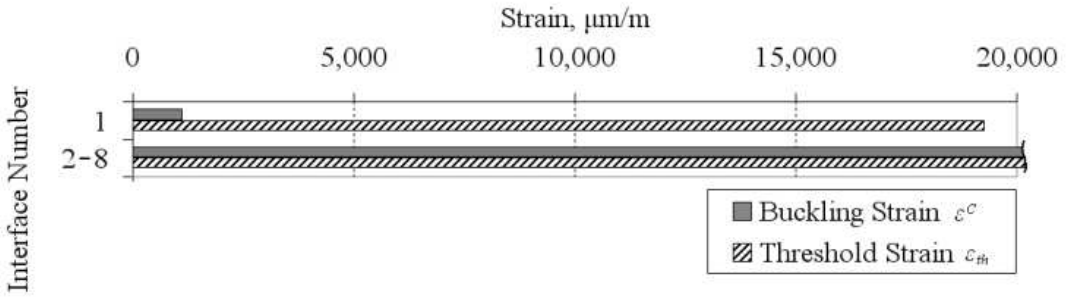

Figure 4-8: CAI model results for damage tolerance optimised (DTO) laminate, d_{1-8} = 32mm, material HTA12K/977-2. At all interfaces below interface 1 buckling and propagation are predicted in excess of 0.02 mm/mm.

of the combination of very low stiffness plies near the surface and 0° plies near the midplane. This design comes about as axial stiffness is an important driver for the optimiser, increasing the load carry capacity of the laminate. This requirement is countered at the surface by the need for less axial stiffness to reduce the threshold strain as calculated by Eq. 3.10. The layup DTO in Table 4.3 is the best performing of all those laminates described, but it differs from the GA derived laminates in having a high overall Poisson's ratio. The benefit of this will be discussed in the next section, but it is of great interest that the GA was unable to produce such a configuration.

Convergence of Genetic Algorithm

The GA was chosen here as a generalised optimisation algorithm that has the potential to deal with the highly non-linear discrete design space that this problem presents. As has been shown however, the GA was unable to reveal the best laminate design for this function. Even when using metaheuristic methods such as this, an optimiser will tend to solutions in an area of the design space populated by other good designs. If a better solution exists within a region of poor designs then it is less likely to be found as there will be no driver to pull the optimiser in that direction. This may mean that the best solutions are missed, and that a different approach to finding damage tolerant laminates may be appropriate. Chapter 5 will begin to look at such approaches.

4.6 Experimental Results

Five laminates were subjected to compression after impact testing; three specimens with the DTO layup (DTO_{1-3}) and two quasi-isotropic (QI_{1-2}). Table 4.5 shows the layups for these specimens. Each sample was impacted using a dynamic impact

testing machine with a steel semi-spherical impactor of diameter 16 mm, over an ASTM impact test window defined in ASTM D7136 [3] of size 125 × 75 mm, where the greater dimension was aligned parallel to the longitudinal (0°) fibre direction. Test impacts were performed on a surplus sample to ensure an impact energy was chosen to give representative BVID damage. Impact energies were chosen so as to produce delaminations of approximately 30 mm maximum diameter. $DTO_{1,2}$ and QI_1 were impacted, before DTO_3 and QI_2. For the second round of impact tests, energies were adjusted according to the reduced fracture toughness of the IM7/8552 material, and the difference in residual energy between the two layups for the three initial tests. Table 4.6 details selected impacts, and Figs. 4-9 and 4-10 show the load and energy traces for the two impacts.

Sample	Material	Layup	Thickness T, mm	E_{xx}, GPa	Propagation Stress σ_{th}, MPa	Failure Stress, MPa
QI_1	HTA12K/977-2	QI	4.24	46.1	-	256
QI_2	IM7/8552	QI	4.03	56.1	251	257
DTO_1	HTA12K/977-2	DTO	4.18	46.3	266	304
DTO_2	HTA12K/977-2	DTO	4.31	40.8	263	290
DTO_3	IM7/8552	DTO	4.05	55.4	339	342

Table 4.5: Experimental results for QI and DTO laminates. Layups are referenced from Table 4.3.

Sample	Peak energy, E_i (J)	Maximum energy, E_{max} (J)	Residual energy, E_r (J)
QI_1	12.54	15.11	2.57
DTO_1	10.12	15.10	4.98

Table 4.6: Energy values recorded for test impacts. Refer to Fig. 2-10 for definitions.

Employing the analysis performed by Hitchen and Kemp[31], Table 4.6 shows the relevant energies for each of the sample impacts. It should be noted that the DTO_1 had a lower peak energy E_i than the QI_1. This indicates that the DTO design is less damage resistant than the quasi-isotropic, meaning that delamination damage will occur in this sample at lower impact energies than the control. This also means that for the same energy impact the graded sample has a higher residual energy E_r, meaning it will absorb more of the impact energy through delamination than the control. This would indicate a larger total delamination area in a DTO sample compared to a quasi-isotropic, given the same impact energy.

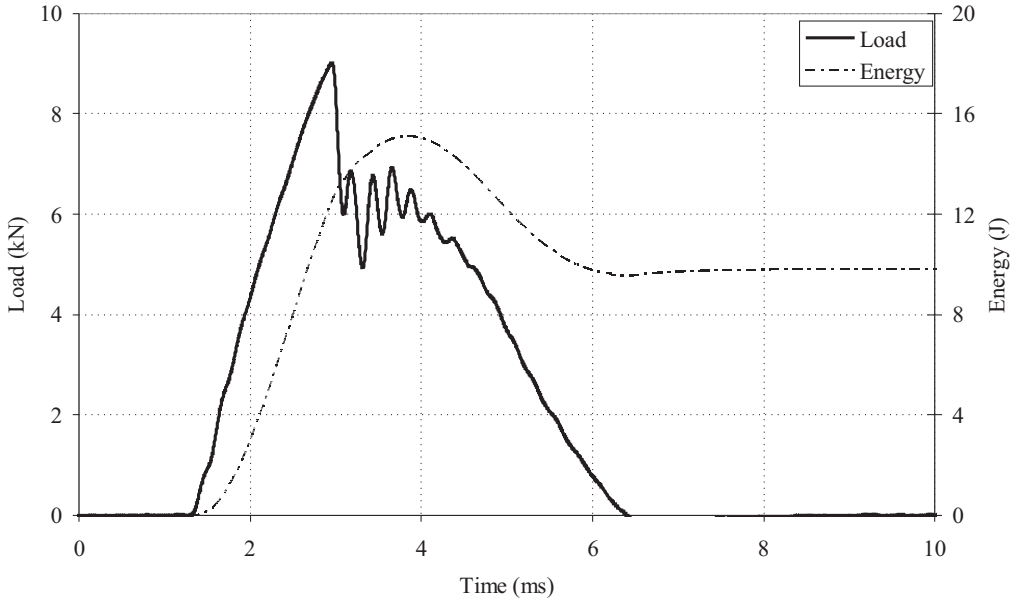

Figure 4-9: Impact data for QI_1 coupon.

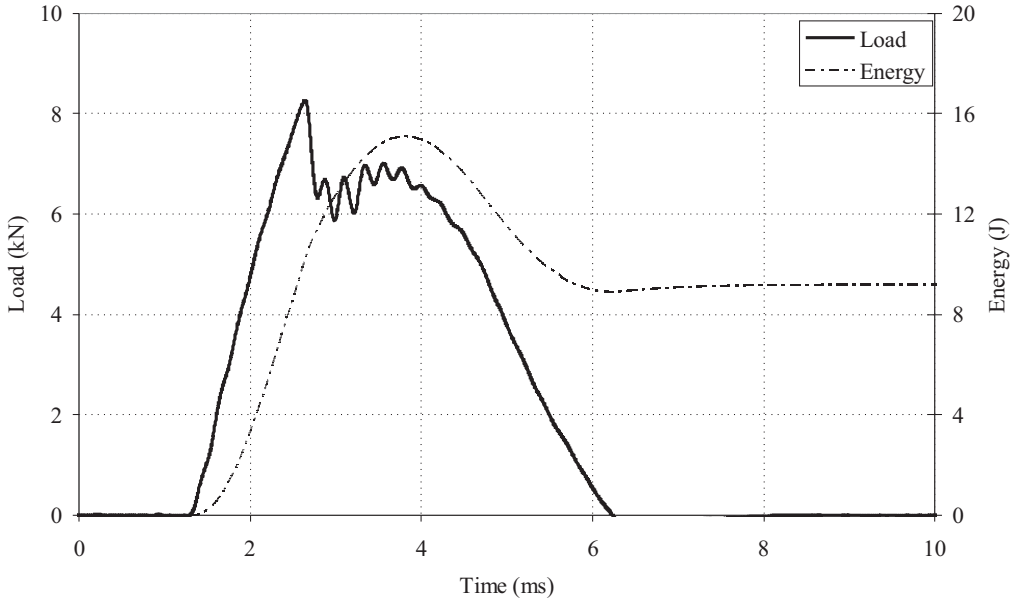

Figure 4-10: Impact data for DTO_1 coupon.

In order to quantify the scale of BVID applied through the impact tests an ultrasonic C-scan technique was used. Images were taken at a resolution of 0.1 mm using a 35 MHz polymer probe. This gives both sufficient scan penetration and through-thickness resolution. Figure 4-11 shows the resulting C-scan images for three samples. The QI sample displays typical BVID, with delaminations near the back face smaller than those deeper in the laminate. In contrast the DTO laminates show large damage near to the back face, with delaminations changing orientation according to the ply angle variation within these laminates.

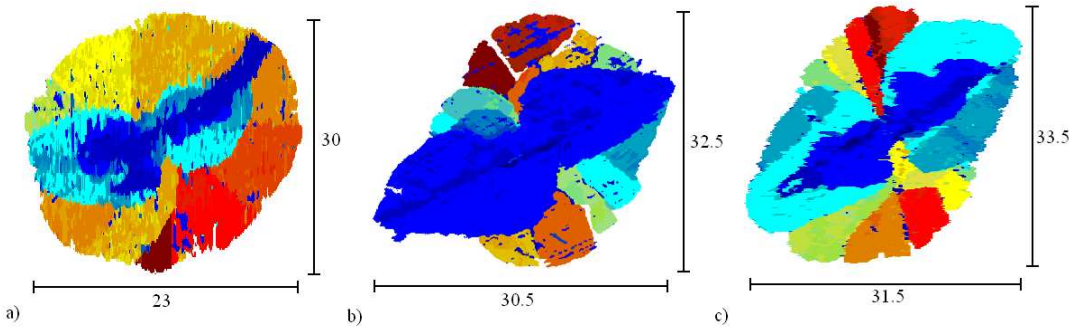

Figure 4-11: Back face C-Scan images of impact damage in a) QI_1, b) DTO_1 and c) DTO_3 samples. Longitudinal axis is aligned vertically, blue represents near surface and red represents deep delaminations. Images and colour maps are individually scaled, dimensions are given in mm.

The compression tests were carried out in an electromechanical compression testing machine under displacement control. End tabs were bonded to the specimens which were held within specially designed end fixtures. In order to restrict overall buckling of the specimens an anti-buckling guide was used, restricting out-of-plane displacement to an 85 mm circular window centred on the impact damage, see Fig. 4-12. The setup is designed to produce clamped conditions at the ends of the test piece.

Measurements in the test were taken using surface strain gauges and a digital image correlation (DIC) system, which allows for 3D visualisation of the deformed sample, along with full field surface strain analysis. Readings from back-to-back strain gauges ensured that the samples were initially loaded under axial compression without significant bending. The strain gauge readings and the DIC allowed for detailed analysis of sublaminate buckling modes that occurred during the tests. The DIC system was used in two modes, the first capturing images at regular intervals during initial loading, the second taking a high speed video of the failure of the sample. This allowed for analysis

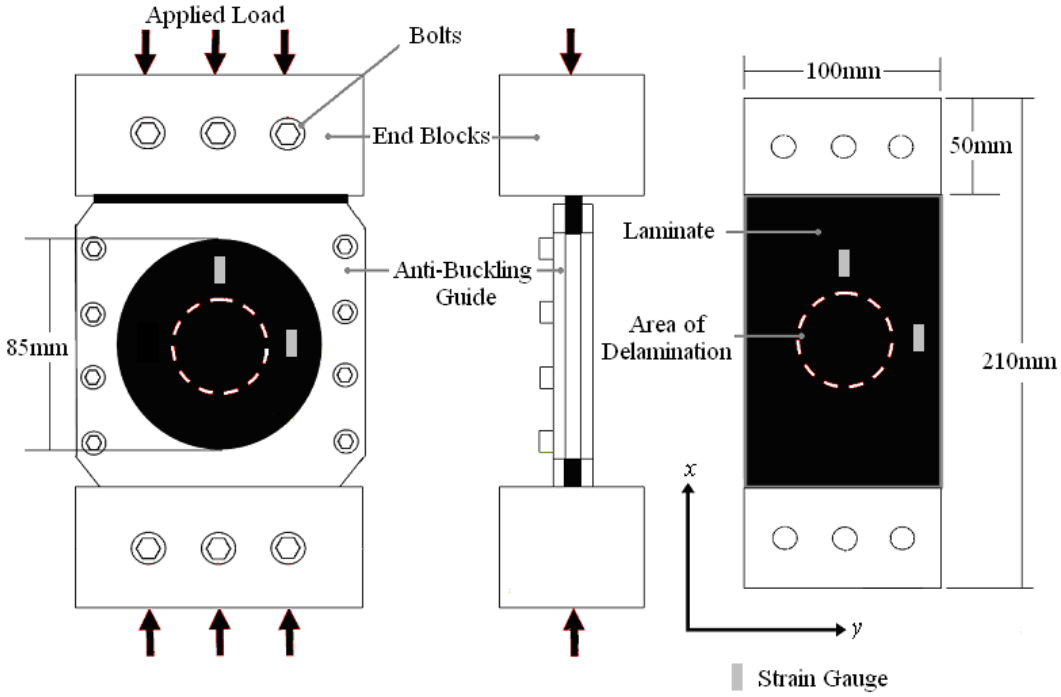

Figure 4-12: Test setup and coupon details for CAI experiment.

of both initial buckling of sublaminates, and the final propagation of the damage.

4.6.1 Results

Figures 4-13 to 4-17 show load-strain plots from the CAI experiments. For the DTO_1 sample a single strain gauge was added transverse to the applied load to aid in confirming the Poisson's ratio of the laminate. The variation of Poisson's ratio as plotted is due initially to the sample settling under load, with slight errors in zero values causing the change in Poisson's ratio. Once global buckling occurs the Poisson's ratio changes again, as the calculation performed is no longer valid for the buckled laminate. Plotting of strain gauge readings is terminated at the point each gauge fails. To allow better understanding of the failure, DIC images of selected laminates are also included. Figure 4-18 shows the out-of-plane displacement of the samples prior to propagation. Table 4.5 summarises the experimental results for each of the samples tested. Note that propagation was observed as a discontinuity in strain readings for the DTO_1. Strain discontinuity in DTO_3 was due to an end tab failure during the test; it was found from DIC data that this did not affect the global buckling mode of this sample compared to the other two DTO samples. Average strain is plotted as a dashed line in Fig. 4-15 to confirm the sample experienced no change in stiffness as a result of this end tab failure.

The strain results for the QI laminate show a change in stiffness at around 89 kN (210 MPa), indicated by the vertical arrow in Fig. 4-13. This is somewhat above the local buckling prediction according to the CAI model (166 MPa); however this prediction was made assuming a constant through-thickness damage diameter; a reduction in diameter of less than 10% at the critical interface would be sufficient to bring the buckling prediction in line with the experiment. The QI laminate shows no signs of propagation before final failure at 108.7 kN (256 MPa).

Both the DTO_1 and DTO_2 laminates show bending early on in the test; DTO_1 from around 42 kN, DTO_2 from 12 kN. This bending leads to contact with the anti-buckling guide, restraining further deflection until the onset of global buckling. DTO_1 shows a propagation event before global buckling occurs, whereas DTO_2 and DTO_3 buckle in an overall mode before propagation (see Fig. 4-21 (b)). Propagation of DTO_1 is indicated by vertical arrows in Fig. 4-15.

4.7 Discussion

The results of the CAI experiments presented here will now be discussed.

Sublaminate Buckling

Figure 4-8 shows that, with the exception of the outermost 60° layer, the DTO laminate is predicted to have very high values of sublaminate buckling strain. This is due to the high Poisson's ratio of this laminate in comparison to the Poisson's ratio of its outer plies, caused by the use of 15° and 30° plies in the core, which exhibit a high Poisson's ratio, as shown in Fig. 4-19. Hence, when uniaxial compression is applied (allowing free strain transverse to this load), a transverse tension is induced in the outer plies of the laminate. Figure 4-20 shows the theoretical in-plane loads for sublaminates in the QI and DTO design, assuming uniaxial load applied to the full laminate with no out-of-plane deformation.

As would be expected, the QI laminate (Fig. 4-20 (a)) shows very little transverse or shear loading, due to the repeating pattern of its layup. This contrasts greatly with the DTO laminate (Fig. 4-20 (b)), which shows high tensile transverse loading. Further, the axial loading in the first four sublaminates is much lower than for the QI layup. For this reason only the first ply is able to buckle, and only then due to its shear loading. Fig. 4-21 shows the buckling modes of sublaminates from the QI and DTO

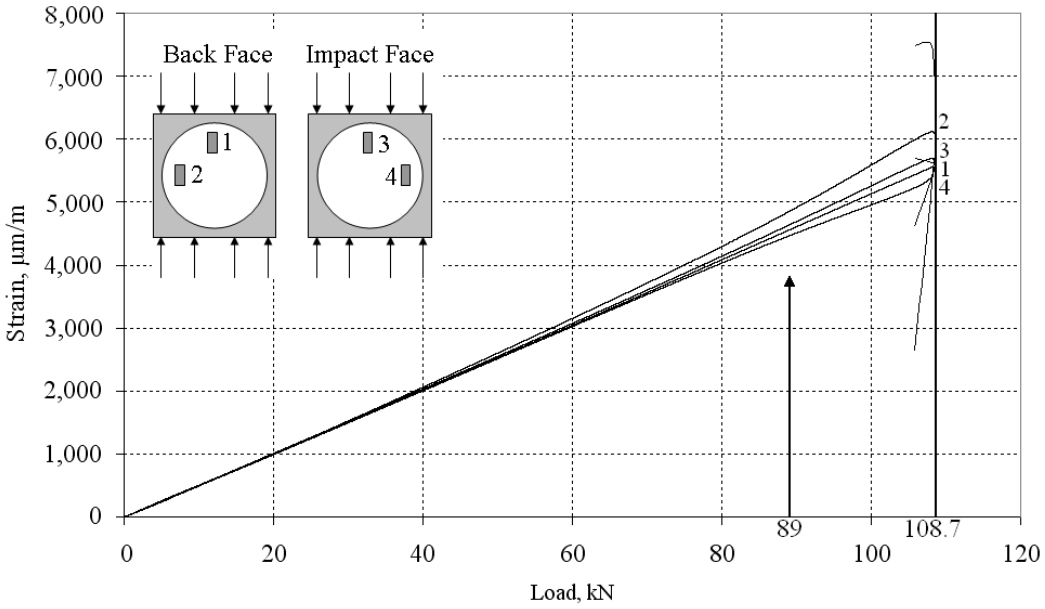

Figure 4-13: Load-strain results for QI_1. Vertical arrow indicates onset of sublaminate buckling. Inset shows positioning of strain gauges.

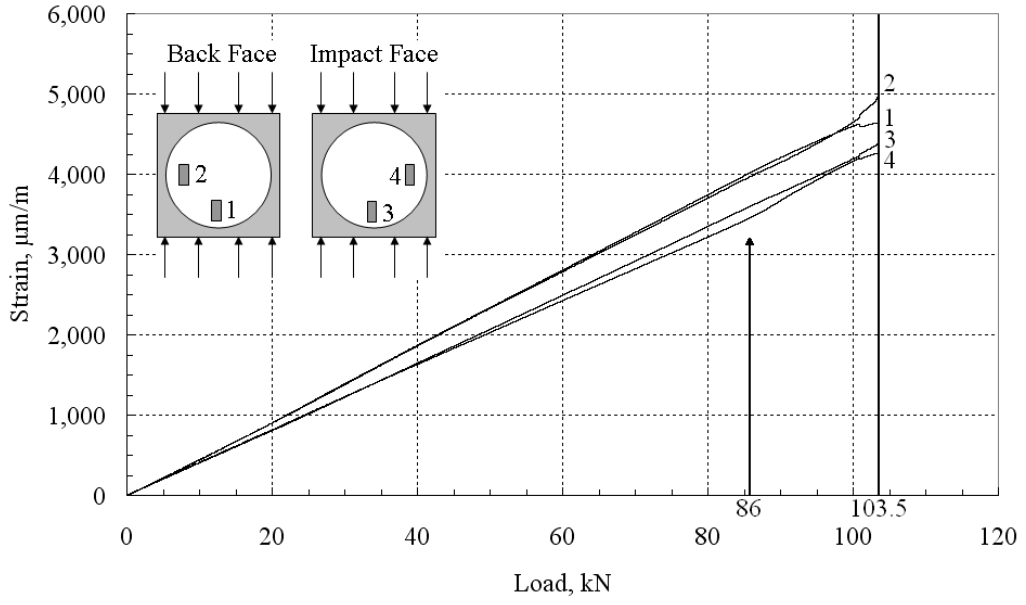

Figure 4-14: Load-strain results for QI_2. Vertical arrow indicates onset of sublaminate buckling. Inset shows positioning of strain gauges.

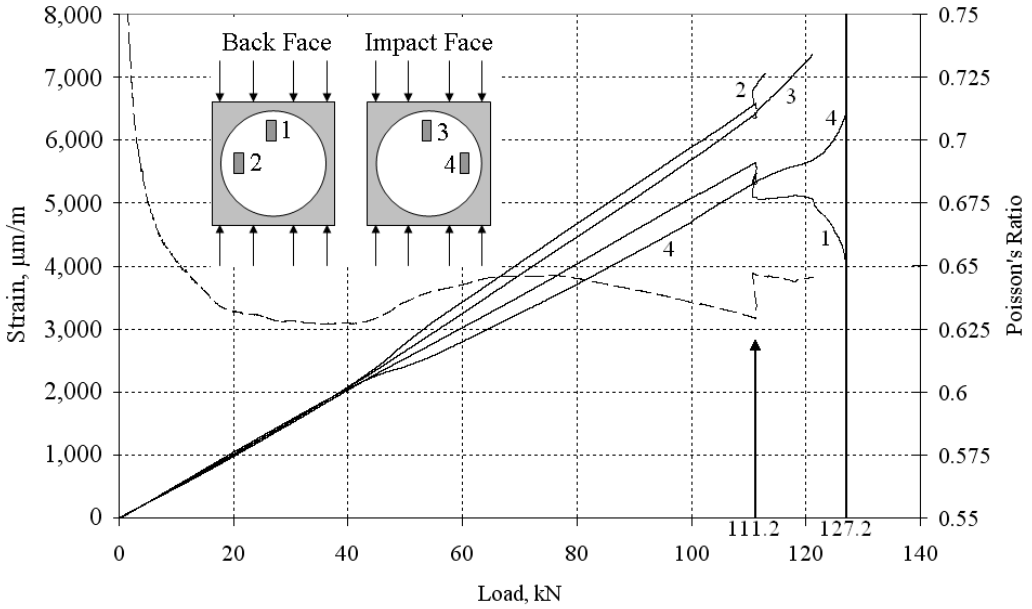

Figure 4-15: Load-strain results for DTO_1. Vertical arrow indicates initial propagation. Inset shows positioning of strain gauges. Dashed line indicates measure surface Poisson's ratio.

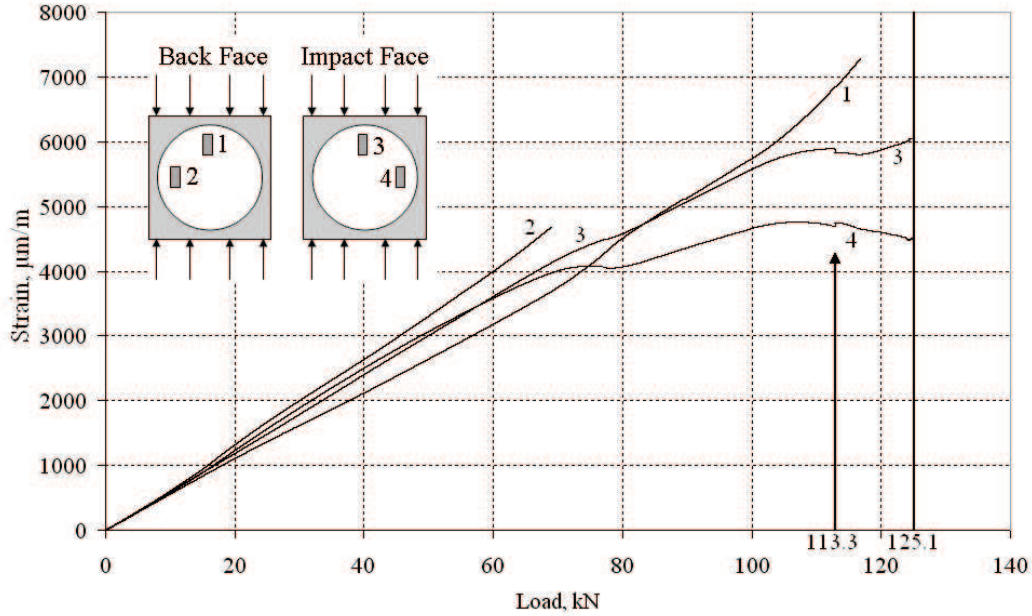

Figure 4-16: Load-strain results for DTO_2. Vertical arrow indicates initial propagation. Inset shows positioning of strain gauges.

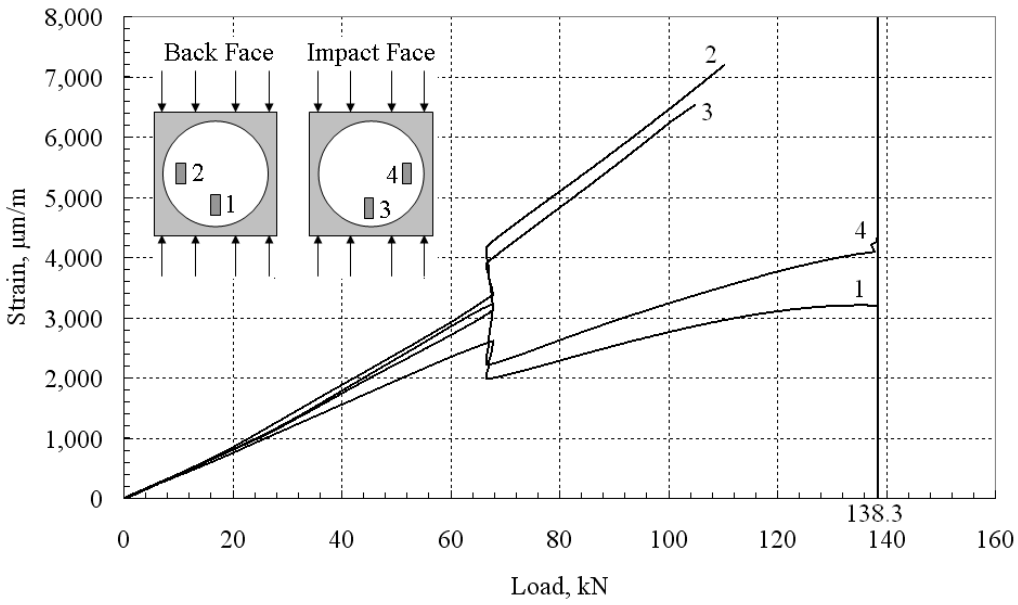

Figure 4-17: Load-strain results for DTO_3. Inset shows positioning of strain gauges.

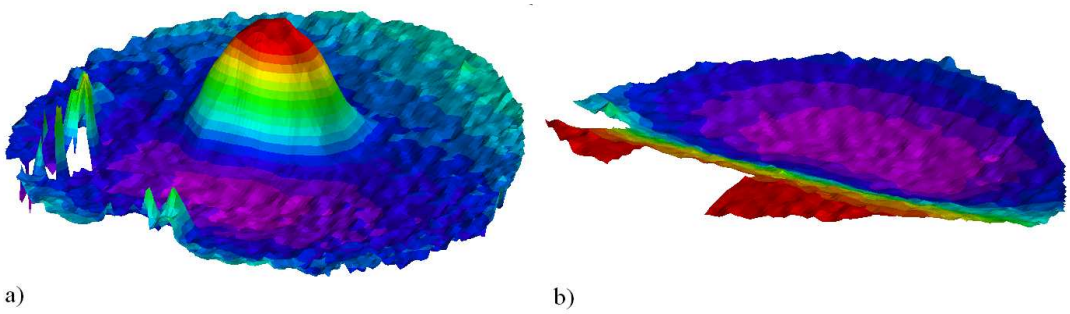

Figure 4-18: Displacement of back face of samples from unloaded shape. a) QI_2 at 100kN, b) DTO_3 at 130kN. Missing data is due to strain gauge positioning on the samples. Red is deformation towards the camera, blue away. Colour map is rescaled for each image.

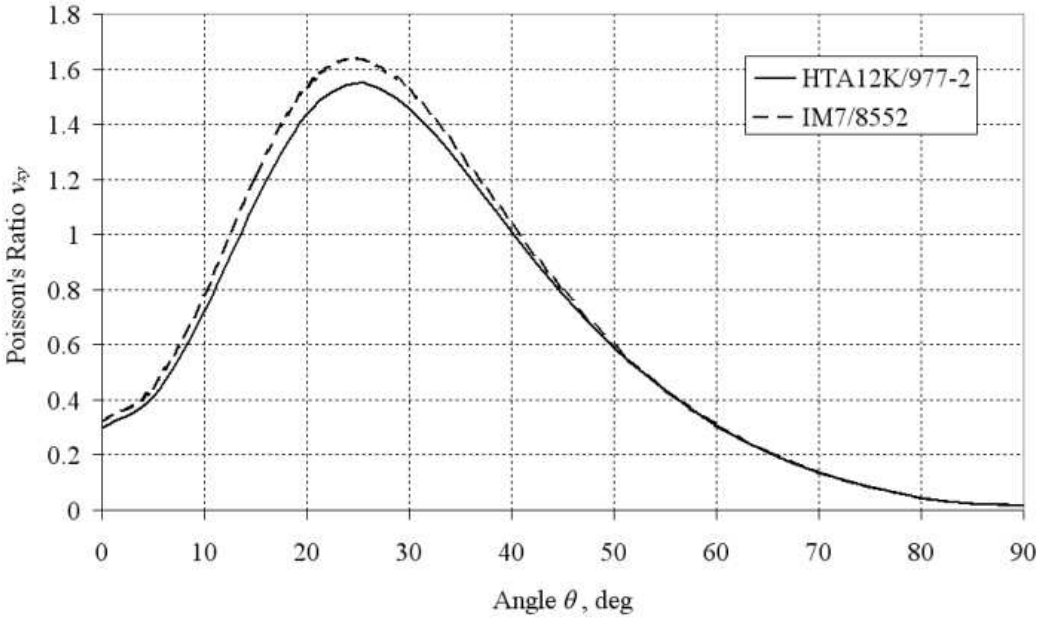

Figure 4-19: Theoretical Poisson's ratio of $(\pm\theta)_n$ laminates, based on classical laminated plate theory.

laminates, taken from VICONOPT analysis. It should be noted that this analysis does not account for contact between the sublaminate and base substrate.

Although the first ply of the DTO design is able to buckle, its lack of stiffness means that it cannot build up enough energy to initiate propagation. All other sublaminates are unable to buckle, so cannot fail by delamination opening. Figure 4-8 shows the results of the model for the DTO laminate. The delay of local buckling means that the laminate no longer fails by delamination opening. The high Poisson's ratio of DTO_1 was confirmed by transverse strain readings taken during the CAI test, and plotted as a dashed line in Fig. 4-15.

Laminates that have previously shown good damage tolerance [57] derive their CAI strength from maximising threshold strain for each interface in the material, and by confining most delamination damage to benign depths within the laminates. For example, a laminate of configuration $[\pm 45_4/(90/0)_4]_S$ was found to have largest delamination damage at the interface between -45° and 90° plies. This delamination was deep enough to delay buckling and improve damage tolerance. The DTO laminates impacted in this work displayed dispersed delamination damage starting near surface, and although

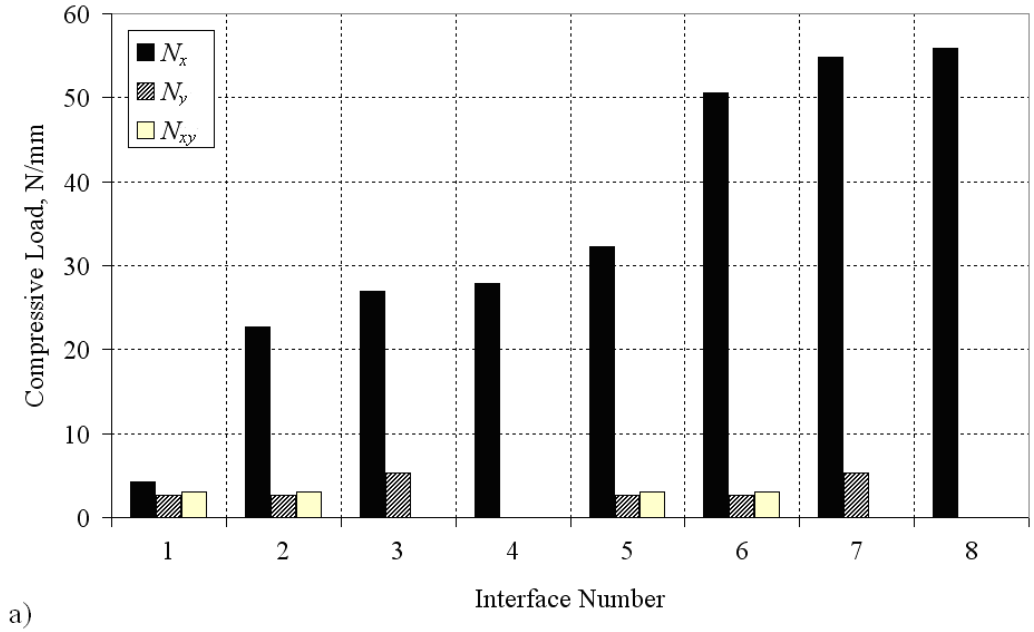

a)

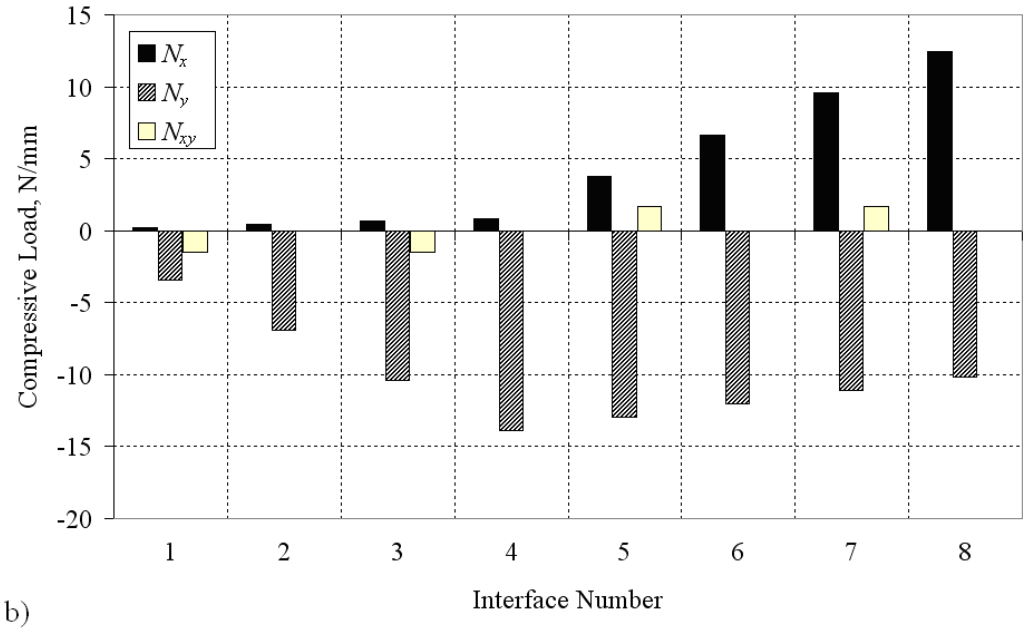

b)

Figure 4-20: Applied loads for sublaminates in a) QI_1 and b) DTO_1 and DTO_2 laminates, given an applied end shortening strain ε_x of 0.001 mm/mm and free strain transverse to this.

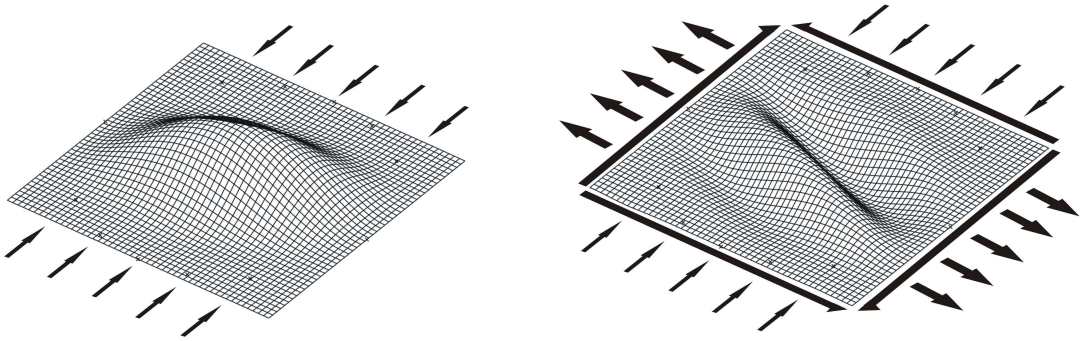

Figure 4-21: Buckling modes of a) 4th interface sublaminate of QI laminate, and b) 1st interface sublaminate of DTO laminate, showing direction of induced sublaminate loads.

this did not cause local buckling before initial propagation it may reduce the overall through-thickness shear stiffness of the laminate within that region. This reduction in shear stiffness could in turn reduce the overall buckling capacity of the damaged plate, and may lead to stress concentrations at which in-plane propagation may occur when the plate deforms out-of-plane.

It is interesting to note that each of the best designs produced by the GA based optimisation exhibited Poisson's ratios well below that of the QI sample. The designs GA_1-GA_3 (see Table 4.3) instead derived their CAI strength from the low axial stiffness of their outer plies allied with a high overall effective modulus. It should be noted that these were not subjected to any laminate design rules, such as those outlined by Niu [52], which has led to undesirable blocking of 0° and 90° plies. However it is possible that a laminate with similar characteristics could be produced without blocking of these angles.

Comparison of CAI Model with Experiments

The experimental results collected for the QI_1 sample show good agreement with the CAI model prediction. Propagation stress is overpredicted by 3%, with strain underpredicted by 11.5%. The deviation between stress and strain is caused by the low experimental value of effective elastic modulus E_{xx} in comparison with that given by classical laminated plate theory. This low effective modulus was evident in all samples manufactured using the HTA12K/977-2 material, indicating that the low stiffness is a material-specific issue. This may be due to inaccuracies in the material properties used, or due to deficiencies in the manufacturing process. If the CAI model is applied

with E_{11}, E_{22} and G_{12} scaled by 0.825 to match the experimental E_{xx}, and with t equal to 1/32 of the experimental laminate thickness, the strain prediction is 7.5% below experimental, with stress 11% below. The discrepancy between experimental and theoretical values is likely to be attributable to the difference between the predicted and actual sublaminate buckling strains. In this work the predicted strains are based on a constant delamination diameter at each interface in the material; in reality this damage was somewhat smaller (see Fig. 4-11 (a)). The increased buckling strain due to this would reduce the difference between experimental and theoretical propagation strains. Propagation in the QI_1 experiment was unstable, as the load-strain plot shows no sign of propagation prior to final failure. This matches the prediction of the CAI model, based upon stability at propagation [55]. The second control sample, QI_2, displayed similar behaviour to that of QI_1, with local sublaminate buckling evident at 80-85% failure load, and laminate failure occurring soon after initial propagation.

The DTO laminate produced here has been shown experimentally to have increased CAI strength in comparison to the QI control laminate. The two DTO laminates manufactured using HTA12K/977-2 (DTO_1 and DTO_2) exhibited 13% and 19% improvements in failure stress and 22% and 33% improvement in failure strain respectively, whilst the DTO_3 sample displayed a 33% improvement in failure stress, albeit with a reduced impact energy. These results do however fall far short of the improvements predicted by the analytical model used in the optimisation process. The mechanism of failure accounted for during optimisation is local delamination propagation, driven by local thin film buckling of delaminated plies at a critical depth. DIC results from the laminates (e.g. see Fig. 4-18 (b)) indicate that local buckling did not occur before propagation for these laminates, precluding this from driving failure of these samples. Comparing these DIC results to those of the QI laminate, for which the model produced a good prediction of failure stress, clear local out-of-plane displacement can be seen, leading to failure triggered by delamination opening for the QI laminate. Hence the DIC results for the DTO laminate show that failure has, most likely, been dominated by in-plane effects.

Damage Resistance

Although not considered in the optimisation process, damage resistance is another consideration in the performance of composites regarding impact. Data from the impact tests indicated that the DTO laminate has a lower damage resistance than the QI laminate; delamination damage initiated in the DTO laminates around 2 J earlier than in the QI. This means that the DTO design is prone to delamination damage from lower

energy impacts, and a larger overall delamination area for the same impact energy. Surface dents were comparable for the two designs, so the reduced damage resistance of the DTO design did not translate into improved visual detectability when compared to the QI layup. Future development of an efficient impact modeling technique could allow damage resistance to be combined with damage tolerance in a laminate with high impact survivability.

Globally Induced Failure of DTO Samples

There are a number of mechanisms by which the DTO laminates may have failed in the absence of local sublaminate buckling. First ply failure analysis using Tsai-Wu predicts failure of the $\pm 15^\circ$ plies at 0.0084 mm/mm, in comparison to the prediction for the QI of 0.0093 mm/mm. Experimental failure strains were within 20% of Tsai-Wu failure for the DTO laminates. Also, the DTO laminate may exhibit a vulnerability to inter-ply cracking from a free edge due to in-plane stresses, as modelled by Fenske and Vizzini [25]. This work indicated that when dealing with laminates of the type $\pm[(\theta)_n]_S$, certain values of θ lead to susceptibility to inter-ply cracking at free edges. Although this is not directly comparable to the DTO design discussed here it does point to free edge inter-ply cracking as a potential failure mode for the DTO laminate. Both of these types of failure are critical for plies of angles around 15°, indicating that the benefits these plies offer in terms of preventing localised buckling may not outweigh their disadvantages regarding in-plane failure.

4.8 Conclusion

An analytical strip model was used as the objective in an optimisation routine to produce a damage tolerance optimised (DTO) composite laminate. Analysis of the CAI experiments performed on the DTO laminate indicated that the optimisation process was successful in eliminating buckling-induced localised delamination propagation, their failure being driven instead by in-plane effects. The layup presented here is an extreme case, with maximum propagation stress as the optimisation objective. It is quite conceivable that the same effect of delaying buckling of locally debonded sublaminates could be achieved in laminates with a more typical layup, although such laminates would still likely require the use of ply angles at more intervals than the standard $0/90/\pm 45^\circ$, to produce the required Poisson's ratio effects.

With the limitations encountered with respect to convergence of the GA on local non-optimum solutions, the next chapter will focus on methods of reducing the compu-

tational analysis of an exhaustive-based method, allowing large numbers of layups to be analysed for little computational effort, and opening the way for possible exhaustive analysis.

Chapter 5

Analysis Techniques Aiding Exhaustive Search for Damage Tolerant Laminates

5.1 Introduction

The previous chapter showed the potential of optimisation of a composite layup for damage tolerance, but also exposed one of the key problems that often occurs in optimisation, especially of discontinuous multimodal design spaces such as this. Much work is done in the tuning and extension of mathematical optimisation methods, especially metaheuristics, to improve convergence and solution quality in such scenarios but this often requires a level of knowledge of the methods applied above that of the user applying them. An alternative to this is presented in this chapter.

For continuous design spaces optimisation or search algorithms are often the only realistic way to obtain optimum solutions. A vast array of methods are available, and for many applications gradient-based methods such as the simplex algorithm [50] are fast and effective in finding optimal designs. In such design spaces there are an infinite number of possible solutions as a result of continuous design variables, but this not the case for discrete design problems.

Due to the finite nature of discrete problems it is possible to solve every known design within a finite design space, given enough computational effort. This is where exhaustive search generally falls down; although an optimum solution is guaranteed, the computational cost is often prohibitive. In some cases however, knowledge of the

design space being analysed can be used to reduce the size of the problem whilst still performing an effective exhaustive search. Reduce the computational effort sufficiently, and exhaustive search becomes a sensible option for finding the optimum solution to a problem.

The features of the compression after impact (CAI) model presented in Chapter 3 facilitate two main methods of reducing the computational effort of an exhaustive design space search. Firstly, the model only analyses thin film buckling and propagation behaviour, so the number of analyses that need to be performed is based on the number of possible thin film sublaminates that may be produced, not the overall number of possible designs within the specified design space. Secondly, the buckling analysis performed using VICONOPT can be replaced with a surrogate alternative, requiring a minimal number of VICONOPT analyses to characterise each sublaminate that may arise. A further method to reduce the computational effort required is to pre-select designs to analyse based on another design criterion, so that only those designs that are fully compliant to all design constraints are examined. The application of these techniques will now be discussed in turn.

The work detailed in this chapter is in part based on that published in Composites Science and Technology in collaboration with Dr R. Butler and Dr C.B. York [6].

5.2 Surrogate Modelling

A surrogate model is a method of describing a relationship between parameters in a wider model in such a way that it is more computationally efficient than solving the relationship through analytical or numerical means. At its simplest, a surrogate model may be a response curve, a set of experimental or analytical data points for a relationship between which interpolation is performed to gain solutions for points at which real data is not available. This can be expanded to further dimensions, with multiple inputs and multiple variables. At its most complete, surrogate modelling incorporates methods of analysing the quality of the model produced, and using this information to choose areas to perform further experiments or analysis to best improve the model.

5.3 Surrogate Buckling Model

Attempting to apply the CAI model exhaustively to a design space is computationally expensive. As an example, to perform full CAI analysis of every fully uncoupled laminate up to 21 plies would require over 680,000 sublaminate buckling calculations, totalling approximately 2 days VICONOPT run time on a desktop quad-core PC (specification shown in Appendix C) [6]. Attempting to analyse design spaces any larger would result in prohibitively long run times, and hence a simple surrogate model has been developed as a replacement for buckling analysis in the search. As the CAI model presented in Chapter 3 predicts propagation of damage under uniaxial loading, there are only three inputs to the VICONOPT analysis for a single delamination; the layup of the sublaminate being analysed, the diameter of the delamination and the Poisson's ratio of the full laminate. Sublaminate loads are calculated as shown in Eq. 5.1.

$$\begin{Bmatrix} N_x \\ N_y \\ N_{xy} \end{Bmatrix} = \begin{bmatrix} A_{11} & A_{12} & A_{16} \\ A_{12} & A_{22} & A_{26} \\ A_{16} & A_{26} & A_{66} \end{bmatrix} \begin{Bmatrix} \varepsilon_x \\ -\varepsilon_x \nu_{xy} \\ 0 \end{Bmatrix} \tag{5.1}$$

where ε_x is the reference applied end shortening, and ν_{xy} is the full laminate Poisson's ratio. For a known sublaminate layup of known material, the loads within the sublaminate when the reference strain ε_x is applied are dependent only on the Poisson's ratio of the full laminate. Hence, a simple relationship can be obtained between full laminate Poisson's ratio and buckling strain for each individual sublaminate. In the case of laminates up to 21 plies thick all sublaminate layups up to 5 plies thick need to be characterised, of which there are 1,364 [6]. Sublaminate buckling analysis within VICONOPT does not account for contact with the base substrate, so further reductions in computational requirements are made by not duplicating analysis of mirrored sublaminate layups, i.e. a [45/0] sublaminate is equivalent to a [0/45] sublaminate. Similarly, anti-symmetric equivalents will also result in the same buckling strain, so for example a [45/0] sublaminate will buckle at the same full laminate end shortening as a [-45/0] sublaminate.

As can be seen in Fig. 5-1, the relationship between sublaminate buckling strain and full laminate Poisson's ratio is monotonic, with sublaminate buckling strain increasing with full laminate Poisson's ratio. For each sublaminate, 12 VICONOPT analyses were performed at evenly spaced values of full laminate Poisson's ratio. The number of analyses was chosen as a result of using a quad-core processor, making computation in sets of four most efficient. This buckling data was stored in a database, within

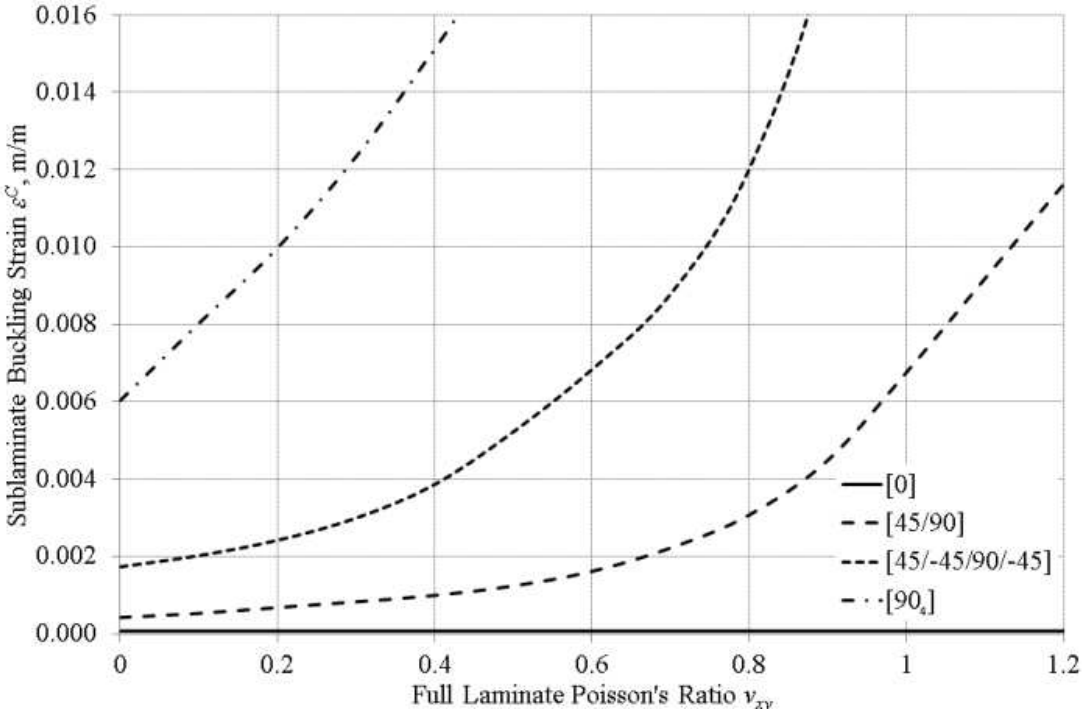

Figure 5-1: Relationship between full laminate Poissons ratio and sublaminate buckling strain for selected sublaminates.

which interpolation could be performed to ascertain the buckling strain of any given sublaminate for any given full laminate Poisson's ratio. Due to the nature of the CAI model (see Eq. 3.10), threshold strain is reasonably insensitive to errors in buckling strain predictions, so the fitting technique is not required to give excessively accurate estimations of buckling strain. Figure 5-2 shows the relationship between buckling strain and threshold strain for selected sublaminates in the 19 ply laminate detailed in Table 6.4. The quadratic relationship means that when buckling strains occur near the minimum threshold strain the model is very insensitive to errors in buckling strain, as for example in the 30 mm diameter [45/-45/45] sublaminate in Fig. 5-2. However, if the buckling strain lies away from the turning point errors translated from buckling strain to threshold strain become nearer 1:1. For the purposes of this work, correlation of the relationship between sublaminate buckling strain and full laminate Poisson's ratio is performed using linear interpolation between the 12 analysis points described above. Although a simple method, the results gained will give a lower bound on computation time for the method, and an initial indication of errors using such a method.

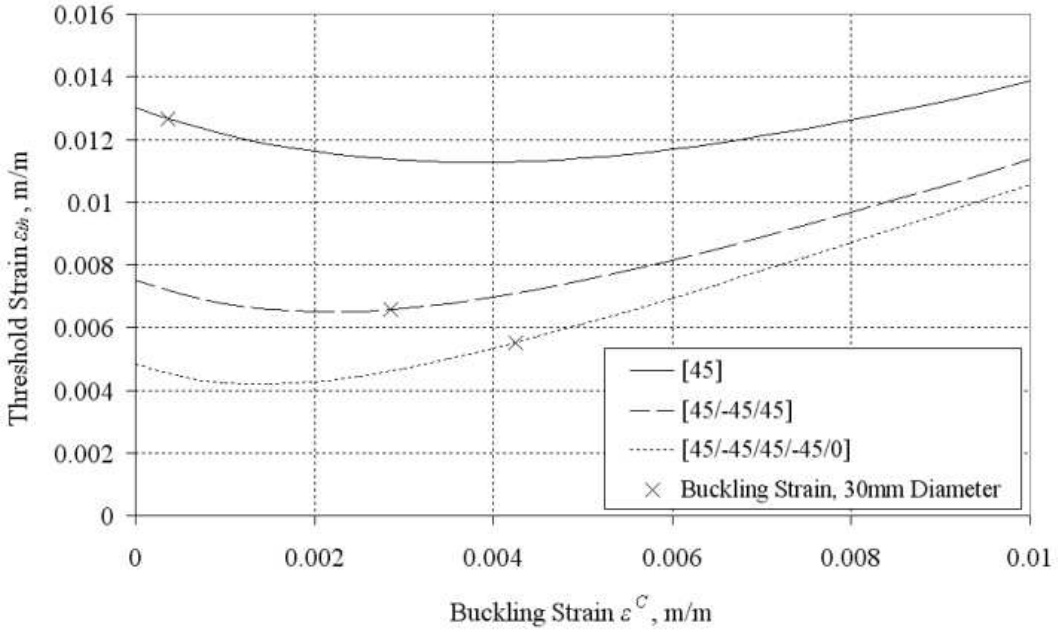

Figure 5-2: Relationship between buckling strain and threshold strain for selected sublaminates in the 19 ply solution shown in Table 6.4.

5.4 Reduction of Number of Buckling Analyses

Taking a 32 ply design space in which each ply can be any one of four different angles as an example, there are a total of 4^{32} possible layups, approximately 18.4×10^{18} designs. Given that to analyse each design using the CAI model will take approximately 0.5 seconds, the total time to analyse every laminate will be around 292 billion years on a standard desktop PC. As the CAI model analyses sublaminate buckling and propagation behaviour, the total number of possible stacking sequences is not the governing factor; rather it is the total number of possible sublaminates that dictates the number of computations required. If the buckling behaviour of each of these sublaminates can be characterised with respect to general characteristics of the full laminate in which it exists, then the number of sublaminates that need to be described can be further reduced.

The total number of possible sublaminates within a design space of laminates made up of plies which can take one of four possible angles can be calculated using Eq. 5.2.

$$N_s = \sum_{i=1}^{n} 4^i \tag{5.2}$$

in which n denotes the maximum depth of plies to be analysed in sublaminate analysis. This is limited by the limit of thin film behaviour, and is generally set at around 25% of the total number of plies in the laminate.

Not every one of these sublaminates need be analysed however, as assumptions made in the VICONOPT modelling of the sublaminates means that certain pairs of sublaminates exhibit identical behaviour. For example, as VICONOPT analyses the sublaminate in isolation from the base laminate; contact has no influence on the VICONOPT buckling result. Also, thin film behaviour is assumed, so there is no out-of-plane displacement at the sublaminate boundary. As a result of this, inverted sublaminate pairs produce equivalent solutions. As an example of this, the buckling strain of a [0/45] sublaminate will be identical to that of a [45/0]. Removing these duplicates from the design space reduces the total number of sublaminates calculated in Eq. 5.2 by 37.5% as n tends to infinity. (see Appendix B for an explanation of this)

5.5 Preselection of Candidate Designs

In a full design space search of laminates with multiple design constraints it will be possible to downsize the space as each constraint is applied. The total number of laminates possible in a design space is given by Eq. 5.3.

$$N_l = \sum_{i=1}^{n} m^i \tag{5.3}$$

where n is the maximum number of plies in the laminate, and m is the number of angles each ply may take. Laminates used in industrial applications my run up to and beyond 100 plies thick, and just limiting the design to standard $[0/90/\pm 45]$ plies still gives 2×10^{60} potential layups. Even smaller design spaces may be vast, for example there are over 18×10^{18} 32 ply laminates in this space. This design space is reduced by stipulations on the design, such as those presented by Niu [52] and discussed in Section 2.3. Applying these along with rules to remove coupling, such as forcing symmetry in the laminate, the design space may be reduced to the point where an exhaustive search for damage tolerance may be performed. Chapter 6 will apply the surrogate sublaminate buckling model to a preselected design space to explore the effectiveness of the surrogate technique both in terms of solution accuracy and computational efficiency.

5.6 Conclusion

Chapter 6 will examine the results provided by the surrogate model through its application to an exhaustive search of a preselected design space of fully uncoupled symmetric and non-symmetric laminates. This study will allow conclusions to be drawn about the accuracy and efficiency of the surrogate sublaminate buckling model presented in this chapter.

Chapter 6

Damage Tolerance of Non-Symmetric Laminates

6.1 Introduction

The previous chapter described a surrogate modelling method for analysing the damage tolerance of a large collection of composite layups using little computational effort. In this chapter this surrogate modelling technique will be applied to a group of non-symmetric laminates that have been selected to have no coupling response to loading. The relaxation of the stipulation of symmetry may allow an increase of the damage tolerance of a composite material, and this idea will be explored. The search will also serve as a basis on which to quantify the effectiveness of the surrogate modelling technique, both in terms of computational efficiency and quality of solution.

6.2 Background

The possibility of coupling is an inherent characteristic of layered orthotropic materials. By tailoring the layup of plies it is possible to produce coupling between any two load and deformation terms in the plate constitutive equations (Eq. 6.1) by ensuring the relevant terms in the **A**, **B**, and **D** matrices are non-zero.

Composite laminate design rules very often call for the use of symmetric layups as a method of suppressing the potential coupling behaviours that can arise in such laminated anisotropic materials. These laminates may however still exhibit bend-twist coupling (indicated by non-zero values for D_{16} and D_{26} in the bending stiffness matrix). Symmetry is in fact sufficient, but not necessary, for a laminate to be uncoupled.

Asymmetric, uncoupled laminates have been explored in the work of York [83], in which it was shown that the design space for asymmetric uncoupled laminates is in fact much greater than for their symmetric counterparts for laminates of thickness greater than 12 plies.

Whilst allowing for an increased layup design space, asymmetric laminate design offers the potential for even greater benefits when combined with an asymmetric design driver. Impact damage is a prime example of this, as impact severities for the two faces of a typical composite laminate in an aerospace application will rarely be equal. This is evident for a wing skin, where, after manufacture, the wing thickness limits the height from which a drop impact can occur on the inner surface, but the outer surface may be exposed to much higher energy impacts, such as bird strike. A further example is that of a composite sandwich panel, in which the composite skins can only be impacted on their outer face. Accounting for this asymmetry in impact threat by using an asymmetric layup may lead to improved CAI performance when compared to a symmetric laminate under the same design constraints.

In this chapter the damage tolerance of symmetric and non-symmetric fully uncoupled laminates up to 21 plies thickness will be analysed both using the standard CAI model described in Chapter 3 and using the surrogate technique presented in Chapter 5. The work detailed in this chapter is in part based on that published in Composites Science and Technology in collaboration with Dr R. Butler and Dr C.B. York [6].

6.3 Coupling in Orthotropic Laminates

In classical laminated plate theory, stiffnesses of a laminated orthotropic material are described by three matrices which describe axial stiffness (**A**), flexural stiffness (**D**), and coupling stiffness (**B**). The derivation of these matrices is fully described elsewhere [47], but shall be used here in brief to describe the coupling effects possible in such laminates.

The plate constitutive equations are fully described (for thin plates) as

$$\begin{Bmatrix} N_x \\ N_y \\ N_{xy} \\ M_x \\ M_y \\ M_{xy} \end{Bmatrix} = \begin{bmatrix} A_{11} & A_{12} & A_{16} & B_{11} & B_{12} & B_{16} \\ A_{12} & A_{22} & A_{26} & B_{12} & B_{22} & B_{26} \\ A_{16} & A_{26} & A_{66} & B_{16} & B_{26} & B_{66} \\ B_{11} & B_{12} & B_{16} & D_{11} & D_{12} & D_{16} \\ B_{12} & B_{22} & B_{26} & D_{12} & D_{22} & D_{26} \\ B_{16} & B_{26} & B_{66} & D_{16} & D_{26} & D_{66} \end{bmatrix} \begin{Bmatrix} \varepsilon_x \\ \varepsilon_y \\ \gamma_{xy} \\ \kappa_x \\ \kappa_y \\ \kappa_{xy} \end{Bmatrix} \tag{6.1}$$

Equation 6.1 shows the coupling terms possible in an orthotropic laminated material. Table 6.1 details each coupling effect, and the terms in the plate constitutive equations that determine that coupling.

Coupling Effect	**A**, **B**, and **D** Matrix Terms
Extension-Shear	A_{16}, A_{26}
Extension-Bending	B_{11}, B_{22}
Extension-Transverse Bending	B_{12}
Extension-Twist	B_{16}, B_{26}
Bend-Shear	B_{16}, B_{26}
Twist-Shear	B_{66}
Bend-Twist	D_{16}, D_{26}

Table 6.1: Coupling terms in the plate constitutive equations.

If any of these terms are non-zero, then the associated coupling will be present in the laminate, with the magnitude of the coupling given by the magnitude of the term. These coupling terms can also lead to changes in effective stiffness of a laminate under certain conditions. For example, if an extension-bending coupled laminate is subjected to uniaxial compression through end shortening and bending of the laminate is restrained, the interaction of extension and bending will produce a different effective stiffness to that if curvature was unconstrained.

6.4 Fully Uncoupled Non-Symmetric Laminates

Fully uncoupled (also known as specially orthotropic) laminates are those that exhibit no coupling responses, other than typical Poisson's ratio effects. Extension-shear terms (Eq. 6.2) and bend-twist terms (Eq. 6.3) in classical lamination theory are zero for these laminates, along with the coupling (**B**) matrix.

$$A_{16} = A_{26} = 0 \tag{6.2}$$

$$D_{16} = D_{26} = 0 \tag{6.3}$$

Fully orthotropic laminates may be desirable when compared to traditional balanced and symmetric layups as a result of possessing no bend-twist coupling (Eq. 6.3), which may have a detrimental effect on the buckling performance of the laminate [84]. Published data [21] contains 75 symmetric sequences, for laminates with up to 21 plies, and 653 anti-symmetric sequences, for laminates with up to 20 plies, together with 49 additional asymmetric sequences, which were derived by combining symmetric and anti-symmetric sequences. The listing reveals that there are no fully uncoupled laminates, containing angle-plies, with fewer than 7 layers; the first fully uncoupled laminate is a single generic 7-ply anti-symmetric stacking sequence. This number increases to 233 generic anti-symmetric sequences with 20 plies. There are no fully uncoupled symmetric stacking sequences with less than 12 plies, and only 25 generic combinations with 20 plies. These twenty-five generic stacking sequences possess balanced and symmetric combinations of angle plies, together with cross plies, which may be 0° and/or 90°, symmetrically disposed about the laminate mid-plane; all possess angle-ply layers on the outer surfaces of the laminate. The derivation [7] adopted in the ESDU data item [21], makes the explicit assumption that cross plies, as well as angle plies, are symmetrically disposed about the laminate mid-plane, i.e. the mixing of 0° and 90° plies is permitted only in one half of the laminate, which is then reflected symmetrically about the laminate mid-plane. This rule applies to both symmetric and anti-symmetric angle-ply stacking sequences.

The relatively small number of fully orthotropic sequences for thin laminates clearly leaves limited scope for composite tailoring and was the key motivation leading to the redevelopment of a definitive list [83] for fully uncoupled laminates with up to 21 plies. In the derivation of this list for (but not restricted to) standard angle-ply configurations, i.e. ±45°, 0° and 90°, the general rule of symmetry is relaxed. Cross plies, as well as angle plies, are therefore no longer constrained to be symmetric about the laminate mid-plane, leading to an increase in the number of possible solutions. To avoid the trivial solution of a stacking sequence with cross plies only, all sequences have an angle-ply on the top outer surface of the laminate, which is in keeping with damage tolerance heuristics. As a result, the bottom outer surface may have an angle-ply of equal or opposite orientation or a cross ply, which may be either 0° or 90°. This relaxation of the rule of symmetry leads to a vastly increased design space; for 16 ply laminates, there are approximately one billion (1×10^9) possible stacking sequence

combinations, of which 360 are fully uncoupled, increasing to approximately one trillion (1×10^{12}) combinations for 21 plies, with a hundred-fold increase in the number of fully uncoupled laminates. The numbers of sequences for each ply number grouping are summarised in Table 6.2, which reveals that symmetric laminates in fact account for a very small percentage of the design space. It should be noted that the stacking sequences derived are fully uncoupled with no bend-twist coupling effects. However, balanced and symmetric configurations continue to be used in studies where the effect of bend-twist coupling is simply ignored[30, 35, 36]. Many other studies of flexural behaviour, e.g., buckling, post-buckling, low velocity impact response, etc., continue to adopt bend-twist coupled laminates as the preferred benchmark configuration, but few consider the effects of the coupling response. For instance, it is now well understood that bend-twist coupling reduces the buckling strength of compression loaded laminated plates, but the magnitude of this strength reduction [84] is often not considered. It is therefore arguably more difficult for the composite laminate designer to apply the lessons learnt in such studies when faced with different laminate designs. Laminates chosen in this study adhere strictly to the definitive listing of fully uncoupled laminates and therefore the conclusions drawn will be independent of the previously un-quantified effect of bend-twist coupling.

Plies	Symmetric	Anti-symmetric	Non-symmetric	Total
7	-	2	-	2
8	-	1	-	1
9	-	6	-	6
10	-	6	-	6
11	-	24	-	24
12	4	21	-	25
13	-	84	-	84
14	12	76	-	88
15	4	288	68	360
16	33	268	59	360
17	50	1002	780	1832
18	110	934	559	1603
19	120	3512	4934	8566
20	352	3290	4284	7926
21	344	12,392	35,521	48,257
Total	1029	21,906	46,205	69,140

Table 6.2: Number of symmetric, anti-symmetric and non-symmetric fully uncoupled laminates with 7 to 21 plies.

6.5 Analysis

The CAI model was applied to every specially orthotropic laminate up to 21 plies thick, as previously characterised by York [83]. Due to the thin film assumption of the model it was applied up to sublaminates 25% thick, on both faces. For this work delamination diameters were fixed at 30 mm for all laminates. Constant delamination diameters were used through-thickness as this gives a worst-case lower bound solution in the absence of a suitable damage modeling method. Any non-symmetric laminates in the design space were analysed for damage tolerance of both faces, with the highest damage tolerance designating the damage tolerance of the laminate. This implies that the laminate would be employed in an environment where impact threats are much larger in magnitude for one face than the other, and that the laminate would be oriented as such. The material used in the analysis is detailed in Table 6.3.

Material	E_{11}, GPa	E_{22}, GPa	G_{12}, GPa	ν_{xy}	t, mm	G_{IC}, J/m^2
HTA12K/977-2 [45]	147	8.5	4.9	0.30	0.125	478

Table 6.3: Material Properties.

As well as forcing special orthotropy in the laminate, manufacturing constraints were also applied, as detailed by Niu [52]. In particular, no more than three layers of the same angle ply were allowed consecutively within the laminate. Niu also recommends a minimum of 10% each of 0°, 90° and ±45° fibres, but this was disregarded as loading is uniaxial in this work. Manufacturing rules pertaining to damage tolerance were also ignored in the presence of the CAI modelling being performed. Results were generated using both VICONOPT sublaminate buckling analysis, and the surrogate sublaminate buckling model described in Chapter 5.

6.6 Results

The CAI model was used to analyse all specially orthotropic laminates up to 21 plies thick. Table 6.4 outlines those laminates with the best damage tolerance for each thickness, and Fig. 6-1 shows the threshold stress of the most damage tolerant laminates by ply percentage breakdown. Figure 6-2 details the best laminates at each ply count, both overall and within the available non-symmetric designs only. The results in these tables and figures have been generated using full VICONOPT analysis throughout so that they may be discussed independently of the surrogate buckling model. All

laminates were also analysed using the surrogate sublaminate buckling model, Fig. 6-3 shows the resulting errors in threshold strain solutions, where both mean and peak error values are given.

Plies	Layup	Threshold Stress σ_{th}, MPa	Running Load, kN/mm	E_{xx}, GPa	ν_{xy}
7	$[45/\text{-}45/\text{-}45/0_{1/2}]_{AS}$	308	0.27	36.3	0.769
8	$[45/\text{-}45/\text{-}45/45]_{AS}$	148	0.15	17.8	0.783
9	$[45/\text{-}45/0/\text{-}45/0_{1/2}]_{AS}$	523	0.59	61.3	0.742
10	$[45/\text{-}45/\text{-}45/45/0]_{AS}$	372	0.47	43.8	0.762
11	$[45/0/\text{-}45/\text{-}45/0/0_{1/2}]_{AS}$	403	0.55	77.1	0.718
12	$[45/\text{-}45/\text{-}45/0/45/0]_{AS}$	398	0.60	61.3	0.741
13	$[45/0/\text{-}45/0/\text{-}45/0/0_{1/2}]_{AS}$	460	0.75	88.1	0.696
14	$[45/\text{-}45/\text{-}45/45/0/90/0]_{AS}$	352	0.62	60.1	0.432
15	$[45/\text{-}45/\text{-}45/45/0_3/90_{1/2}]_{AS}$	447	0.84	73.0	0.538
16	$[45/\text{-}45/\text{-}45/45/0_2/90/0]_{AS}$	415	0.83	71.0	0.429
17	$[45/\text{-}45/45/\text{-}45/0_2/\text{-}45/0_{1.5}]_{AS}$	472	1.00	71.5	0.727
18	$[45/\text{-}45/\text{-}45/45/0_3/90/0]_{AS}$	464	1.04	79.4	0.426
19	$[45/\text{-}45/45/\text{-}45/0_3/\text{-}45/0_{1.5}]_{AS}$	440	0.90	79.4	0.713
20	$[45/\text{-}45/\text{-}45/45/90/0_3/90/0]_{AS}$	423	1.06	74.1	0.308
21	$[45/\text{-}45/45/\text{-}45/90/0_3/\text{-}45/0_{1.5}]_{AS}$	458	1.20	77.2	0.464

Table 6.4: Fully orthotropic laminates up to 21 plies thickness with highest CAI threshold stress, using VICONOPT buckling analysis. The subscript AS denotes that the layup has symmetric crossplies, and anti-symmetric angle plies.

6.7 Discussion

Each of the best designs shown in Table 6.4 exhibits traits highlighted to be beneficial to damage tolerance in previous work [5, 56], namely that the outer layers are softer in the loading direction, with central layers dominated by stiffer plies. This configuration produces higher buckling strains for the thin sublaminates, and also means they accrue strain energy more slowly in the post-buckled regime. Stiffer plies in the core of the laminate increase the effective modulus, raising the threshold stress. As the model incorporates both the axial and transverse stiffnesses of the sublaminates, the best designs are all those whose sublaminates have similar values of A_{11} and A_{22}. If either of these were excessively high, i.e. if the sublaminates had large numbers of 0° or 90° plies, then threshold strain would drop significantly, leading to a non-optimal solution. Figure 6-1 gives an indication of the best ply percentage breakdowns for damage tolerance. It can be seen that the best layups are generally those with over 40% 0° fibres, and 15%

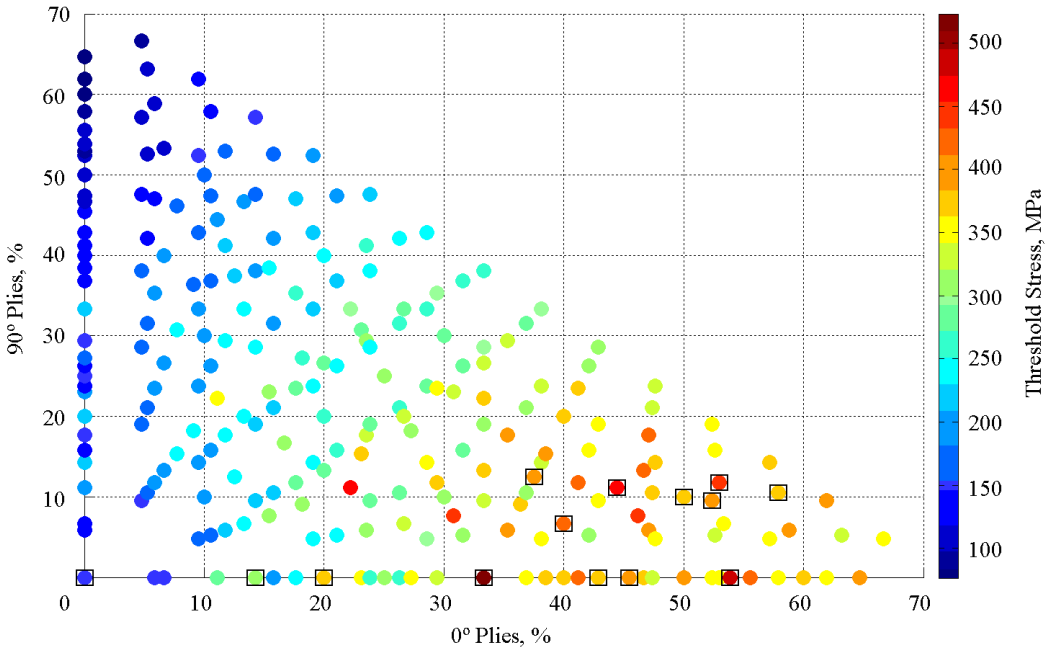

Figure 6-1: Threshold stress of fully orthotropic laminates up to 21 plies thick by ply percentage breakdown. Best designs for each ply count are boxed for clarity.

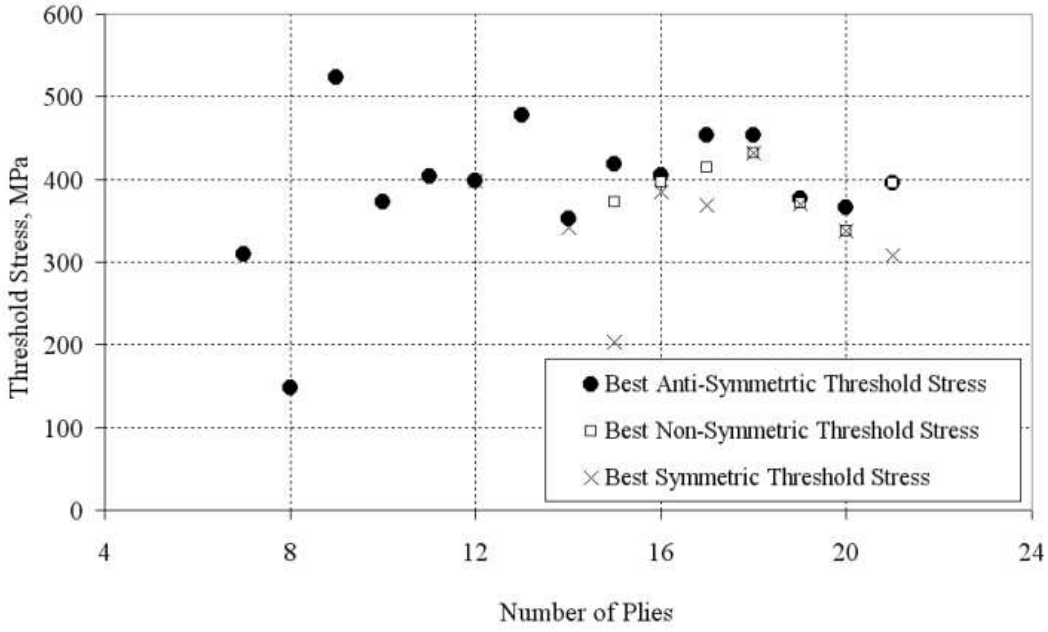

Figure 6-2: Threshold stress of fully orthotropic laminates by ply count.

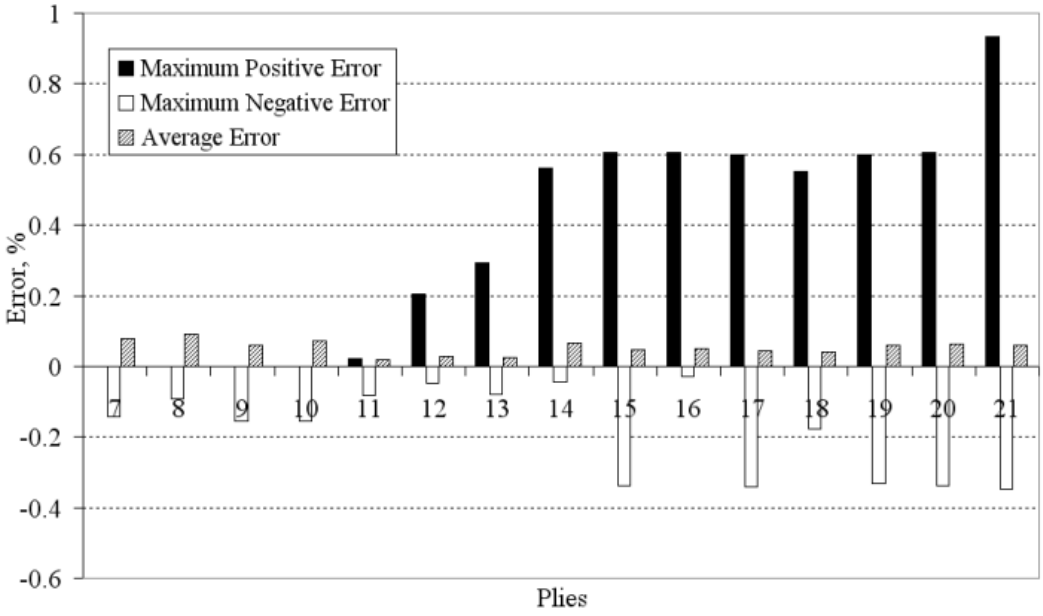

Figure 6-3: Error data for threshold strains calculated using linear interpolation of buckling strain data.

or less 90°. Within this region lie commonly used ply breakdowns in skins (44/44/12) and stiffeners (60/30/10), so these layups are practical for use in aerospace from an in-plane stiffness perspective.

The general trend of peak threshold stress with respect to ply count (Fig. 6-2) is affected by a number of factors. Firstly, the small number of specially orthotropic candidate laminates at lower ply numbers means that no conclusions may be drawn for laminates up to 10 plies thickness. Secondly, a step change in the relationship is seen between 13 and 14 plies, the point at which an extra ply is added to the CAI analysis within the 25% thin film sublaminate. This new sublaminate gives a lower threshold stress and so drops the damage tolerance of the 14 ply laminate. This feature is not seen for the next increase in number of sublaminates between 17 and 18 plies, as the design space is at this point large enough that a good solution may still be found. Finally, when the ply blocking manufacturing constraints becomes an issue at 14 plies, 90° fibres need to be used to unblock the central 0° plies as in many cases the addition of only a pair of ±45° plies would cause bend-twist coupling in the laminate. The effect of this unblocking requirement can be seen in Table 6.4, where increases in the number of plies do not necessarily bring improvements in running load capacity. In the

worst case, the best 19 ply specially orthotropic laminate is outperformed in outright load carrying capacity by the best 17 ply laminate with respect to damage tolerance. Furthermore, the inclusion of progressively more 0° and 90° fibres in the thicker layups acts to reduce the full laminate Poisson's ratio, where a high full laminate Poisson's ratio has been shown to help laminates resist localised delamination buckling (Chapter 4, [5]). Omitting the minimum ply percentage rule from the manufacturing constraints applied to the laminates made these high Poisson's ratios possible, especially in the thinner laminates (7-13 plies thick). These designs did not include 90° fibres, the presence of which would reduce the Poisson's ratio significantly. This means these designs could be less practical in a skin/stiffener configuration, as matching such high Poisson's ratios to other laminates might be troublesome.

For the design space investigated here, it has been shown that the inclusion of non-symmetric, specially uncoupled layups has not been of benefit with regards to damage tolerance. In all instances it is an anti-symmetric design that offers the best damage tolerance, and as such these solutions do not offer differing damage tolerances for each face. The gap between the best anti-symmetric and non-symmetric layup is generally small however, indicating that non-symmetric layups are not a great disadvantage in terms of damage tolerance.

6.7.1 Surrogate Sublaminate Buckling Model

The sensitivity of the best 21 ply laminate to errors in buckling strain prediction was explored by plotting buckling/threshold strain curves for each of the possible sublaminates, Fig. 6-4. For this laminate the critical interface is interface 4. Figure 6-4 shows that the buckling strain for this interface lies near the turning point, and threshold strain is less sensitive to changes in buckling strain than for interfaces 1, 2 and 5. As with the 19 ply results shown in Fig. 5-2, at extremes of buckling strain the error ratio between buckling strain and threshold strain still does not exceed 1. The majority of laminates investigated in this work tend to have their critical interface at the 25% boundary for thin film buckling behavior. This means that those thin laminates tested here will have low values of buckling strain, i.e. sublaminate responses on the left of the 1 and 2 ply curves shown in Fig. 6-4. Thicker laminates will be critical for sublaminates 4 or 5 plies thick, with buckling occurring to the right of the point of minimum threshold strain on these curves. It is in these regions that the error transmitted from buckling strain estimation to threshold strain is largest, and this helps to explain the error data shown in Fig. 6-3.

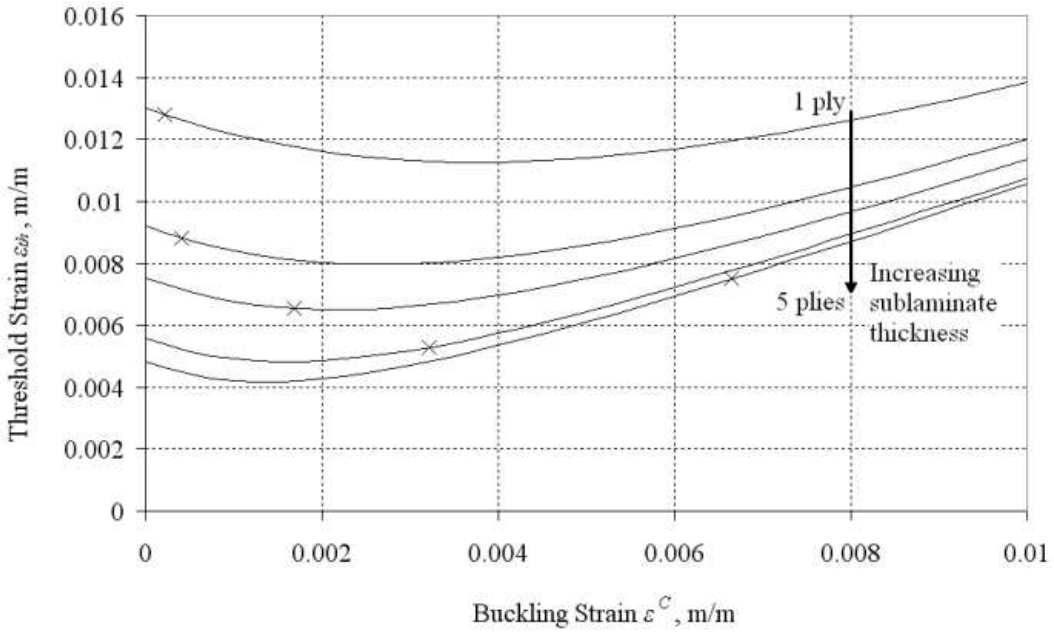

Figure 6-4: Relationship between buckling strain and threshold strain for sublaminates in the 21 ply solution shown in Table 6.4.

As can be seen in Fig. 6-3, non-conservative errors in threshold strain are less than 1% for all layups. Average absolute errors for each ply count are below 0.1%. These results are excellent when one accounts for the reduction in computation time achieved. Exhaustive analysis of all specially orthotropic laminates up to 21 plies thick on a standard desktop PC takes in the order of 2 days to complete, with the implementation of parallel processing on a quad-core CPU. Analysis of the same design space using the surrogate, including all VICONOPT analyses required to build the model, takes approximately 18 minutes, around 0.625% of the full analysis. The surrogate model presented here has practical applications beyond the specially orthotropic case study provided. As a facilitator of an exhaustive search it allows users to find an optimum damage tolerant laminate from within any given design space without uncertainty over whether the solution is a true optimum, so often the case with typical optimisation techniques used in laminate optimisation, such as genetic algorithms. These design spaces may contain many millions of designs, but would still be manageable using the surrogate method.

6.8 Conclusion

CAI analysis of specially orthotropic laminates up to 21 plies thick has shown that the inclusion of non-symmetric laminates in the potential design space does not allow for higher threshold stresses than more traditional symmetric or anti-symmetric layups. However, non-symmetric designs do not show a significant disadvantage from the point of view of damage tolerance, under the assumption that the laminate requires only one damage tolerant face. For some laminate thicknesses it was found that adding plies may actually reduce overall load capacity as a result of ply unblocking and the requirement for special orthotropy. For laminates more than 14 plies thick, the maximum damage tolerant strength achieved was between 400 and 480 MPa. It was found that two types of damage tolerant laminate dominate, one without 90° plies and high Poisson's ratio, the other with one or two 90° plies and lower Poisson's ratio. The use of a simple surrogate sublaminate buckling model reduced computation time by over 99%, the results of which showed average errors less than 0.1%, and maximum non-conservative errors less than 1%.

Chapter 7

Design of Composite Structures Subject to Damage Tolerance and Buckling Stiffness

7.1 Introduction

The development of efficient methods of analysing the damage tolerance of composite laminates presented to this point show the theoretical potential of utilising such methods when designing composite laminates. In reality, damage tolerance will not be the objective in a laminate optimisation routine, but will instead be used as a constraint on the design of a wider composite structure, with the objective being weight, or perhaps cost. In this chapter damage tolerance will be set as a constraint in a panel design scenario. Buckling will also be considered, and the panels will be optimised for minimum weight.

7.2 Optimisation

It is first important to understand the possible methods of optimising such a problem. For larger scale problems, such as the optimisation of a wing cover panel, genetic algorithms become too inefficient to be practical due to the high computational effort required to search such a wide range of solutions. In order to alleviate some of this effort, bi-level optimisation approaches have been developed, looking to combine the efficiency of numerical optimisation techniques with the ability of GAs to search a highly non-linear, discrete design space.

7.2.1 Bi-Level Optimisation

B. Liu et al. [43] performed two-level optimisation of a wing structure using a response surface method. A large number of lower (panel) level optimisations were performed for a range of global (wing) design variables. These results were used to produce a response surface for use at the global optimisation level. This work performs panel optimisation using a GA, with discrete design variables. Here the number of plies in each orientation are pre-specified, and the problem becomes a permutation one. The response surface is used to estimate buckling loads for the panels in the wing level optimisation, given the wing loading and calculated skin thickness. At the wing optimisation level the breakdown of ply angles is continuous, meaning that the solution thicknesses needs to be rounded after being found. These rounded ply thicknesses are then used in the GA to produce the final panel design. Some manual design was applied at this point, as the rounding process could potentially break buckling constraints. It was found that the response surface method was effective in allowing the efficient wing-level optimisation to find an optimum solution. It should be noted that this method still requires some manual design following the rounding procedure, thereby increasing time to solution, and introducing the possibility of a non-optimal solution being produced.

W. Liu et al. [45] performed bi-level optimisation of a number of composite panel designs, and validated the panel modelling technique using experimental results. The bi-level strategy in this work was based on a higher panel level, and a lower laminate level procedure. Analysis and higher level continuous optimisation was performed using VICONOPT, the results of which were compared to FEA performed in ABAQUS. This higher level analysis was performed given a set percentage breakdown of ply angles for the skin and stiffener, with variable panel geometry. The optimum design found was then rounded down in the lower level to give manufacturable ply thicknesses. The stacking sequence was designed manually so as not to violate defined stacking sequence rules arising from expert knowledge. This design was analysed in VICONOPT to check it still fulfilled the design criteria after the rounding. If it did not plies were added to the laminate until the design was feasible. The panel analysis performed was compared to experimental results from three panel tests, one designed for skin buckling (two stiffener panel), one for stiffener buckling (three stiffener panel), and a third Z stiffened panel based upon the results of the bi-level optimisation routine. VICONOPT and ABAQUS showed good agreement to experimental results for the two and three blade stiffened panels; however for the Z stiffened panel the radius of the bends in the stiffener were initially not taken into account, leading to a potentially non-optimum solution, and an under prediction of the initial buckling load. The bi-level optimisation routine was

shown to reduce the mass of a typical aerospace panel by 13% compared to a datum panel design. It should be noted that the design process for the datum panel is not given.

W. Liu et al. [44] presented a bi-level approach to optimisation of a stiffened panel using the finite strip method and optimisation package VICONOPT at the continuous level, and either GA or a manual stacking approach at the discrete level. A number of different stiffener designs were considered. Panel level optimisation is performed in VICONOPT, assuming orthotropic plates at this stage. This optimises the geometry of the panel for a given compressive load. As the variables in this routine are continuous the solution is rounded to the nearest ply integer to allow the layup to be picked. Firstly, a manual selection process is used, in which a layup is picked, then tested in VICONOPT. If the chosen layup does not satisfy the constraints then plies are added until all constraints are fulfilled. A second approach is also presented, whereby a GA is used to select the layups for each of the parts of the stiffened panel. The routine is constrained by the orthotropic laminate layup rules presented by Niu [52]. The GA's fitness function was based on maximising the buckling factor and material reserve factor for the plate, and penalty functions based on the orthotropic laminate layup rules. As in Liu et al. [45] cycling of this bi-level approach can be used to obtain better solutions. This method was shown to offer weight savings of between 13 and 17% compared to a datum panel design. This compares with a saving of 13% over the same datum in previous work by Liu et al. [45]. As mentioned previously, it should be noted again that the design process for the datum panel is not described.

For this work a bilevel approach to optimisation is more suitable, similar to that of Liu et al. [44]. The use of a multi-objective optimisation method is unnecessary as damage tolerance will here be embedded as a constraint, rather than added as a second objective along with weight minimisation. VICONOPT will be used for the higher level of panel optimisation, with the layup design performed with the aid of the CAI model as the lower level of optimisation.

7.3 Modelling and Optimisation in VICONOPT

Chapter 3 discussed the use of the exact finite strip analysis tool VICONOPT in the buckling analysis of thin film sublaminates produced by delamination damage. In this chapter, VICONOPT is used to analyse the buckling of prismatic stiffened assemblies, and perform optimum design analysis. Section 3.5.2 describes the analysis methodology

within VICONOPT, the optimum design methodology also employed in VICONOPT will be discussed here.

7.3.1 VICONOPT Sizing Strategy

The design problem in VICONOPT is a constrained minimisation problem of the form:
Minimise

$$W(\mathbf{X}) \tag{7.1}$$

Subject to

$$G_m(\mathbf{X}) \leqslant 0 \quad m = 1, .2, .3, \ldots, n_c \tag{7.2}$$

where $\mathbf{X}$ is a vector of design variables, $W(\mathbf{X})$ is the objective function, the $G_m(\mathbf{X})$ are inequality constraint functions and n_c is the number of inequality constraints. These inequality constraints include buckling constraints, material strength constraints, and any geometric constraints specified by the user. The objective function is the mass of the structure. Design variables may be made up of plate breadths, layer thicknesses and ply angles.

Buckling constraint information is provided by the analysis methods in VICONOPT. This includes sensitivity analysis with respect to the design variables, used to set up approximate analyses based on a first order Taylor series expansion. This approximate analysis is used in a linear optimisation step within the sizing strategy.

The sizing strategy takes place in two phases, designed to minimise computational effort. The inner sizing cycle uses the approximate analyses based on the first order Taylor series expansion. This performs linear optimisation within move limits calculated so that the linear approximation is valid within the bounds of movement. Buckling sensitivities may then be recalculated in the outer sizing cycle, followed by further linear optimisation. Analysis is terminated after a user specified maximum number of sizing cycles, or when convergence in the relative mass difference in subsequent sizing cycles is achieved. Figure 7-1 outlines the sizing strategy. A fuller description of this methodology can be found in [80].

7.3.2 Assemblies in VICONOPT

The sublaminate buckling analysis performed using VICONOPT in Chapter 3 was a flat plate analysis with point constraints added to approximate a circular boundary. In order to position these point constraints the plate was split into a number of strips, the

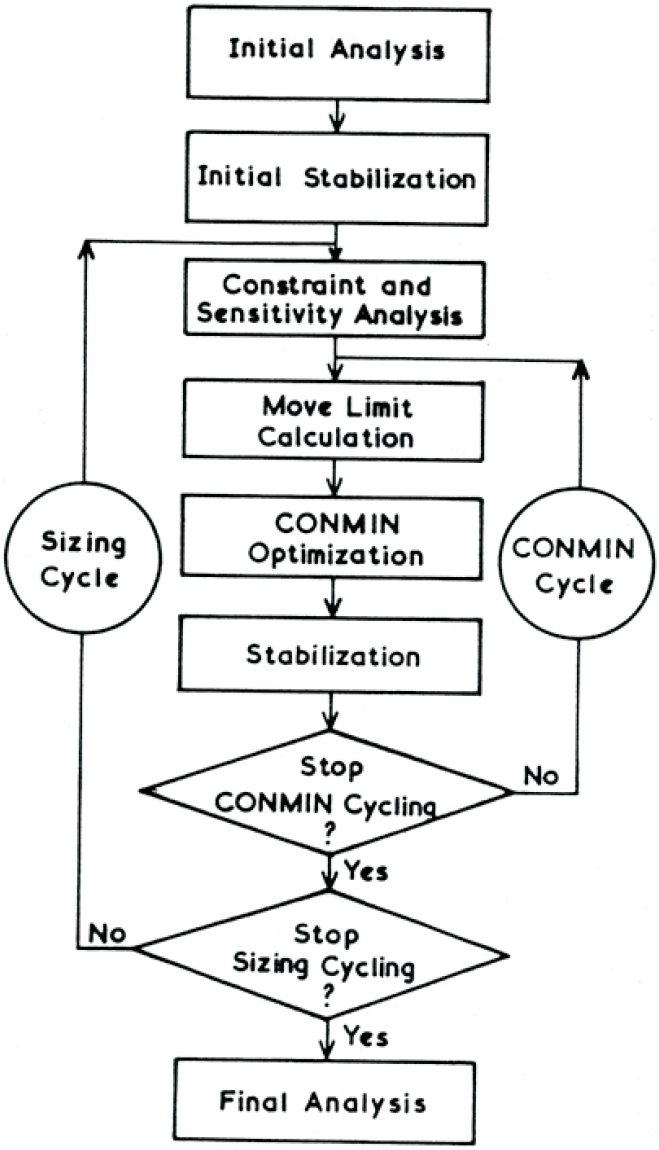

Figure 7-1: VICONOPT Sizing Strategy.

interfaces of which were the locations for the point constraints. In this case the strips were attached parallel to each other, producing a 2D plate. VICONOPT may also be used to analyse 3D prismatic structures, with strips connected at predefined angles to define stiffeners for example. Figure 7-2 shows a typical VICONOPT assembly. In this case an assembly of a finite width has been produced by connecting strips rotated to produce both skin and stiffeners. Constraints may then be applied at nodes to approximate the boundary conditions required. It is also possible to model an infinitely wide panel by using a repeating section, as shown in Fig. 7-3.

7.3.3 Out-of-Plane Loading in VICONOPT

The position of the upper wing skin within the wing structure means that it is subject to an out-of-plane pressure loading that needs to be accounted for in the buckling analysis. This loading occurs as a result of the combined external suction due to lift being produced, and internal pressure due to fuel held in the wing box. Figure 7-4 shows the pressure distribution around an aerofoil in flight, demonstrating the suction on the upper wing panel.

During flight the upper wing skin is in compression due to wing bending root to tip, and can also be seen from Fig. 7-4 to be experiencing suction due to lift, as well as pressure exerted due to the fuel held in the wing box. This out-of-plane loading complicates the buckling problem as pre-buckling is now non-linear. The infinite strip analysis tool VICONOPT used here includes methods to account for out-of-plane pressure loading.

As VICONOPT pre-buckling analysis does not allow for out-of-plane deformation directly, pressure loadings are included in the form of critical bending moments. These are calculated for two potentially critical positions in the plate, namely mid-bay and at the rib boundary. These moments are used to calculate additional longitudinal loads in each plate, which are added to those already calculated from in-plane applied loads or plate internal stresses. As the VICONOPT analysis is prismatic these loads may not be applied together, so two analyses are performed, one with the rib boundary bending moment added, the other with the mid-bay bending moment added. The lower of the two critical factors calculated will dictate the buckling factor for the panel. Figure 7-5 shows these moments on a clamped strut with a uniformly distributed load.

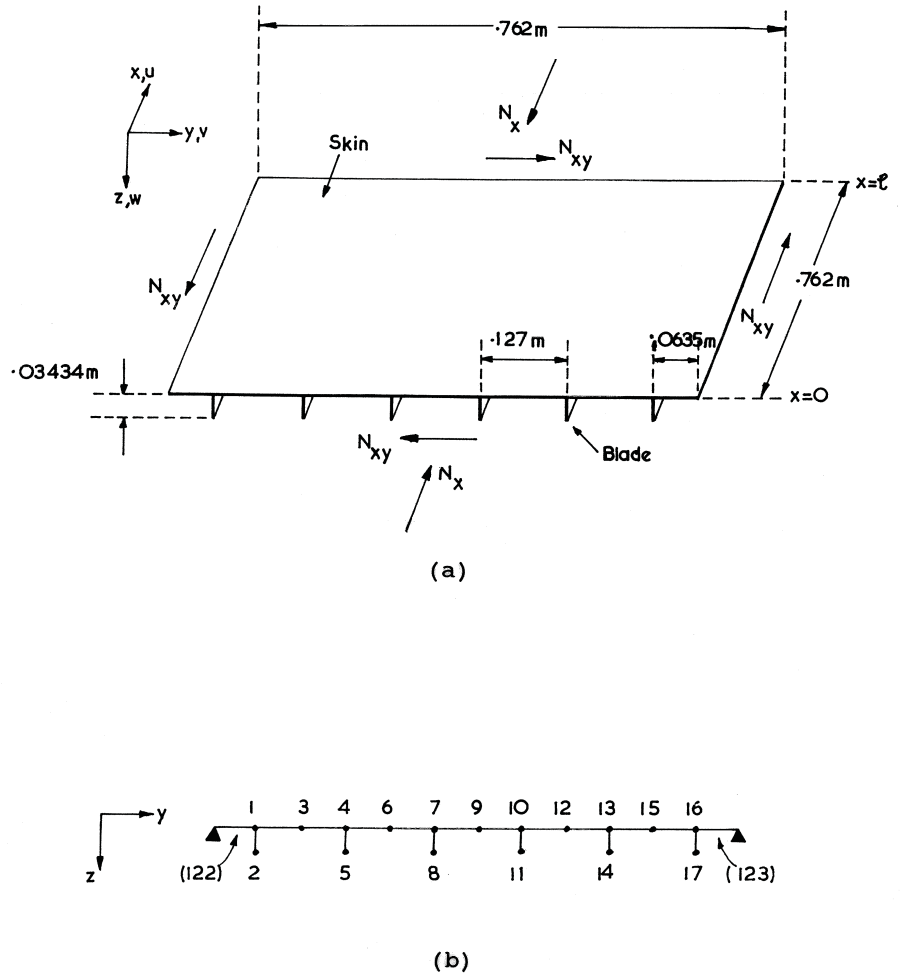

Figure 7-2: Blade stiffened panel with constraints in VICONOPT. a) Isometric view showing dimensions and typical loading. b) Panel cross-section, showing node numbering, showing line supports (solid triangles) and point supports (solid circles). Taken from [75].

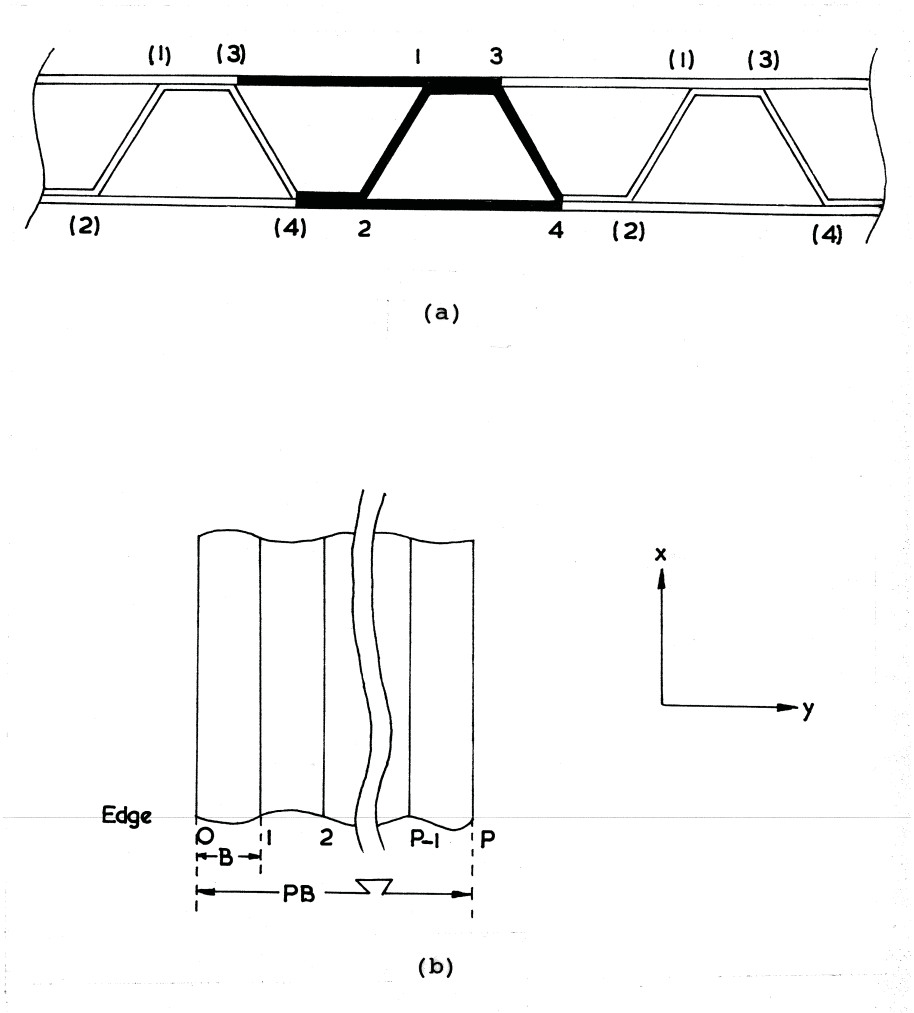

Figure 7-3: Plate assemblies that consist of repeating portions. a) A typical repetitive cross-section, with the datum repeating portion shown bold. The numbers are node numbers, with the brackets indicating that all repeating portions have an implied node numbering identical to that of the datum portion. b) Plan view of a repetitive plate assembly with P repetitions. Taken from [75].

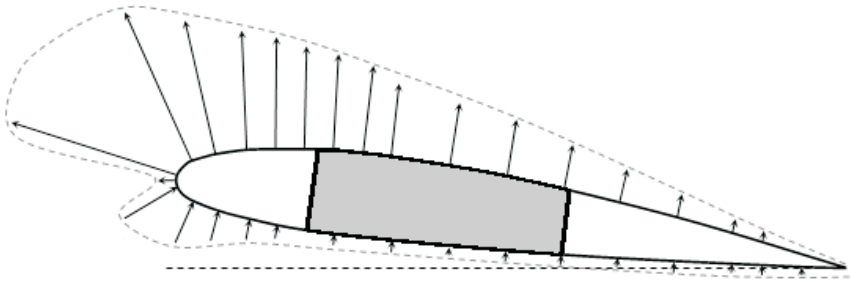

Figure 7-4: Pressure distribution around a NACA 2415 aerofoil at 8° angle of attack. Arrows pointing away from the aerofoil surface indicated pressures lower than free stream, arrows points towards indicate higher. Greyed section shows wing box.

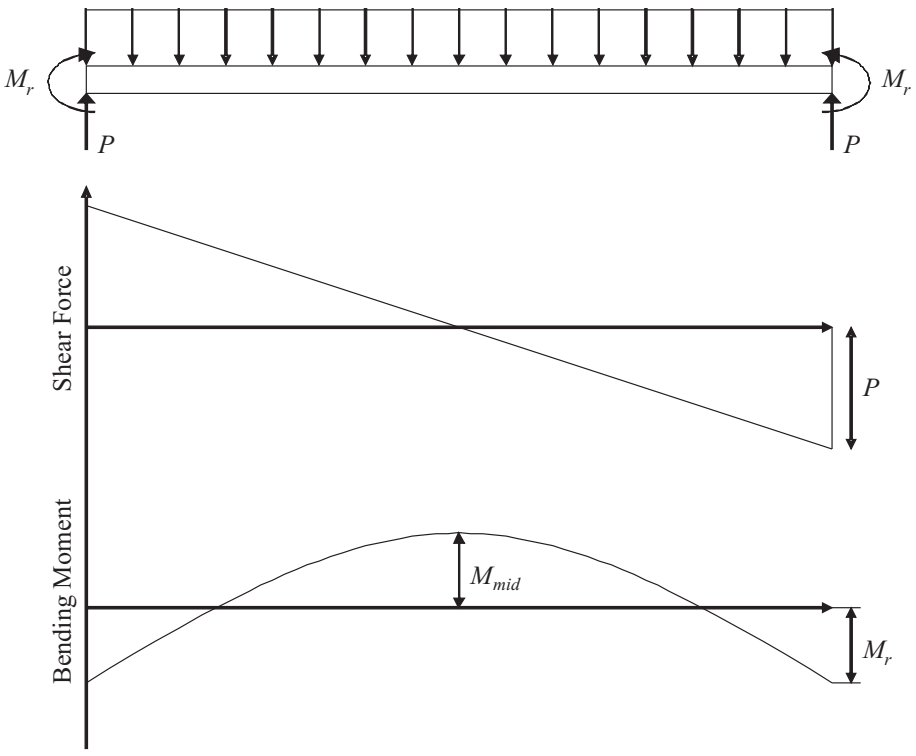

Figure 7-5: Bending moments due to out-of-plane pressure load in VICONOPT. Moments M_r and M_{mid} are applied to the buckling analysis in turn.

7.4 Buckling Analysis - Stiffened Panels

Traditional metal wing skin structures in commercial aircraft are generally stringer stiffened panels, supported at their edges by ribs and wing spars. Figure 7-6 shows a typical composite stiffened panel.

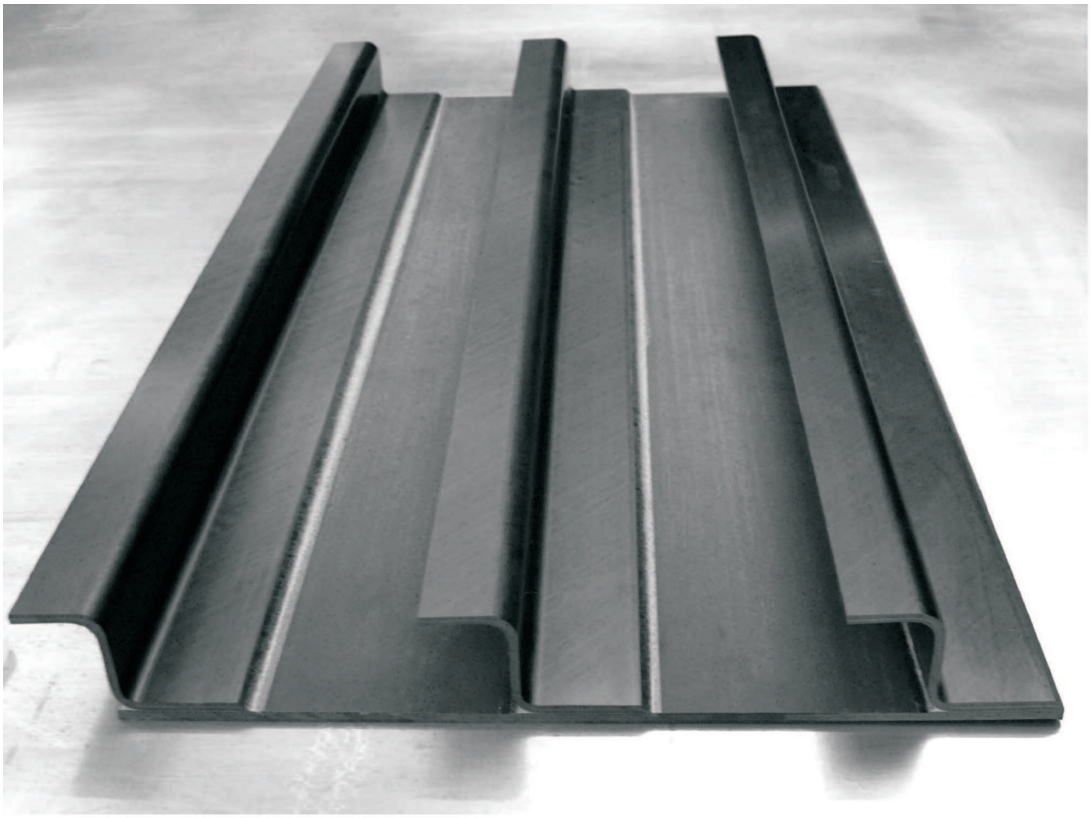

Figure 7-6: Typical stiffened panel configuration. Test panel uses Z stiffeners, image taken from bilevel optimisation work by Liu et al. [45].

This method of skin design is long standing, and acts to break up the skin into smaller panels which are harder to buckle, increasing the overall buckling load of the skin-stiffener panel. The critical buckling modes for such a structure tend to be skin buckling, stiffener buckling and overall interactive buckling.

There are a range of stiffener cross sections employed in stiffened panels; in this work three will be discussed: Blade, I and hat. Figures 7-7, 7-8 and 7-9 show each of these cross sections.

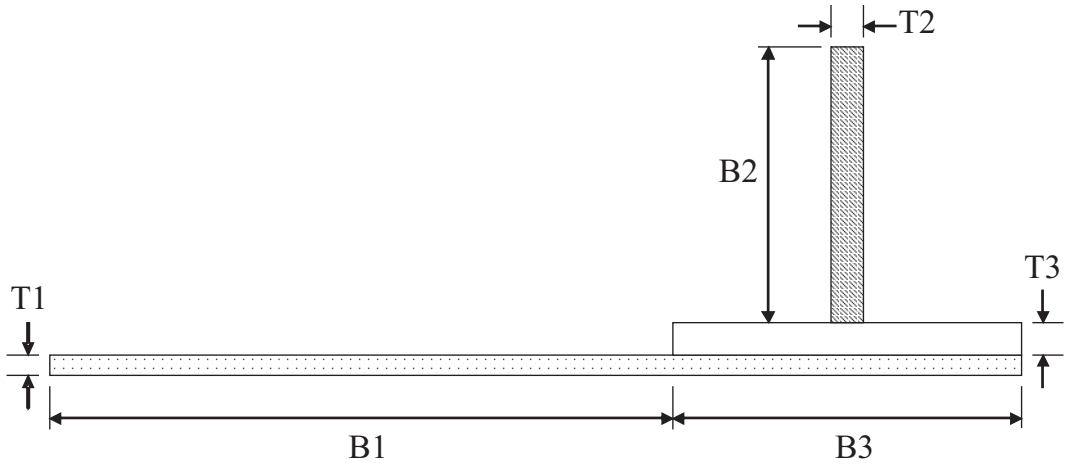

Figure 7-7: Geometry and variables for blade stiffened wing skin panel.

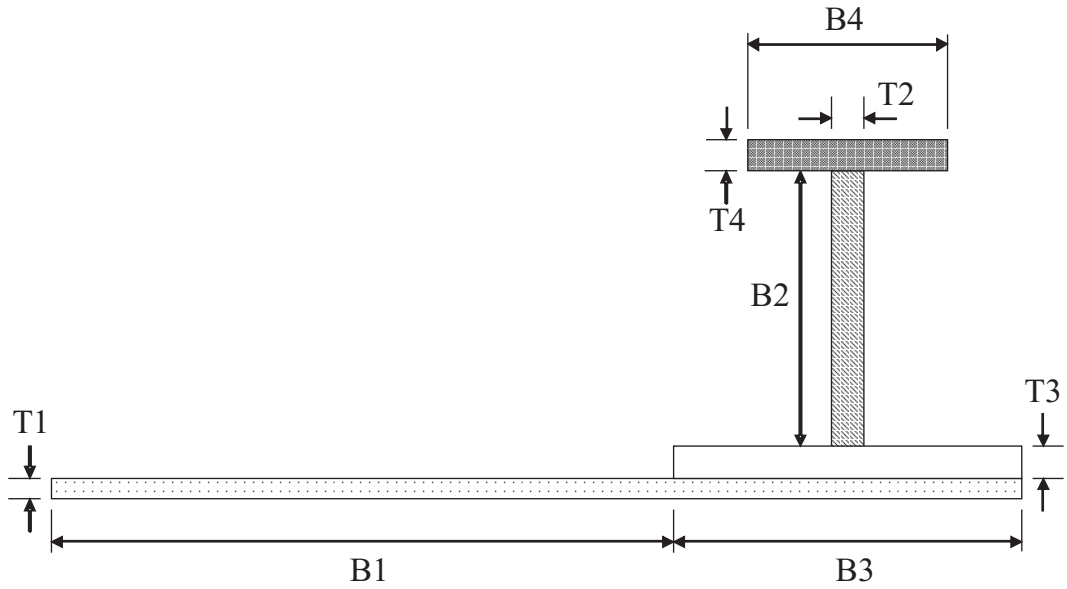

Figure 7-8: Geometry and variables for I stiffened wing skin panel.

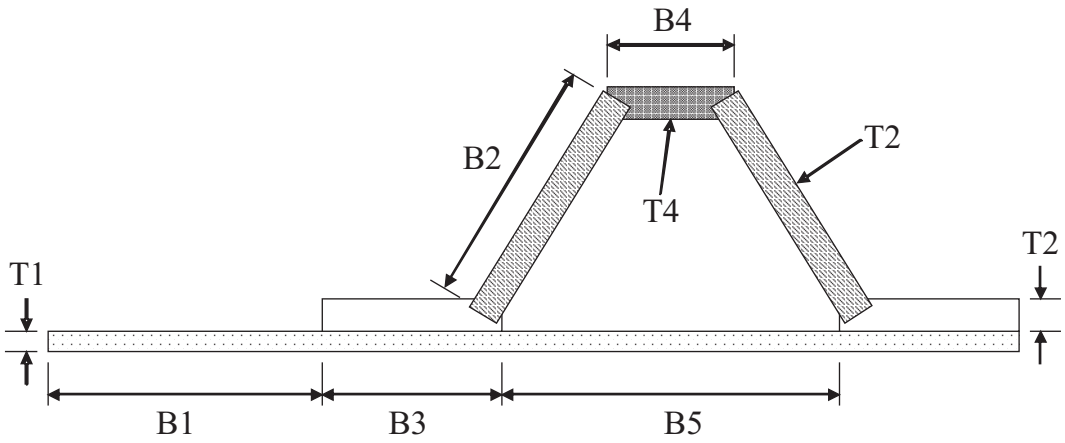

Figure 7-9: Geometry and variables for hat stiffened wing skin panel.

As with the sublaminate buckling analysis performed in the CAI model, plate buckling analysis is performed using VICONOPT.

7.4.1 Problem Definition

The problem is structured as a simple generic wing cover panel optimisation problem. Geometric dimensions are specified in Table 7.1 and loads in Table 7.2. A panel is optimised for each load case separately.

Panel Width	Infinite
Rib Pitch	600 mm
Foot Width	60 mm
Stringer Pitch	Variable
Thicknesses T1-T4	Variable
Breadths B1, B2, B4, B5	Variable

Table 7.1: Geometries in stiffened panel optimisation.

Load Case	Running Load, kN/mm	Pressure Load, MPa
1	1.00	0.13
2	2.00	0.13
3	4.00	0.13
4	6.00	0.13

Table 7.2: Loadings in stiffened panel optimisation.

These parameters are applied to three stringer geometries: Blade (Fig. 7-7), I (Fig. 7-8), and hat (Fig. 7-9). For each of these all dimensions are initially treated as continuous

variables, apart from foot width B3, which is kept constant at 60 mm for the blade and I designs, and 30 mm for the hat.

7.4.2 Assumptions

The CFRP laminates are initially modelled as homogeneous through thickness, based on the ply percentages specified in Table 7.3. The spar is not considered here, but is included for completeness. This assumption has been used previously in stiffened composite panel optimisation work [44, 45]. Table 7.4 details the material properties used in this work.

Component	0° plies, %	±45° plies, %	90° plies, %	Laminate Poisson's Ratio
Wing Skin	44	44	12	0.399
Wing Stiffener	60	30	10	0.362
Wing Spar	15	70	15	0.450

Table 7.3: Nominal ply percentage fractions and Poisson's ratios for various composite wing components.

Material	E_{11}, GPa	E_{22}, GPa	G_{12}, GPa	ν_{12}	t, mm	G_{IC}, J/m^2
Standard CFRP	120	9	5	0.30	0.125	478

Table 7.4: Material Properties.

These properties are calculated as follows: a symmetric laminate is created consisting of an equal number of 0°, 90° and 45° plies, the thicknesses of which are directly proportional to the ply percentages specified in Table 7.3. The effective in-plane properties of this laminate can then be used as the properties of an equivalent homogenous material for use in the VICONOPT optimisation routine. Table 7.5 details this homogenised material.

Material	E_{xx}, GPa	E_{yy}, GPa	G_{xy}, GPa	ν_{xy}	t, mm	G_{IC}, J/m^2
Standard CFRP Skin	65.7	32.7	16.5	0.399	0.125	478
Standard CFRP Stiffener	81.2	27.9	12.8	0.362	0.125	478

Table 7.5: Material properties for homogenised composite.

The panel is modelled as being infinitely wide between two ribs, using recurrence equations so that only a datum repeating portion is computed. Compatibility at the rib interface is satisfied by the buckling wavelengths chosen. For all designs, buckling half-wavelengths from the 40 mm to the defined rib pitch are analysed. Analysing half-wavelengths in this range will cover both global buckling and local skin or stiffener buckling. Strains presented in this report are end-shortening strains due to the applied running load, without the non-linear out-of-plane pressure effects.

7.4.3 Results

Results are presented here, initially for panels without a damage tolerance constraint. Therefore, a limit strain of 0.004 mm/mm is added to the optimisation problem as an assumed safe life strain in the absence of any damage tolerance modelling. Tables 7.6 to 7.8 give the dimensions for the optimum panel configurations produced.

Load Case	B1, mm	B2, mm	B3, mm	T1, mm	T2, mm	T3, mm
1	36.9	35.1	60.0	1.10	5.47	2.83
2	34.2	48.9	60.0	1.03	8.14	3.00
3	111	68.1	60.0	3.43	13.0	13.9
4	107	58.1	60.0	3.30	22.3	23.8

Table 7.6: Dimensions of optimum blade stiffened panels.

Load Case	B1, mm	B2, mm	B3, mm	B4, mm	T1, mm	T2, mm	T3, mm	T4, mm
1	33.6	35.1	60.0	28.0	2.25	2.98	1.49	1.20
2	37.0	58.9	60.0	51.6	1.41	4.72	2.36	2.26
3	58.1	60.7	60.0	9.22	1.82	13.5	6.73	13.3
4	64.8	57.1	60.0	4.08	2.01	23.9	11.9	24.7

Table 7.7: Dimensions of optimum I stiffened panels.

Load Case	B1, mm	B2, mm	B3, mm	B4, mm	B5, mm	T1, mm	T2, mm	T4, mm
1	51.9	42.1	30.0	23.1	62.3	1.86	2.99	2.03
2	37.5	74.1	30.0	19.6	39.9	1.20	3.16	6.01
3	66.4	87.4	30.0	17.0	62.2	2.06	8.28	8.75
4	72.1	73.2	30.0	25.8	72.9	2.17	16.1	9.25

Table 7.8: Dimensions of optimum hat stiffened panels.

Figure 7-10 shows the masses for each stiffener type of the buckling optimised panels without damage tolerance analysis. Figure 7-11 shows the end shortening strain in each panel. These strains are below the strain allowable of 0.004 mm/mm as the non-linear effects of the out-of-plane pressure loading mean that localised areas of the panel are reaching the strain allowable due to bending.

7.4.4 Discussion

Firstly, it should be noted that in all cases the optimised panels presented here were at the strain allowable constraint value. This is not shown in Fig. 7-11 as the strain plotted is the end shortening strain, approximated assuming axial compression. Being on the strain allowable constraint limits greatly the ability to reduce the mass of the panel through use of different stiffener geometries, hence the similar panel masses shown in Fig. 7-10. This may be as a result of the relatively small rib pitch of 600 mm chosen for this study. Even so, it can be seen that the blade stiffened designs are generally heavier than the I and hat stiffened equivalents. As applied load increases the difference in mass between the I and hat solutions also closes. This behaviour is contrary to what might be expected, as the higher second moment of area of the I design should improve buckling efficiency. If the strain allowable constraint is removed from these designs, then this becomes clearer. Figure 7-12 shows the masses for these panels without strain allowable constraints, and Fig. 7-13 gives the critical end shortening strains for these panels.

As can be seen in Fig. 7-12, relaxation of the strain allowable reduces significantly the mass of the I and hat stiffened panels in relation to the blade stiffened design. This shows that increasing the strain allowables on the panel will help designers extract more from a stiffened panel through cross section selection.

The end shortening strains plotted in Fig. 7-11 indicate that the behaviour of the blade and I stiffened panels is very similar as the applied load in the optimisation is increased. The trend is as would be expected, with end-shortening strain tending to the strain allowable as applied load increases. This is because as the mass of the panel increases with the increased load, the bending deformation caused by the out-of-plane loading reduces, meaning local peak strains converge to the overall end shortening strain. It should be noted at this point that, as shown in Table 7.2, the out-of-plane pressure loading is effectively applied as a dead load, not scaling with applied end load but instead fixed at 0.13 MPa. This is a realistic assumption to make as lift suction pressure will not change greatly with increase in applied end load. This trend is not

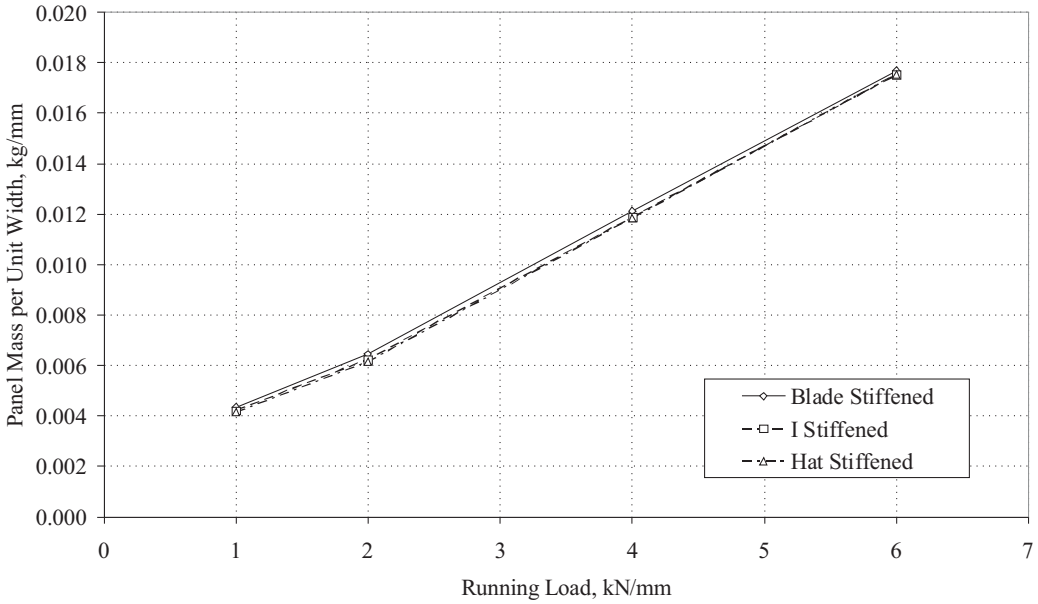

Figure 7-10: Optimised panel masses for selected stiffener geometries.

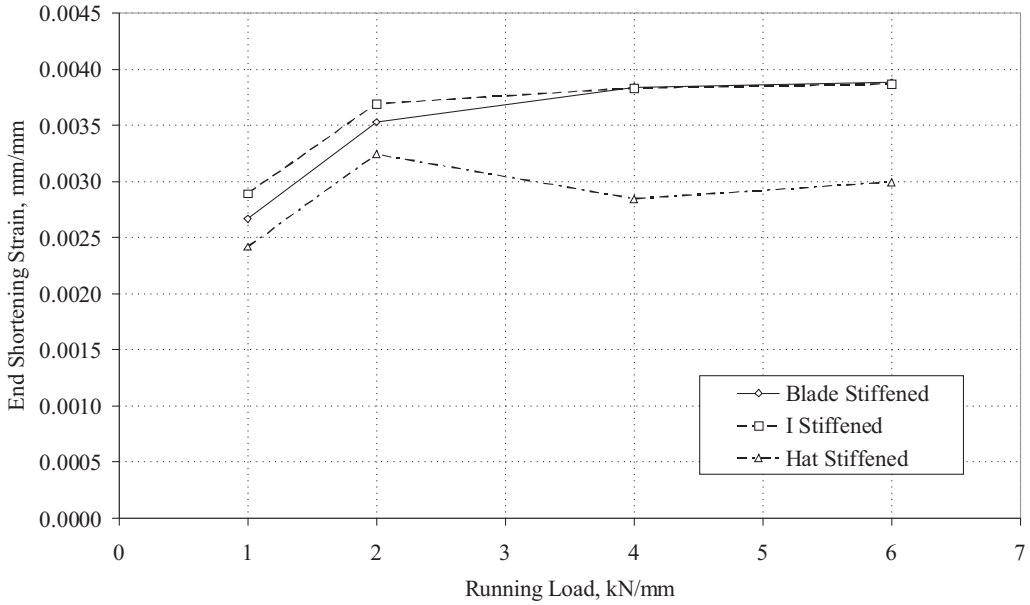

Figure 7-11: End shortening strains of optimised panels for selected stiffener geometries.

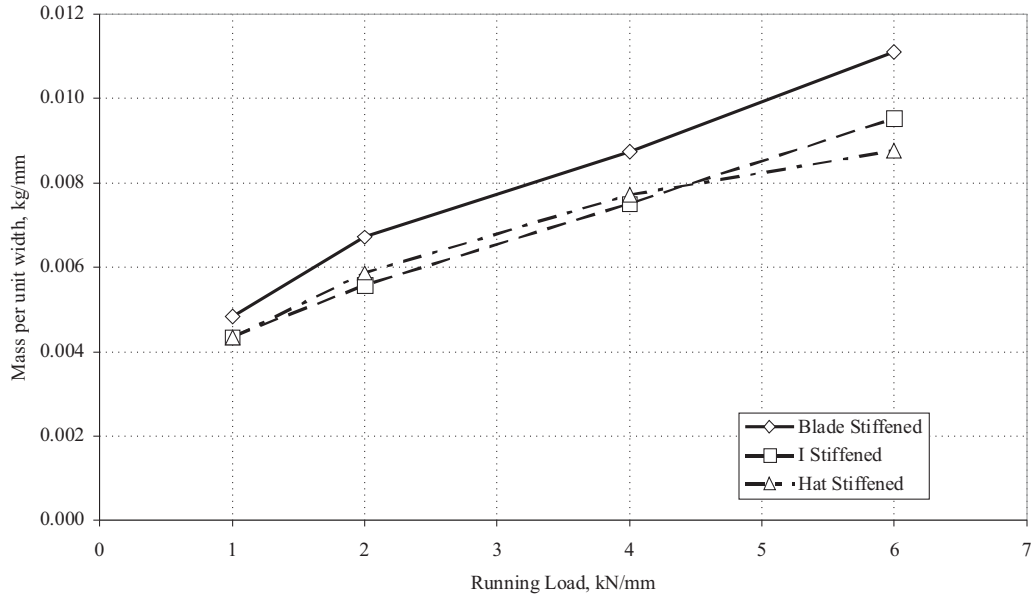

Figure 7-12: Optimised panel masses for selected stiffener geometries, without strain allowable constraint applied.

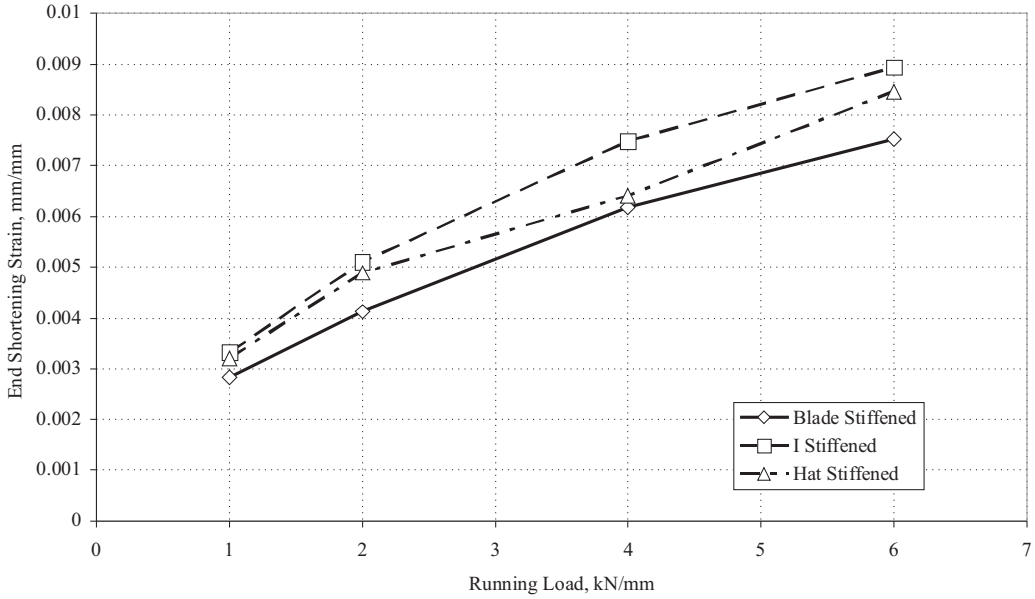

Figure 7-13: End shortening strains of optimised panels for selected stiffener geometries, without strain allowable constraint applied.

exhibited by the hat stiffened panel however, but this may be explained by examining the mean thickness of the skin and stiffener for each configuration. Figure 7-14 shows the mean thickness of each panel for both skin and stiffener, and Fig. 7-15 shows the percentage of skin in each panel by mass.

As can be seen particularly in Fig. 7-15, the ratio of skin mass to stiffener mass for the blade stiffened panel differs greatly from that of the I and hat stiffened solutions. For all solutions the general trend is for skin percentage to reduce as applied load is increased. This is because, as shown in Table 7.5, the stiffener displays a higher effective modulus than the skin. As the applied load on the panel is increased, the mass must increase to ensure the strain allowables are not violated, and due to this increase buckling becomes less of a concern. As such, the optimiser can then choose to redistribute the mass of the panel to the stiffener, which due to its higher stiffness can carry higher load for less weight than the skin.

Figure 7-15 can also help to explain the drop in end shortening strain at the higher applied loads for the hat stiffened panels, exhibited in Fig. 7-11. At lower applied loads the hat stiffened panels have a lower proportion of skin compared to the I stiffened panels, but as applied load increases the trend switches, and I stiffened panels have a lower percentage of skin.

The optimisation of a number of stiffened wing skin panels has highlighted some of the limitations that strain allowables can have on stiffened panel design, and provides a strong case for exploring ways to increase this strain allowable. One such way is to incorporate damage tolerance into the design routine and using this to set the strain allowables of the panel, rather than setting generalised conservative allowables for the whole panel. The next section will discuss a methodology for including damage tolerance in a panel optimisation routine.

7.5 Incorporating Damage Tolerance

Chapter 5 described a surrogate modelling method for analysing sublaminate buckling which calculated sublaminate buckling strain based only on the full laminate Poisson's ratio. This was required because the Poisson's ratio may vary greatly for a generalised range of laminates, and is the only variable in sublaminate buckling once a number of simplifying assumptions have been made. By applying standard industry methodology in terms of ply percentages it is possible to treat laminate Poisson's ratio

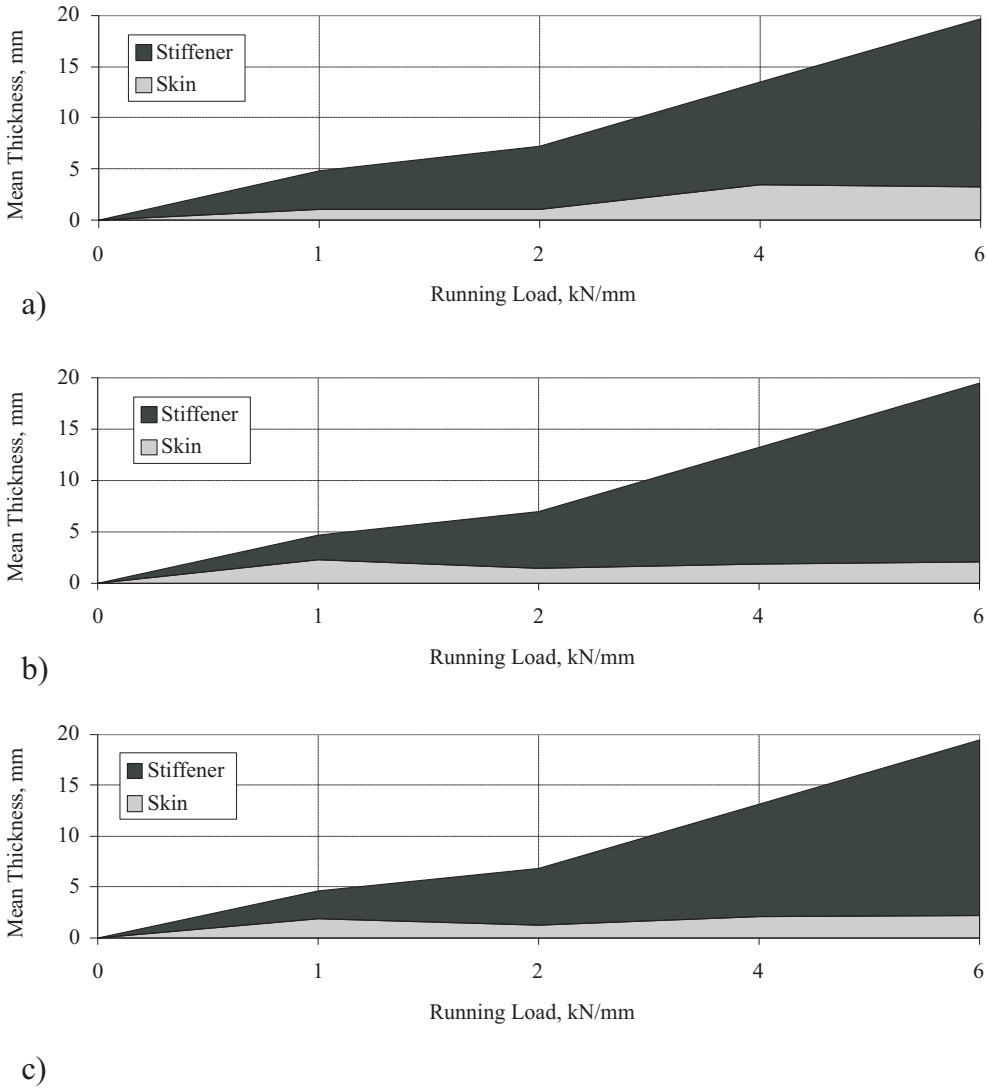

Figure 7-14: Mean thickness of skin and stiffener for optimised panel configurations. a) blade stiffened, b) I stiffened, c) hat stiffened

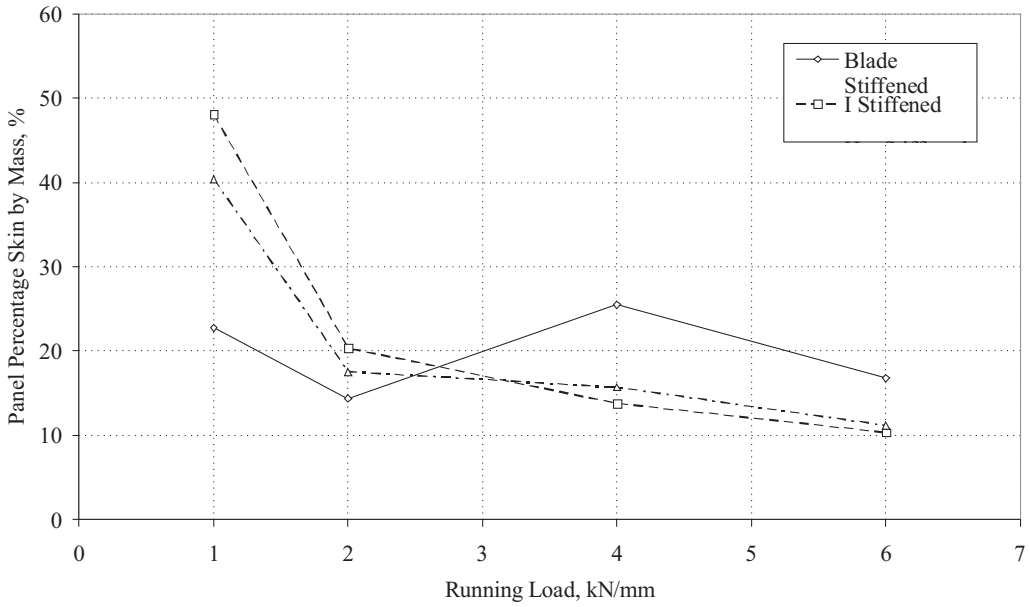

Figure 7-15: Percentage of skin in optimised panel configurations.

as a constant, allowing damage tolerance to be incorporated into a structural design problem for minimal computational effort.

In current composite design methodology it is very often the case that ply percentages will be specified for different components within a structure. Table 7.3 shows typical ply percentages for some composite wing components. With these percentages fixed, or near fixed as is the case once a design is dicretised and layups are chosen, the Poisson's ratio of the laminate is also fixed. From the plate constitutive equations (Eq. 6.1):

$$N_y = A_{12}\varepsilon_x + A_{22}\varepsilon_y + A_{26}\gamma_{xy} \tag{7.3}$$

For a symmetric laminate under uniaxial compression, N_y and γ_{xy} become zero, ε_y can be expressed as $\varepsilon_x\nu_{xy}$, and Eq. 7.3 can be rearranged to give Poisson's ratio, as shown in Eq. 7.4.

$$\nu_{xy} = \frac{A_{12}}{A_{22}} \tag{7.4}$$

From Matthews and Rawling [47],

$$A_{\mathrm{rs}} = \sum_{j=1}^{p} \bar{Q}_{\mathrm{rs}\,j} t_j \tag{7.5}$$

where $\bar{Q}_{\mathrm{rs}\,j}$ is value [r, s] of the translated stiffness matrix for layer j. Substituting Eq. 7.5 into Eq. 7.4:

$$\nu_{xy} = \frac{\sum_{j=1}^{p} \bar{Q}_{12\,j} t_j}{\sum_{j=1}^{p} \bar{Q}_{22\,j} t_j} \tag{7.6}$$

When Eq. 7.5 is used in laminate analysis, t_j refers to the thickness of the j^{th} layer in the laminate. In this case it can be used to define the percentage of plies in each direction in the laminate p_k, where in this case k is either 0°, 90°, or ±45°. Again from Matthews and Rawling,

$$\bar{Q}_{12} = \quad (Q_{11} + Q_{22} - 4Q_{33})n^2m^2 + Q_{12}(m^4 + n^4) \tag{7.7}$$

$$\bar{Q}_{22} = \quad Q_{11}n^4 + 2(Q_{12} + 2Q_{33})n^2m^2 + Q_{22}m^4 \tag{7.8}$$

where $m = cos(\theta)$ and $n = sin(\theta)$, and θ is the ply angle. The stiffness matrix $\mathbf{Q}$ is defined as

$$\mathbf{Q} = \begin{bmatrix} \frac{E_{11}}{1-\nu_{12}\nu_{21}} & \frac{\nu_{21}E_{11}}{1-\nu_{12}\nu_{21}} & 0 \\ \frac{\nu_{12}E_{22}}{1-\nu_{12}\nu_{21}} & \frac{E_{22}}{1-\nu_{12}\nu_{21}} & 0 \\ 0 & 0 & G_{12} \end{bmatrix} \tag{7.9}$$

In Eq. 7.9 E_{11}, E_{22}, G_{12} and ν_{12} are defined material properties, and ν_{21} is calculated using the relationship

$$\frac{\nu_{12}}{E_{11}} = \frac{\nu_{21}}{E_{22}} \tag{7.10}$$

Substituting Eqs. 7.7 and 7.8 into Eq. 7.6, and redefining ply thicknesses t_j as ply fractions p_k yields

$$\nu_{xy} = \frac{2Q_{12}(2p_{0^\circ} + p_{\pm 45^\circ} + 2p_{90^\circ}) + (Q_{11} + Q_{22} - 4Q_{33})p_{\pm 45^\circ}}{4Q_{11}p_{90^\circ} + 2Q_{22}(2p_{0^\circ} + p_{\pm 45^\circ}) + (Q_{11} + 2Q_{12} + 4Q_{33})p_{\pm 45^\circ}} \tag{7.11}$$

Equation 7.11 may then be used to calculate the Poisson's ratio for a balanced symmetric laminate given the ply fractions in each of the standard ply directions. Table 7.3 shows these Poisson's ratio values for standard laminates in a composite wing, for the material specified in Table 7.4.

As discussed in Chapter 5, the CAI model sublaminate analysis takes only one input from the full laminate of which it is part, its Poisson's ratio. Assuming a fixed Poisson's

ratio, as is close to the case for laminates with specified ply fractions, even when discretised, means that there is one optimal sublaminate for each sublaminate thickness. Using this knowledge, a quick exhaustive search can be performed for each sublaminate thickness, and a database of optimum sublaminate designs can be produced. Figure 7-16 shows the flow chart for this sublaminate analysis.

7.5.1 Optimum Sublaminate Layup Search

A computer program is developed, incorporating the CAI analysis modules described in Chapter 3, to search for optimum sublaminate layups given a fixed laminate ply fraction. As this chapter looks at a real design case, layup rules for composite laminate design stated by Niu [52] are adhered to. In particular, the stipulation of $\pm 45^\circ$ plies at the outer faces of the laminate serves to reduce the size of the design space explored.

The program analyses each potential sublaminate within a $0/90/\pm 45$ design space for a given material, at a Poisson's ratio calculated using Eq. 7.11. The delamination diameter is set at a maximum of 35 mm for BVID as described by Han et al. [28]. The analysis described in Fig. 7-16 is performed to sublaminates up to 7 plies thick, at which point sublaminates are too thick to buckle locally. For thin laminates (up to $\sim$30 plies thickness) this is governed by the interaction of local buckling with global laminate curvature. A 2D representation of this behaviour in a homogeneous material has been presented by Hunt et al. [32]. The mode of buckling depends of the ratio of sublaminate thickness to laminate thickness. Figure 7-17 shows the modes of buckling that may occur.

For very thin delaminations a thin film type delamination buckling will occur, as in Fig. 7-17 a). In this case there is very little out-of-plane displacement of the base substrate. As the thickness of the delaminated sublaminate is increased, its buckling induces curvature in the base substrate (Fig. 7-17 b)). Here the delamination still opens, allowing propagation, but curvature in the base substrate may reduce the accuracy of predictions made by the CAI model as interaction begins. Figure 7-17 c) shows the closing mode that occurs for sublaminates greater than $\sim$25% laminate thickness. Here the buckling of the sublaminate pulls the substrate up, closing the delamination and restraining Mode I propagation of the delamination. Delaminations at such depths are assumed to be benign in this analysis due to this phenomenon. With a database of sublaminate propagation threshold strains produced, the optimum surface ply layup can be found by a search of this data.

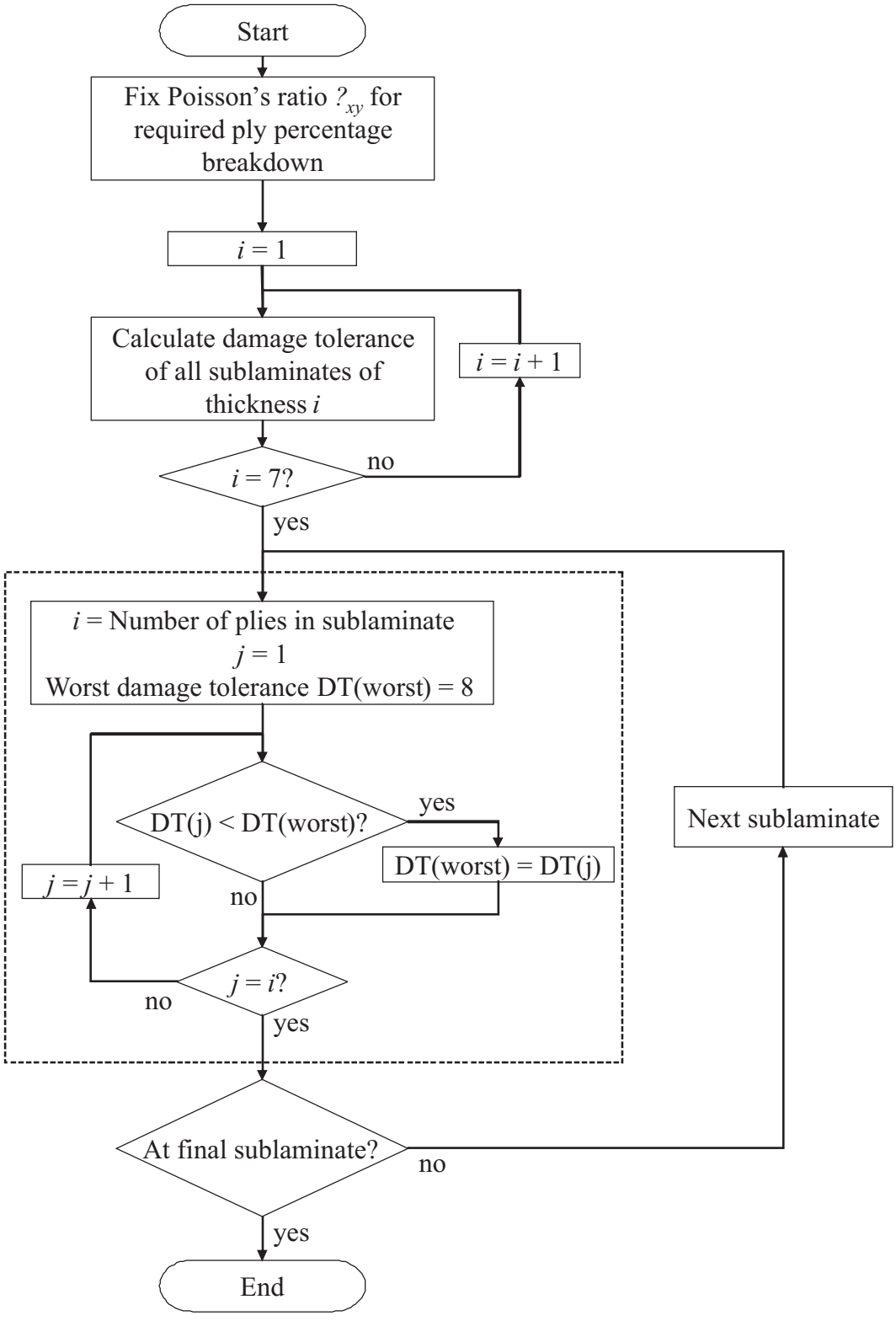

Figure 7-16: Flowchart for calculation of damage tolerance of each possible sublaminate.

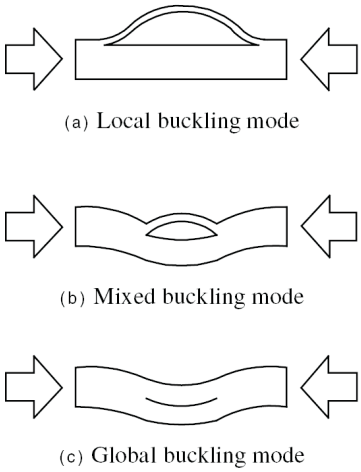

Figure 7-17: Three types of buckling mode shape. Figure taken from Hwang and Liu [33].

The sublaminate analysis takes place in two stages; firstly the threshold strain for each individual sublaminate is calculated, then results are combined so that each sublaminate threshold strain is the lowest strain of each sublaminates within it. Finally, for each total sublaminate thickness the highest threshold strain design is chosen, giving the optimum surface sublaminate layup for each total laminate thickness. Table 7.9 shows the optimum skin sublaminate layups for each laminate thickness, with Table 7.10 showing the optimum sublaminate layups for stiffeners. As the depth to which thin film delamination buckling is critical is around 25% of the total laminate thickness, the optimum surface ply layup may change with laminate thickness.

Laminate Thickness, mm	Skin Sublaminate Layup	Critical Interface	Critical Strain, mm/mm
0-0.75	45	1st	0.015
0.875-1.25	± 45	2nd	0.010
1.375-1.75	$\pm 45/0$	3rd	0.0062
1.875-2.25	$[\pm 45]_2$	4th	0.0065
2.375-2.75	$\pm 45/45/0/90$	4th	0.0053
2.875-3.25	$\pm 45/0_2/\pm 45$	5th	0.0043
3.375+	$[\pm 45]_2/90/0_2$	7th	0.0055

Table 7.9: Optimum damage tolerant sublaminate layups for standard CFRP material in Table 7.4 for skins.

Laminate Thickness, mm	Stiffener Sublaminate Layup	Critical Interface	Critical Strain, mm/mm
0-0.75	45	1st	0.015
0.875-1.25	± 45	2nd	0.010
1.375-1.75	$\pm 45/0$	3rd	0.0062
1.875-2.25	$\pm 45/0_2$	4th	0.0047
2.375-2.75	$\pm 45/45/0/90$	4th	0.0053
2.875-3.25	$\pm 45/0_2/\pm 45$	5th	0.0043
3.375-3.75	$\pm 45/0_2/\pm 45/0$	5th	0.0043
3.875-4.25	$\pm 45/0_2/\pm 45/0_2$	5th	0.0043
4.375+	$[\pm 45]_2/90/0_2$	7th	0.0055

Table 7.10: Optimum damage tolerant sublaminate layups for standard CFRP material in Table 7.4 for stiffeners.

These two tables form the quick look-up for strain allowables for use within an optimisation routine. As strain allowables vary with thickness and Poisson's ratio, different limits may be set for different components in the assembly. The bilevel optimisation approach can now be described.

7.6 Optimisation of Stiffened Panels with Damage Tolerance Constraints

Figure 7-18 shows the flow diagram for the bilevel routine, optimising a stiffened panel for minimum mass based on buckling and damage tolerance constraints. This bilevel method of optimisation only uses an optimiser on one level, with the damage tolerance and layup analysis predetermined by an exhaustive search.

The nature of the optimisation routine, and the discrete changes in strain allowable with respect to laminate thickness displayed in Tables 7.9 and 7.10 mean that the flow chart in Fig. 7-18 may produce an infinite loop between two solutions. In this case the lowest mass solution of these two designs is selected.

7.6.1 Design Case

As discussed in Section 3.3.2, free edge damage in composites is a major limiting factor in strain allowables, and does not allow for as great improvements in damage tolerant strain as enclosed damage by stacking sequence optimisation. For this reason the optimisation here will be initially performed on hat stiffened panels (Fig. 7-9), as

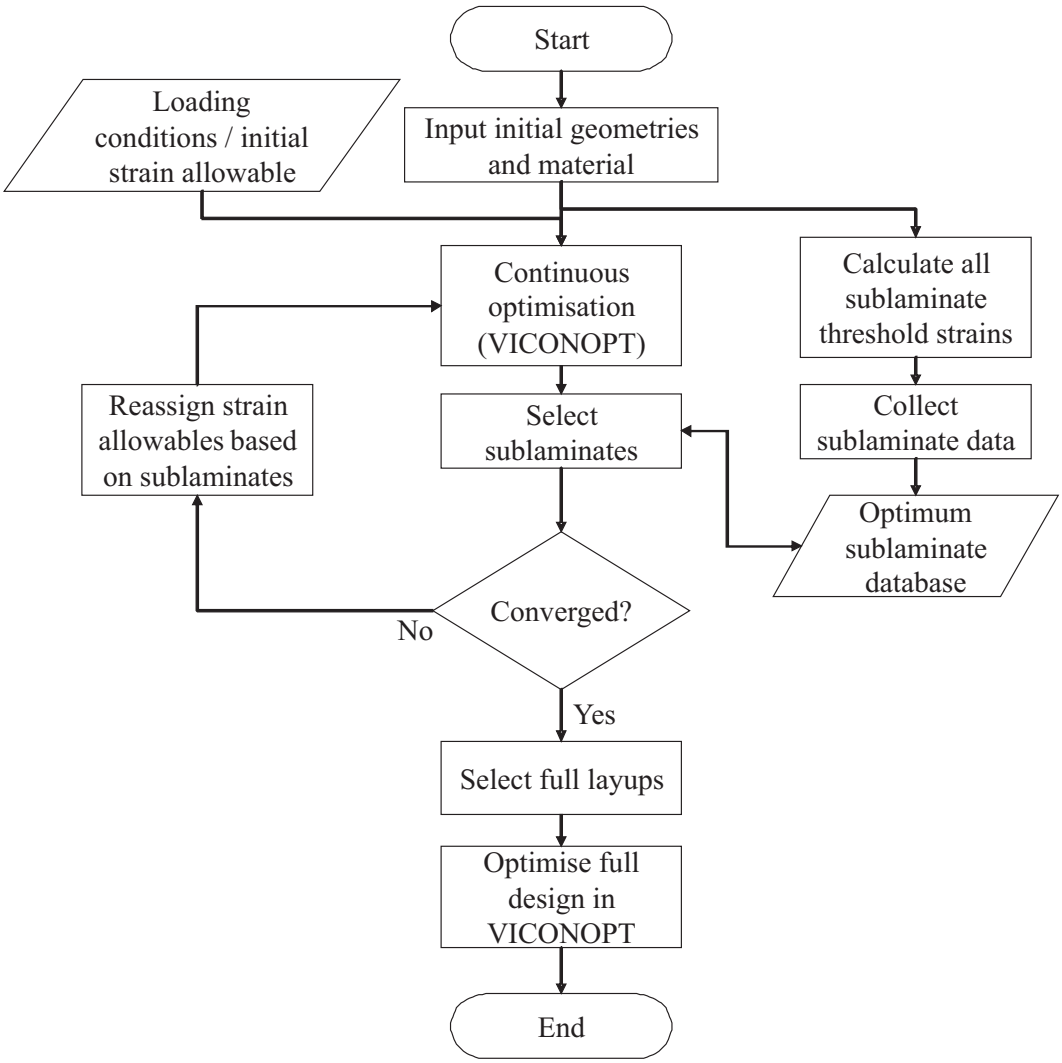

Figure 7-18: Flowchart for bilevel optimisation process.

they exhibit only one free edge, which is bonded to the wing skin. Geometries and load cases will be the same as those specified in Tables 7.1 and 7.2.

7.6.2 Results

Figure 7-19 shows the panel masses for hat stiffened panels optimised both with a nominal strain allowable set, and with CAI strength used to set allowable strain. In both design cases, once the panel thicknesses have been set in the initial optimisation process, layups are chosen and the panel is rerun with only breadth variables to produce final masses. This accounts for the difference in masses for the non damage tolerant hat stiffened panels here and in Fig. 7-10. Table 7.11 shows the geometries and Table

7.12 shows the layups for each damage tolerant hat stiffened panel. It should be noted that the damage tolerant 6 kN/mm hat stiffened panel did not fully converge, leading to a higher mass solution than may be possible.

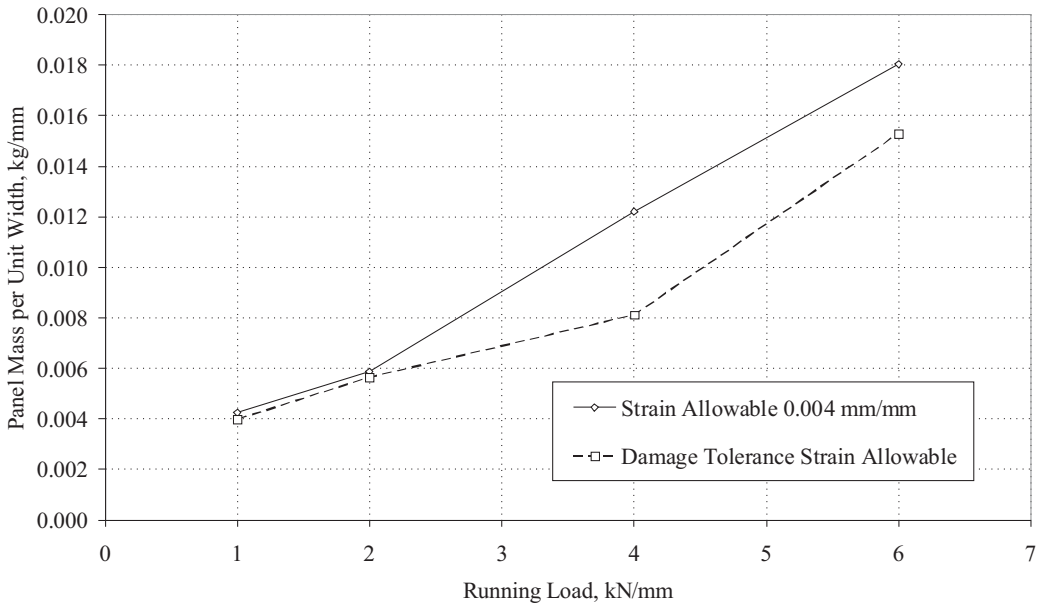

Figure 7-19: Mass of damage tolerance and buckling optimised hat stiffened panel compared to buckling optimised panel with nominal strain allowable of 0.004 mm/mm.

Load Case	B1, mm	B2, mm	B3, mm	B4, mm	B5, mm	T1, mm	T2, mm	T4, mm
1	45.0	41.1	30.0	24.4	80.9	1.875	2.875	1.50
2	64.0	54.0	30.0	24.0	24.5	1.75	3.5	3.5
3	64.0	54.0	30.0	24.0	8.0	1.75	4.75	6.75
4	66.6	104.5	30.0	33.3	63.5	2.00	9.50	9.25

Table 7.11: Dimensions of optimum hat stiffened panels with damage tolerance analysis.

7.6.3 Discussion

The integration of damage tolerance as a constraint into a panel optimisation routine has allowed for further mass reductions when compared to applying a strain allowable as a method of controlling damage growth. Although the allowable strain set for the non damage tolerance optimised panel was nominal, it is representative of the current methods used currently in the aviation industry. By using analysis of the failure modes

Load Case	Section	Layup
1	T1	$[[\pm 45]_2/0_3/90/0_3/[\mp 45]_2]_T$
1	T2	$[\pm 45/0_2/\pm 45/0_3/90/0_3/90/0_3/\mp 45/0_2/\mp 45]_T$
1	T4	$[\pm 45/0_2/90/0]_S$
2	T1	$[\pm 45/0_2/90]_S$
2	T2	$[\pm 45/0_2/\pm 45/0_3/90/0_3/90]_S$
2	T4	$[\pm 45/0_2/\pm 45/0_3/90/0_3/90]_S$
3	T1	$[\pm 45/0_2/90]_S$
3	T2	$[[\pm 45]_2/90/0_4/\pm 45/0_5/90/0_2]_S$
3	T4	$[[\pm 45]_2/90/0_4/\pm 45/0_4/90/0_4/\pm 45/0_4/90]_S$
4	T1	$[\pm 45/0_2/90/0/\pm 45]_S$
4	T2	$[[[\pm 45]_2/90/0_4][\pm 45/0_4/90/0_2]_3[\pm 45]]_S$
4	T4	$[[[\pm 45]_2/90/0_4][\pm 45/0_4/90/0_2]_2[\pm 45/0_4/\pm 45/0_2]]_S$

Table 7.12: Stacking sequences for each section in hat stiffened panels with damage tolerance analysis.

that this strain allowable is designed to stop, it has been shown that further weight savings can be made in composite stiffened panels.

The benefits of an increased strain in the damage tolerant panels are not fully realised until higher values of applied load. This is because at lower load levels buckling is more critical, and the increased strain allowables cannot be fully utilised. As load is increased buckling strains increase, and the extra strain afforded by the damage tolerance inclusion can be utilised to produce a lower mass panel.

The bilevel optimisation approach presented here is a simple way of including damage tolerance constraints in a VICONOPT design sizing, but may not be the most effective way of doing so. It may be more effective to include thickness-based strain allowables within the VICONOPT code itself. Currently the algorithm may loop without convergence as the damage tolerance feedback is out of step with the VICONOPT analysis; integration of the two methods would stop this occurring. This integration of thickness-based strain allowables would not however be a trivial task, and the bilevel approach here gives an indication as to the benefits of including damage tolerance analysis as a constraint in VICONOPT optimisation, without the need to fully integrate the process within the VICONOPT code itself.

Although the issue of free edge impact damage makes the use of this method less applicable to panel geometries that exhibit free edges, it is still of interest to perform the bi-level optimisation for the blade and I stiffened panel configurations. Interest in these

configurations may also be improved by the use of an extrusion-type manufacturing technique, producing blade stiffeners that do not have a typical free edge at the end of the web. Figure 7-20 shows the optimum panel masses for blade stiffened panels, and Fig. 7-21 shows the masses for I stiffened designs. Critical end shortening strains are given in Figs. 7-22 and 7-23 respectively.

Running of the blade and I stiffened configurations with the damage tolerance analysis constraint allows for direct comparison of the masses of these solutions. Figure 7-24 shows the masses of these three configurations.

Figure 7-24 reconfirms the poor convergence of the 6 kN/mm hat stiffened solution, with this being the only hat stiffened design with a higher mass than both the blade and I stiffened equivalents. It can be seen that as with the panels with a fixed strain allowable applied, the damage tolerance strain allowable panels do not show significant changes in optimum panel mass with stiffener cross section. When comparing to the optimised panel masses with no strain allowable set (Fig. 7-12) it can be seen that some of the disadvantage in mass for the blade stiffened design is lost when damage tolerance strain allowables are set.

7.6.4 Limitations of the Design Algorithm

The design algorithm presented here seeks to show the possibilities of including a simple damage tolerance analysis method within a stiffened panel optimisation routine. Due to its inherent simplicity there are a number of limitations associated with it, some modelling based, others manufacturing. These will be addressed in turn.

Local-Global Buckling Interaction

One of the major limitations with this design algorithm, and one that exists with many similar investigations, is that it isolates the two significant failure modes for the structure, stability-based buckling and strength-based damage tolerance. There is a very great danger that such an assumption could lead to non-conservative designs, with interaction of the two modes reducing the failure strain of the structure below that for which it has been designed [2]. The nature of this interaction is not easy to model, as it depends on the position at which impact damage occurs within the panel. A designer may be able to make assumptions about the critical locations for impact damage and design for these, but ultimately this problem should be addressed by buckling analysis incorporating the destiffening effects of impact induced inter-ply

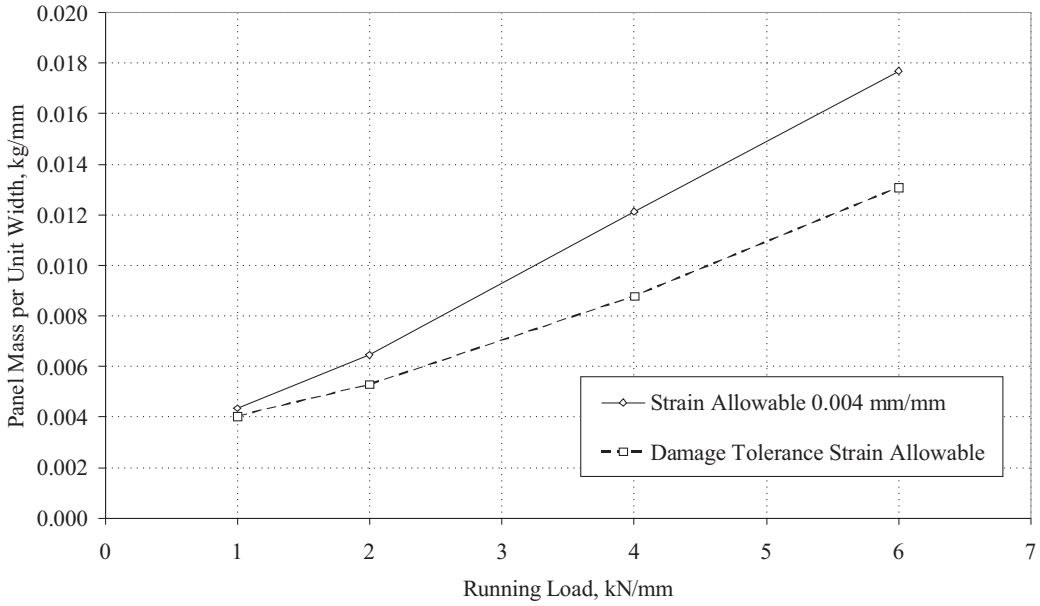

Figure 7-20: Mass of damage tolerance and buckling optimised blade stiffened panel compared to buckling optimised panel with nominal strain allowable of 0.004 mm/mm.

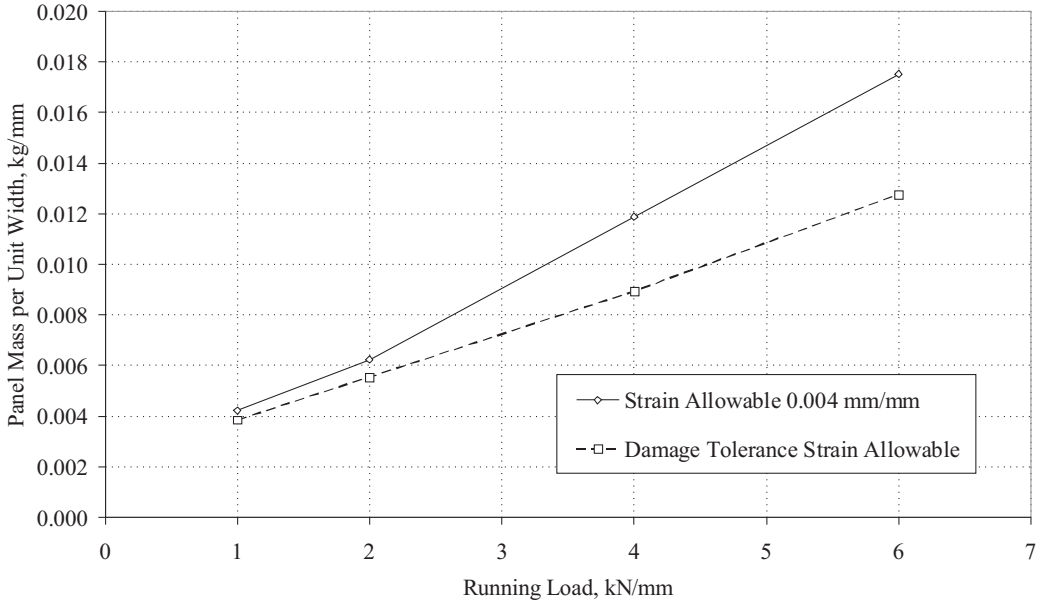

Figure 7-21: Mass of damage tolerance and buckling optimised I stiffened panel compared to buckling optimised panel with nominal strain allowable of 0.004 mm/mm.

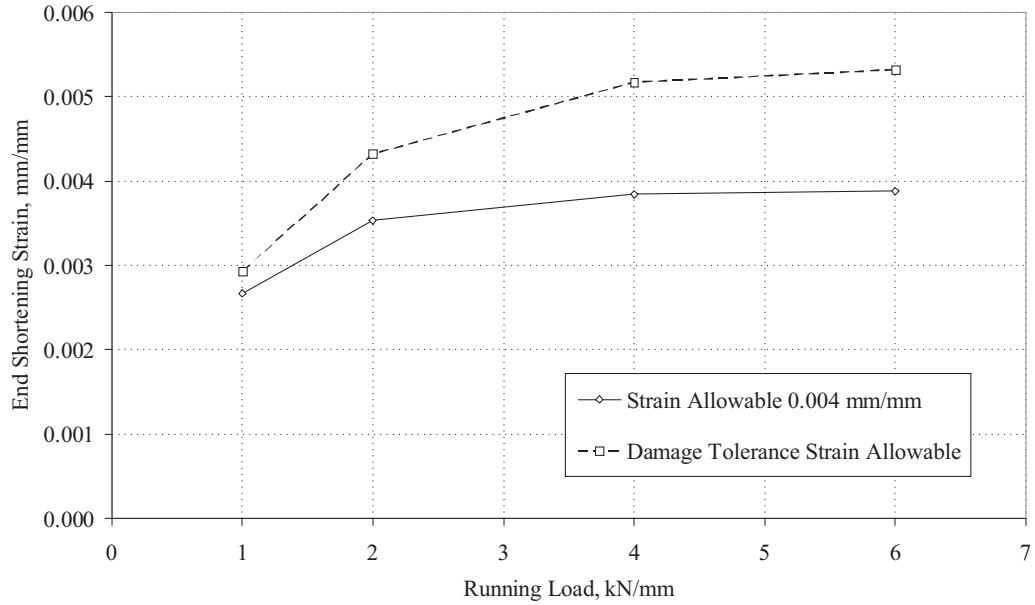

Figure 7-22: End shortening strain of damage tolerance and buckling optimised blade stiffened panel compared to buckling optimised panel with nominal strain allowable of 0.004 mm/mm.

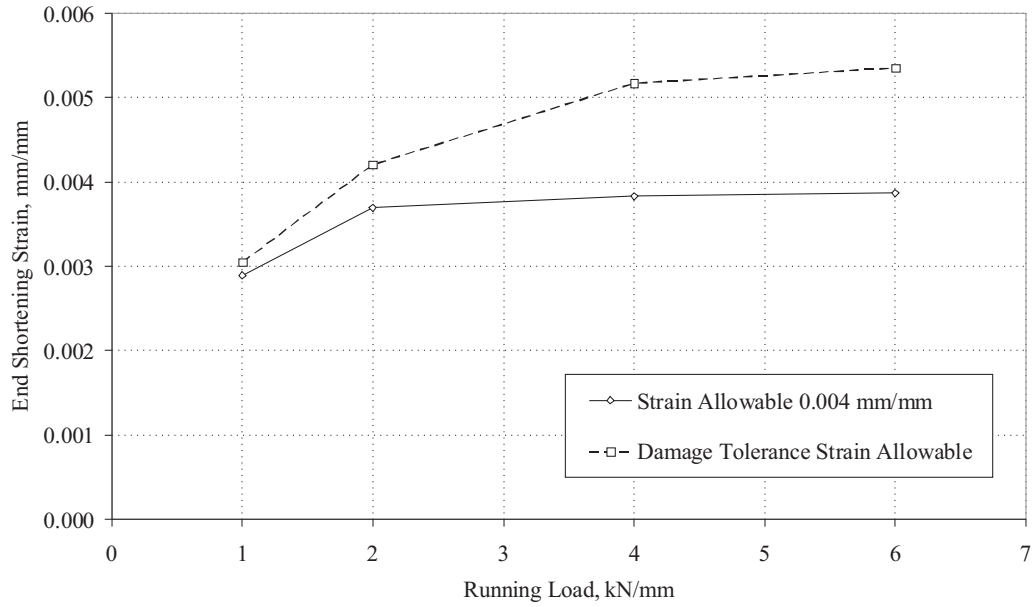

Figure 7-23: End shortening strain of damage tolerance and buckling optimised blade stiffened panel compared to buckling optimised panel with nominal strain allowable of 0.004 mm/mm.

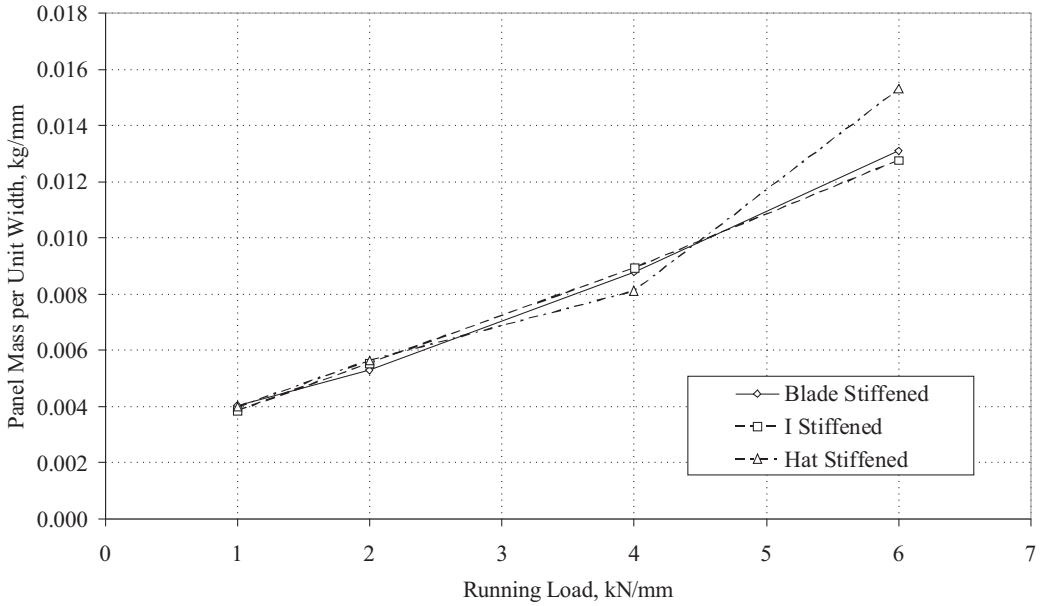

Figure 7-24: Mass of damage tolerance optimised panels with blade, I, and hat stiffeners.

delaminations, and delamination propagation analysis that includes the postbuckled behaviour of the panel.

Laminate Continuity Across Ply Drops

Another limitation of the bilevel method as presented here is that it does not account for the possible requirement of layup continuity between regions of thickness change. A clear example where this may be needed is in the crown of a hat stiffener. In the optimisation routines presented here the crown has been allowed to take a different thickness to the web. As the web and crown would be formed together this change in thickness would be achieved in manufacturing by dropping or adding plies to attain the desired thickness. For this to be possible the thinner laminate must be a subset of the thicker laminate; it must be possible to create the thinner laminate from the thicker laminate by only removing plies. The selection of layups in this optimisation routine does not include such interaction, and although ply drops may be possible in the layups chosen this is not guaranteed.

As well as ply drops within each stiffener cross section, there will also be requirements for ply drops within the skin and stiffener in the primary loading direction, with loads reducing towards the wing tip. For simplicity this routine looks at a single stiffened

wing panel in isolation, so cannot account for the restrictions in layup design imposed by these ply drops. A more complete design routine might look at multiple stiffened wing skin panels simultaneously, allowing it to deal with the continuity of fibres from one skin panel to the next.

7.6.5 Computational Efficiency

It is difficult to directly compare the computational efficiency of the damage tolerance strain allowable method to that with a fixed strain allowable as much of the extra analysis performed for the damage tolerance strain allowable is preprocessing, and need only be performed once for a given material. This preprocessing takes somewhere in the region of 30 minutes to perform. As the VICONOPT sizing analysis is looped in the damage tolerance strain allowable method there is also an increased number of VICONOPT analyses, but for all of the design studies presented here the number of VICONOPT analyses does not exceed six. With a single analysis taking around 2-3 seconds this is an acceptable increase in computation time given the improvements in design mass produced. All performance measures given here are taken on the PC described in Appendix C

7.7 Conclusion

It has been shown here that inclusion of damage tolerance analysis to set the strain allowables in a buckling optimised panel design routine yields lower mass solutions than those designed using a fixed strain allowable. The method is also computationally efficient, as while it does require preprocessing to compile the optimum sublaminate data, the increase in computation time after this is only a matter of seconds over analysis using a fixed strain allowable.

Chapter 8

Final Conclusions

This thesis has explored the use of a simple semi-analytical compression after impact (CAI) model as a design tool, and the methods by which it may be integrated into composite component design. An efficient CAI model was chosen, and a program was written to automate its use, allowing for it to be used within other computer programs. Initially the model was used as the objective function in the optimisation of a composite layup. The results of this optimisation showed the characteristics of a damage tolerant composite laminate; namely that the near surface sublaminates should be compliant in the load direction, and have a Poisson's ratio lower than that of the full laminate for best damage tolerance. The use of a genetic algorithm (GA) in the optimisation also showed the difficulty of tuning such metaheuristic search methods, and that in this case this method often did not find an optimum or near optimum solution.

The difficulty of tuning GAs for good convergence for damage tolerance optimisation lead to the development of a surrogate buckling method to reduce the computational effort of the model, with the aim of allowing the use of exhaustive search methods with the CAI model. A simple linear interpolation method was used to map sublaminate buckling strains to the Poisson's ratio of the full laminate in which the delaminated sublaminate resided. This method allowed for the analysis of all fully uncoupled symmetric and non-symmetric laminates up to 21 plies thick in less than 1% of the time of a full exhaustive search, with average solution errors less than 0.1% as a result of the surrogate model.

The analysis of a design space of symmetric and non-symmetric fully uncoupled laminates using the surrogate sublaminate buckling model showed that in the case of a requirement for no coupling in a laminate, including bend-twist coupling, symmetric laminates do not give the most damage tolerant solution. In this case for optimal

damage tolerance an anti-symmetric or non-symmetric laminate gives much higher compression after impact strength. Although this holds for laminates up to 21 plies thick, conclusions for thicker laminates could not be drawn as databases of fully uncoupled laminates with larger numbers of plies were unavailable, and trends within the data produced were inconclusive.

The principles by which the surrogate sublaminate buckling model was created were finally applied to allow inclusion of damage tolerance as a constraint within a stiffened composite panel optimisation routine. The CAI model was used to produce a strain allowable for each component of stiffened panels with various stiffener geometries within a panel optimisation routine, and these results were compared to those for panels optimised using a fixed nominal strain allowable. A bilevel approach was adopted, with damage tolerance analysis performed based on laminate thicknesses produced by VICONOPT sizing analysis. The bilevel optimisation strategy was shown to produce viable panel designs, with strain allowables tailored for each component within the panel depending on the damage tolerance of that component. Masses of these panels were similar at low load, but at high load weight savings of up to 30% were achieved.

8.1 Future Work

As with any piece of research work, results presented in this thesis have given indications as to a number of areas in which further research may be undertaken.

8.1.1 Optimistion of Composite Laminates for Damage Tolerance

The use of a GA in combination with the CAI model presented in this thesis gave an insight into the characteristics of a damage tolerant composite laminate. The optimisation process itself however was shown to be difficult to tune to achieve good convergence. Further work into the reasons for this, or the selection of another optimisation technique such as particle swarm optimisation, may provide further details as to what makes a good damage tolerant laminate. The relaxation of the design space searched may also yield interesting results.

8.1.2 Further Incorporation of CAI Analysis in Design

The bilevel approach for inclusion of damage tolerance strain allowable constraints in a composite stiffened panel optimisation routine presented here was a simple method of indicating the potential benefits of including damage tolerance analysis at the panel design stage. The implementation separated panel geometry optimisation from layup

optimisation, and as such the higher level geometry optimisation was performed with no knowledge of the effect a laminate thickness change had on its strain allowable. It would not be a trivial task to incorporate damage tolerance into the main geometry optimisation, as the strain allowable is a discrete function of thickness; however if this integration could be achieved the optimisation would be faster, and the results potentially even better as current practice described here, although producing improved designs, may not be exploiting the concept of damage tolerance analysis strain allowables to the full.

8.1.3 Non-Symmetric Laminates in Aerostructures

With current practice in composite laminate design calling for laminates to be symmetric to suppress potential coupling interactions within the laminate, the results presented in this thesis for the damage tolerance of symmetric and non-symmetric fully uncoupled laminates asks interesting questions as to the limitations this stipulation imposes on the designer. As with any change in the aerospace industry however, more research and evidence is required before manufacturers begin to use these more exotic layups in their products. Part of this research must show the true benefits of non-symmetric and anti-symmetric laminates to act as drivers for changes, as well as the disadvantages that restricting the designer to symmetric designs bring. A wider investigation of the damage tolerance of these laminates, in particular focussing on bend-twist coupled laminates which are typically used today, may provide further evidence that the potential benefits of non-symmetric and anti-symmetric laminates may outweigh the difficulties in implementing them.

Appendix A

Calculation of Poisson's Ratio for Fully Coupled Laminates

The calculation of Poisson's ratio for a symmetric laminate is a simple rearrangement of the plate constitutive equations. If the laminate is non-symmetric however assumptions need to be made about the clamping conditions of the laminate and the definition of a Poisson's ratio. Here it is assumed that the plate is free to deform such that a uniaxial load does not induce secondary loads either in-plane or out-of-plane. Making this assumption, the plate constitutive equations may be rearranged as described here to calculate the ratio of free transverse strain to end-shortening.

Classical Lamination Theory states:

$$\begin{Bmatrix} \mathbf{N} \\ \mathbf{M} \end{Bmatrix} = \begin{bmatrix} \mathbf{A} & \mathbf{B} \\ \mathbf{B} & \mathbf{D} \end{bmatrix} \begin{Bmatrix} \varepsilon^{\mathbf{0}} \\ \kappa \end{Bmatrix} \tag{A.1}$$

The stresses $\mathbf{N}$ are then

$$\mathbf{N} = \mathbf{A}\varepsilon^{\mathbf{0}} + \mathbf{B}\kappa \tag{A.2}$$

Rearranging in terms of $\varepsilon^{\mathbf{0}}$:

$$\varepsilon^{\mathbf{0}} = \mathbf{A}^{-1}\mathbf{N} - \mathbf{A}^{-1}\mathbf{B}\kappa \tag{A.3}$$

Making $\mathbf{F} = \mathbf{A}^{-1}\mathbf{B}$ the constituent strains become:

$$\varepsilon_x^0 = A'_{11}N_x + A'_{12}N_y + A'_{13}N_{xy} - F_{11}\kappa_x - F_{12}\kappa_y - F_{13}\kappa_{xy} \tag{A.4a}$$
$$\varepsilon_y^0 = A'_{21}N_x + A'_{22}N_y + A'_{23}N_{xy} - F_{21}\kappa_x - F_{22}\kappa_y - F_{23}\kappa_{xy} \tag{A.4b}$$
$$\gamma_{xy}^0 = A'_{31}N_x + A'_{32}N_y + A'_{33}N_{xy} - F_{31}\kappa_x - F_{32}\kappa_y - F_{33}\kappa_{xy} \tag{A.4c}$$

Equation A.1 also gives the moments of the system:

$$\mathbf{M} = \mathbf{B}\varepsilon^0 + \mathbf{D}\kappa \tag{A.5}$$

Rearranging in terms of κ:

$$\kappa = \mathbf{D}^{-1}\mathbf{M} - \mathbf{D}^{-1}\mathbf{B}\varepsilon^0 \tag{A.6}$$

Making $\mathbf{G} = \mathbf{D}^{-1}\mathbf{B}$ the constituent curvatures become:

$$\kappa_x = D'_{11}M_x + D'_{12}M_y + D'_{13}M_{xy} - G_{11}\varepsilon_x^0 - G_{12}\varepsilon_y^0 - G_{13}\gamma_{xy}^0 \tag{A.7a}$$
$$\kappa_y = D'_{21}M_x + D'_{22}M_y + D'_{23}M_{xy} - G_{21}\varepsilon_x^0 - G_{22}\varepsilon_y^0 - G_{33}\gamma_{xy}^0 \tag{A.7b}$$
$$\kappa_{xy} = D'_{31}M_x + D'_{32}M_y + D'_{33}M_{xy} - G_{31}\varepsilon_x^0 - G_{32}\varepsilon_y^0 - G_{33}\gamma_{xy}^0 \tag{A.7c}$$

The longitudinal laminate Poisson's Ratio is found when a uniaxial load N_x is applied. By setting all other stresses and moments to zero Eqs. A.4 and A.7 become

$$\varepsilon_x^0 = A'_{11}N_x - F_{11}\kappa_x - F_{12}\kappa_y - F_{13}\kappa_{xy} \tag{A.8a}$$
$$\varepsilon_y^0 = A'_{21}N_x - F_{21}\kappa_x - F_{22}\kappa_y - F_{23}\kappa_{xy} \tag{A.8b}$$
$$\gamma_{xy}^0 = A'_{31}N_x - F_{31}\kappa_x - F_{32}\kappa_y - F_{33}\kappa_{xy} \tag{A.8c}$$
$$-\kappa_x = G_{11}\varepsilon_x^0 + G_{12}\varepsilon_y^0 + G_{13}\gamma_{xy}^0 \tag{A.8d}$$
$$-\kappa_y = G_{21}\varepsilon_x^0 + G_{22}\varepsilon_y^0 + G_{23}\gamma_{xy}^0 \tag{A.8e}$$
$$-\kappa_{xy} = G_{31}\varepsilon_x^0 + G_{32}\varepsilon_y^0 + G_{33}\gamma_{xy}^0 \tag{A.8f}$$

Substituting Eqs. A.8d, A.8e and A.8f into eqn A.8c, and rearranging:

$$\gamma_{xy}^0 = \frac{A'_{31}N_x + \varepsilon_x^0 P_2 + \varepsilon_y^0 P_3}{P_1} \tag{A.9}$$

where

$$P_1 = (1 - F_{31}G_{13} - F_{32}G_{23} - F_{33}G_{33}) \tag{A.10a}$$

$$P_2 = (F_{31}G_{11} + F_{32}G_{21} + F_{33}G_{31}) \tag{A.10b}$$

$$P_3 = (F_{31}G_{12} + F_{32}G_{22} + F_{33}G_{32}) \tag{A.10c}$$

Substituting Eqs. A.8d, A.8e, A.8f and A.9 into eqn A.8a and A.8b, and rearranging:

$$\varepsilon_x^0 = \frac{A'_{11}N_x + \varepsilon_y^0 P_5 + P_6}{P_4} \tag{A.11a}$$

$$\varepsilon_y^0 = \frac{A'_{21}N_x + \varepsilon_x^0 P_8 + P_9}{P_7} \tag{A.11b}$$

where

$$P_4 = (1 - F_{11}G_{11} - F_{12}G_{21} - F_{13}G_{31} - \frac{P_2 P_{10}}{P_1}) \tag{A.12a}$$

$$P_5 = (F_{11}G_{12} + F_{12}G_{22} + F_{13}G_{32} + \frac{P_3 P_{10}}{P_1}) \tag{A.12b}$$

$$P_6 = A'_{31}N_x \frac{P_{10}}{P_1} \tag{A.12c}$$

$$P_7 = (1 - F_{21}G_{12} - F_{22}G_{22} - F_{23}G_{32} - \frac{P_3 P_{11}}{P_1}) \tag{A.12d}$$

$$P_8 = (F_{21}G_{11} + F_{22}G_{21} + F_{23}G_{31} + \frac{P_2 P_{11}}{P_1}) \tag{A.12e}$$

$$P_9 = A'_{31}N_x \frac{P_{11}}{P_1} \tag{A.12f}$$

and

$$P_{10} = (F_{11}G_{13} + F_{12}G_{23} + F_{13}G_{33}) \tag{A.12g}$$

$$P_{11} = (F_{21}G_{13} + F_{22}G_{23} + F_{23}G_{33}) \tag{A.12h}$$

Substituting Eq. A.11b into Eq. A.11a and rearranging yields:

$$\varepsilon_x^0 = \frac{N_x(A'_{11} + \frac{P_5}{P_7}A'_{21}) + \frac{P_5 P_9}{P_7} + P_6}{P_4 - \frac{P_5 P_8}{P_7}} \tag{A.13}$$

Equation A.13 can then be used to find the strain ε_x^0 for a reference stress N_x, and this value can then be used in Eq. A.11b to find the associated strain ε_y^0. The longitudinal laminate Poisson's Ratio ν_{xy} is then given by:

$$\nu_{xy} = -\frac{\varepsilon_y^0}{\varepsilon_x^0} \tag{A.14}$$

The effective modulus of the laminate in the x direction can also be found using these parameters. From Eq. A.1 it is known that:

$$N_x = A_{11}\varepsilon_x^0 + A_{12}\varepsilon_y^0 + A_{13}\gamma_{xy}^0 + B_{11}\kappa_x + B_{12}\kappa_y + B_{13}\kappa_{xy} \tag{A.15}$$

The effective modulus $E_{xx} = \frac{N_x}{\varepsilon_x^0 t}$, so dividing Eq. A.15 by ε_x^0:

$$E_{xx}t = A_{11} - A_{12}\nu_{xy} + A_{13}\frac{\gamma_{xy}^0}{\varepsilon_x^0} + B_{11}\frac{\kappa_x}{\varepsilon_x^0} + B_{12}\frac{\kappa_y}{\varepsilon_x^0} + B_{13}\frac{\kappa_{xy}}{\varepsilon_x^0} \tag{A.16}$$

Equations A.8d, A.8e, A.8f and A.9 can then also be divided by ε_x^0 to give:

$$-\frac{\kappa_x}{\varepsilon_x^0} = G_{11} - G_{12}\nu_{xy} + G_{13}\frac{\gamma_{xy}^0}{\varepsilon_x^0} \tag{A.17a}$$

$$-\frac{\kappa_y}{\varepsilon_x^0} = G_{21} - G_{22}\nu_{xy} + G_{23}\frac{\gamma_{xy}^0}{\varepsilon_x^0} \tag{A.17b}$$

$$-\frac{\kappa_{xy}}{\varepsilon_x^0} = G_{31} - G_{32}\nu_{xy} + G_{33}\frac{\gamma_{xy}^0}{\varepsilon_x^0} \tag{A.17c}$$

$$\frac{\gamma_{xy}^0}{\varepsilon_x^0} = \frac{A'_{31}E_{xx}t + P_2 - P_3\nu_{xy}}{P_1} \tag{A.17d}$$

Substituting Eqs. A.17 into Eq. A.16 and rearranging:

$$E_{xx} = \frac{P_{12}(P_2 - P_3\nu_{xy})}{(P_1 - A'_{31}P_{12})t} + \frac{P_{13}}{(1 - A'_{31}\frac{P_{12}}{P_1})t} \tag{A.18}$$

where

$$P_{12} = A_{13} - B_{11}G_{13} - B_{12}G_{23} - B_{13}G_{33} \tag{A.19a}$$

$$P_{13} = A_{11} - A_{12}\nu_{xy} + B_{11}(G_{12}\nu_{xy} - G_{11}) + B_{12}(G_{22}\nu_{xy} - G_{21}) + B_{13}(G_{32}\nu_{xy} - G_{31}) \tag{A.19b}$$

Appendix B

Proof of Reduction in Problem Size through Removal of Duplicate Sublaminates in Exhaustive Analysis

This proof shows the reduction in the number of buckling analyses required in the surrogate sublaminate buckling model by removing duplicate sublaminates that are reflected about their midplane, for example the [45/0] and [0/45] sublaminates. These sublaminates yield the same buckling result in VICONOPT so only one need be analysed in constructing the surrogate model. The author would like to credit Tim Dodwell for the final derivation here. The total number of possible sublaminates for layups made up of typical [0/90/ $\pm$ 45] fibres is

$$N_s = \sum_{i=1}^{n} 4^n \tag{B.1}$$

where n is the maximum number of plies in the sublaminate. Of this the total number of unique buckling solutions (removing those that are mirrored copies of other sublaminates) is given by

$$N_{s,unique} = 4 + \sum_{j=2}^{n} \left(\sum_{i=1}^{4} (4^{j-1} - 4^{j-2}(i-1)) \right) \tag{B.2}$$

Eqs. B.1 and B.2 may be used as a ratio to work out the percentage of all sublaminates that need to be analysed, as shown by Eq. B.3.

$$F = \frac{N_{s,unique}}{N_s} = \frac{4 + \sum_{j=2}^{n}(\sum_{i=1}^{4}(4^{j-1} - 4^{j-2}(i-1)))}{\sum_{j=1}^{n} 4^j} \tag{B.3}$$

Multiplying out and combining sums in the numerator, Eq. B.3 becomes

$$F = \frac{\sum_{j=1}^{n} 4^j - 6\sum_{j=2}^{n} 4^{j-2}}{\sum_{j=1}^{n} 4^j} \tag{B.4}$$

and hence

$$F = 1 - 6\left(\frac{\sum_{j=2}^{n} 4^{j-2}}{\sum_{j=1}^{n} 4^j}\right) \tag{B.5}$$

Aside:

$$\sum_{j=2}^{n} 4^{j-2} = 1 + 4 + 16 + \ldots + 4^{n-2} \tag{B.6}$$

$$\sum_{j=1}^{n} 4^j = 4 + 16 + \ldots + 4^n \tag{B.7}$$

hence

$$\sum_{j=2}^{n} 4^{j-2} = 1 + \sum_{j=1}^{n} 4^j - (4^{n-1} + 4^n) \tag{B.8a}$$

$$= 1 + \sum_{j=1}^{n} 4^j - \frac{5}{4}4^n \tag{B.8b}$$

so

$$F = 1 - 6\left(\frac{1 + \sum_{j=1}^{n} 4^j - \frac{5}{4}4^n}{\sum_{j=1}^{n} 4^j}\right) \tag{B.9}$$

As n becomes large first term goes hence

$$F = 1 - 6\left(1 - \frac{5}{4}\left(\frac{4^n}{\sum_{j=1}^{n} 4^j}\right)\right) \tag{B.10}$$

As $n \to \infty$

$$F = 1 - 6\left(1 - \frac{5}{4}\left(\frac{1}{1 + \frac{1}{4} + \frac{1}{16} + \ldots}\right)\right) \tag{B.11}$$

Sum of infinite series $= \frac{1}{1-\frac{1}{4}} = \frac{4}{3}$ hence

$$F = 1 - 6\left(1 - \frac{5}{4} \cdot \left(\frac{3}{4}\right)\right) \tag{B.12}$$

so

$$F = 1 - \frac{6}{16} = 0.625 \tag{B.13}$$

Equation B.13 shows that the computation time saved by removing duplicate sub-laminates is 37.5%.

Appendix C

Computer Specifications

The specifications of the PC on which optimisation and analysis in this thesis was performed are given here for completeness.

Processor Intel Core 2 Quad Q9550, 4 cores, 2.93GHz 12MB L2 cache

RAM 4GB DDR2-800 (3GB usable due to operating system limitations)

Chipset Intel Q35 Express

Operating System Microsoft Windows XP Professional 32-bit, Service Pack 2

References

[1] M.S. Anderson and D. Kennedy. Inclusion of transverse shear deformation in the exact buckling and vibration analysis of composite plate assemblies. Technical Report NASA-CR-4510, NASA, 1993.

[2] Z. Aslan and M. Sahin. Buckling behavior and compressive failure of composite laminates containing multiple large delaminations. *Composite Structures*, 89(3):382–390, 2009.

[3] Standard test method for measuring the damage resistance of a fiber-reinforced polymer matrix composite to a drop-weight impact event. Technical Report ASTM D7136 / D7136M - 07, ASTM International, 2005.

[4] N. Baker. Optimisation of aerospace composites for damage tolerance. Master's thesis, Department of Mechanical Engineering, University of Bath, 2008.

[5] N. Baker and R. Butler. Compression after impact modeling of damage tolerant composite laminates. In *Proceedings of the 51st AIAA/ASME/ASCE/AHS/ASC Structures, Structural Dynamics and Materials Conference*, Orlando FL, 2010.

[6] N. Baker, R. Butler, and C.B. York. Damage tolerance of fully orthotropic laminates in compression. *Composites Science and Technology*, 72(10):1083–1089, 2012.

[7] P. Bartholomew. Ply stacking sequences for laminated plates having in-plane and bending orthotropy. *Fibre Science and Technology*, 10(4):239–253, 1977.

[8] M.W. Bloomfield, C.G. Diaconu, and P.M. Weaver. On feasible regions of lamination parameters for lay-up optimization of laminated composites. *Proceedings of the Royal Society A*, 465(2104):1123–1143, 2009.

[9] R. Butler, D.P. Almond, G.W. Hunt, B. Hu, and N. Gathercole. Compressive fatigue limit of impact damaged composite laminates. *Composites: Part A*, 38(4):1211–1215, 2007.

[10] R. Butler, N. Baker, and W. Liu. Damage tolerance of buckling optimized variable angle tow panels. In *Proceedings of the 50th AIAA/ASME/ASCE/AHS/ASC Structures, Structural Dynamics, and Materials Conference*, Palm Springs CA, 2009.

[11] R. Butler, A.T. Rhead, W. Liu, and N. Kontis. Compressive strength of delaminated aerospace composites. *Philosophical Transactions of the Royal Society A*, 2011. (Submitted).

[12] P.P. Camanho, P. Maimí, and C.G. Dávila. Prediction of size effects in notched laminates using continuum damage mechanics. *Composites Science and Technology*, 67(13):2715–2727, 2007.

[13] F. Cesari, V. Dal Re, G. Minak, and A. Zucchelli. Damage and residual strength of laminated carbonepoxy composite circular plates loaded at the centre. *Composites Part A: Applied Science and Manufacturing*, 38(4):1163–1173, 2007.

[14] H. Chai and C.D. Babcock. Two-dimensional modelling of compressive failure in delaminated laminates. *Journal of Composite Materials*, 19(1):67–98, 1985.

[15] H. Chai, C.D. Babcock, and W.G. Knauss. One dimensional modelling of failure in laminated plies by delamination buckling. *International Journal of Solids and Structures*, 17(11):1069–1083, 1981.

[16] M. Clerc. *Particle Swarm Optimisation*. ISTE Ltd., first edition, 2006.

[17] M.W. Czabaj, A.T. Zehnder, B.D. Davidson, A.K. Singh, and D.P. Eisenberg. Compression after impact of sandwich composite structures: Experiment and modeling. In *Proceedings of the 51st AIAA/ASME/ASCE/AHS/ASC Structures, Structural Dynamics and Materials Conference*, pages 55–64, Orlando FL, 2010.

[18] D. Dalmas and A. Laksimi. On the method of determination of strain energy release rate during fatigue delamination in composite materials. *Applied Composite Materials*, 6(5):327–340, 1999.

[19] C.G. Diaconu and P.M. Weaver. Approximate solution and optimum design of compression-loaded, postbuckled laminated composite plates. *AIAA Journal*, 43(4):906–914, 2005.

[20] J. Dréo, P. Siarry, A. Pétrowski, and E. Taillard. *Metaheuristics for Hard Optimization: Simulated Annealing, Tabu Search, Evolutionary and Genetic Algorithms, Ant Colonies, Methods and Case Studies*. Springer-Verlag, 2006.

[21] Laminate stacking sequences for special orthotropy (application to fibre reinforced composites). Technical Report 82013, Engineering Sciences Data Unit, 1982.

[22] Buckling of rectangular specially orthotropic plates. Technical Report 80023, Engineering Sciences Data Unit, 1995.

[23] Certification specifications for large aeroplanes. Technical Report CS-25, European Aviation Safety Agency, 2008.

[24] Certification specifications for large aeroplanes - acceptable means of compliance. Technical Report CS-25 Book 2, European Aviation Safety Agency, 2008.

[25] M.T. Fenske and A.J. Vizzini. The inclusion of in-plane stresses in delamination criteria. *Journal of Composite Materials*, 35(15):1325–1342, 2001.

[26] M.P. Flanagan, M.A. Zikry, J.W. Wall, and A. El-Shiekh. An experimental investigation of high velocity impact and penetration failure modes in textile composites. *Journal of Composite Materials*, 33(12):1080–1103, 1999.

[27] A.C. Garg. Delamination - a damage mode in composite structures. *Engineering Fracture Mechanics*, 29(5):557–584, 1988.

[28] H.T. Han and S.W. Choi. The effects of loading parameters on fatigue of composite laminates: Part V. Technical Report DOT/FAA/AR-01/24, U.S. Department of Transportation Federal Aviation Administration, 2001.

[29] R. Hassan, B. Cohanim, O. de Weck, and G. Venter. A comparison of particle swarm optimization and the genetic algorithm. In *Proceedings of the 46th AIAA/ASME/ASCE/AHS/ASC Structures, Structural Dynamics and Materials Conference*, 2005.

[30] M.J. Hinton, A.S. Kaddour, and P.D. Soden. *Failure Criteria in Fibre Reinforced Polymer Composites: The World-Wide Failure Exercise*. Elseveier Science Ltd., 2004.

[31] S.A. Hitchen and R.M.J. Kemp. The effect of stacking sequence on impact damage in a carbon fibre/epoxy composite. *Composites*, 26(3):207–214, 1995.

[32] G.W. Hunt, B. Hu, R. Butler, D.P. Almond, and J.E. Wright. Nonlinear modeling of delaminated struts. *AIAA Journal*, 42(11):2364–2372, 2004.

[33] S-F. Hwang and G-H. Liu. Buckling behavior of composite laminates with multiple delaminations under uniaxial compression. *Composite Structures*, 53(2):235–243, 2001.

[34] M.W. Hyer and R.F. Charette. The use of curvilinear fiber format in composite structure design. In *Proceedings of the 30th AIAA/ASME/ASCE/AHS/ASC Structures, Structural Dynamics and Materials Conference*, New York NY, 1989.

[35] A.S. Kaddour and M.J. Hinton. Failure criteria for polymer composites under 3D stress states: The second world-wide failure exercise. In *Proceedings of the 17th International Conference on Composite Materials*, Edinburgh, Scotland, 2009.

[36] A.S. Kaddour, M.J. Hinton, S. Li, and P.A. Smith. Damage prediction in polymer composites: Update of part a of the third world-wide failure exercise (wwfe-iii). In *Proceedings of the 17th International Conference on Composite Materials*, Edinburgh, Scotland, 2009.

[37] G.A. Kardomateas. The initial post-buckling and growth behavior of internal delaminations in composite plates. *Journal of Applied Mechanics*, 60(4):903–910, 1993.

[38] G.A. Kardomateas and A.A. Pelegri. The stability of delamination growth in compressively loaded composite plates. *International Journal of Fracture*, 65(3):261–276, 1994.

[39] D.G. Katerelos, A. Paipetis, and V. Kostopoulos. A simple model for the prediction of the fatigue delamination growth of impacted composite panels. *Fatigue and Fracture of Engineering Materials and Structures*, 27(10):911–922, 2004.

[40] H. Kim, D.A. Welch, and K.T. Kedward. Experimental investigation of high velocity ice impacts on woven carbon/epoxy composite panels. *Composites Part A: Applied Science and Manufacturing*, 34(1):25–41, 2003.

[41] R. Le Riche and R.T. Haftka. Optimisation of laminate stacking sequence for buckling load maximization by genetic algorithm. *AIAA Journal*, 31(5):951–956, 1993.

[42] W.C. Liao and C.T. Sun. The determination of mode III fracture toughness in thick composite laminates. *Composites Science and Technology*, 56(4):489–499, 1996.

[43] B. Liu, R.T. Haftka, and M.A. Akgün. Two-level composite wing structural optimization using response surfaces. *Structural and Multidisciplinary Optimization*, 20(2):87–96, 2000.

[44] W. Liu, R. Butler, and H.A. Kim. Optimization of composite stiffened panels subject to compression and lateral pressure using a bi-level approach. *Structural and Multidisciplinary Optimization*, 36(3):235–245, 2008.

[45] W. Liu, R. Butler, A.R. Mileham, and A.J. Green. Bilevel optimization and post-buckling of highly strained composite stiffened panels. *AIAA Journal*, 44(11):2562–2570, 2006.

[46] E. Madenci and R.A. Westmann. Local delamination growth in layered systems under compressive load. *Journal of Applied Mechanics*, 60(4):895–902, 1993.

[47] F.L. Matthews and R.D. Rawlings. *Composite Materials: Engineering and Science*. Chapman and Hall, first edition, 1994.

[48] Microsoft. Microsoft Visual Studio C♯ 2010. Computer Program, 2010.

[49] S. Nagendra, D. Jestin, Z. Gürdal, R.T. Haftka, and L.T. Watson. Improved genetic algorithm for the design of stiffened composite panels. *Computers and Structures*, 58(3):543–555, 1996.

[50] S.G. Nash, editor. *A History of Scientific Computing*, pages 141–151. ACM Press, 1990.

[51] K.-F. Nilsson, J.C. Thesken, P. Sindelar, A.E. Giannakopoulos, and B. Storåkers. A theoretical and experimental investigation of buckling induced delamination growth. *Journal of the Mechanics and Physics of Solids*, 41(4):749–782, 1993.

[52] M.C.Y Niu. *Composite Airframe Structures*. Conmilit Press Ltd., second edition, 1996.

[53] T. Nyman, A. Bredberg, and J. Schön. Equivalent damage and residual strength for impact damaged composite structures. *Journal of Reinforced Plastics and Composites*, 19(6):428–448, 2000.

[54] C.R. Reeves and J.E. Rowe. *Genetic Algorithms: Principles and Perspectives*. Kluwer Academic Publishers, second edition, 2004.

[55] A.T. Rhead and R. Butler. Buckling, propagation and stability of delaminated isotropic layers. In *Proceedings of the 14th European Conference on Composite Materials*, 2010.

[56] A.T. Rhead and R. Butler. Compressive static strength model for impact damaged laminates. *Composites Science and Technology*, in press.

[57] A.T. Rhead, R. Butler, and N. Baker. Analysis and compression testing of laminates optimised for damage tolerance. *Applied Composite Materials*, 18(1):85–100, 2011.

[58] A.T. Rhead, R. Butler, and G.W. Hunt. Post-buckled propagation model for compressive fatigue of impact damaged laminates. *International Journal of Solids and Structures*, 45(16):4349–4361, 2008.

[59] A.T. Rhead, D. Marchant, and R. Butler. Compressive strength of composite laminates following free edge impact. *Composites Part A: Applied Science and Manufacturing*, 41(9):1056–1065, 2010.

[60] A. Riccio and M. Gigliotti. A novel numberical delamination growth initiation approach for the preliminary design of damage tolerant composite structures. *Journal of Composite Materials*, 41(16):1939–1960, 2007.

[61] M. Schmidt and S. Robinson. *Microsoft Visual C♯ .NET 2003 Developer's Cookbook*. Sams Publishing, first edition, 2003.

[62] L.A. Schmit Jnr. and B. Farshi. Optimum laminate design for strength and stiffness. *International Journal for Numerical Methods in Engineering*, 7(4):519–536, 1973.

[63] L.A. Schmit Jnr. and B. Farshi. Optimum design of laminated fibre composite plates. *International Journal for Numerical Methods in Engineering*, 11(4):623–640, 1979.

[64] S. Setoodeh, M.M. Abdalla, and Z. Gürdal. Design of variable-stiffness laminates using lamination parameters. *Composites Part B: Engineering*, 37(4-5):301–309, 2006.

[65] K.N. Shivakumar and J.D. Whitcomb. Buckling of a sublaminate in a quasi-isotropic composite laminate. *Journal of Composite Materials*, 19(1):2–18, 1985.

[66] G. Soremekun, Z. Gürdal, R.T. Haftka, and L.T. Watson. Composite laminate design optimization by genetic algorithm with generalized elitist selection. *Computers and Structures*, 79(2):131–143, 2001.

[67] W.-H. Steeb. *The Nonlinear Workbook: Chaos, Fractals, Cellular Automata, Neural Networks, Genetic Algorithms, Gene Expression Programming, Support Vector Machine, Wavelets, Hidden Markov Models, Fuzzy Logic with C++, Java and SymbolicC++ Programs*. World Scientific Publishing Co. Pte. Ltd., fourth edition, 2008.

[68] H. Suemasu. Effects of multiple delaminations on compressive buckling behaviors of composite panels. *Journal of Composite Materials*, 27(12):1172–1192, 1992.

[69] B.F. Tatting and Z. Gürdal. Design and manufacture of elastically tailored tow placed plates. Technical Report NASA/CR-2002-211919, NASA, 2002.

[70] T.E. Tay. Characterisation and analysis of delamination fracture in composites: An overview of developments from 1990 to 2001. *ASME Applied Mechanics Review*, 56(1):1–31, 2003.

[71] J.M.T. Thompson and G.W. Hunt. *Elastic Instability Phenomena*. Wiley and Sons Ltd., first edition, 1984.

[72] V. Tita, J. de Carvalho, and D. Vandepitte. Failure analysis of low velocity impact on thin composite laminates: Experimental and numerical approaches. *Composite Structures*, 83(4):413–428, 2008.

[73] S.W. Tsai and H.T. Hahn. A general theory of strength for anisotropic materials. *Journal of Composite Materials*, 5(1):58–80, 1971.

[74] S.W. Tsai and H.T. Hahn. *Introduction to Composite Materials*. Technomic Publishing Co., Inc., 1980.

[75] University of Cardiff. VICONOPT 1.4. Computer Program, 2007.

[76] J.D. Whitcomb. Parametric analytical study of instability-related delamination growth. *Composites Science and Technology*, 25(1):19–48, 1986.

[77] J.D. Whitcomb and K.N. Shivakumar. Strain-energy release rate analysis of plates with postbuckled delaminations. *Journal of Composite Materials*, 23(7):714–734, 1989.

[78] J.M. Whitney and R.J. Nuismer. Stress fracture criteria for laminated composite containing stress concentrations. *Journal of Composite Materials*, 8(3):253–265, 1974.

[79] J.F.M. Wiggenraad, P. Arendsen, and J.M.S. da Silva Pereira. Design optimization of stiffened composite panels with buckling and damage tolerance constraints. Technical Report NLR-TP-98024, National Aerospace Laboratory NLR, 1998.

[80] F.W. Williams, M.S. Anderson, D. Kennedy, R. Butler, and G. Aston. User manual for VICONOPT: An exact analysis and optimum design program covering the buckling and vibration of prismatic assemblies of flat in-plane loaded, anisotropic

plates, with approximations for discrete supports and transverse stiffeners. Technical Report NASA-CR-181966, NASA, 1990.

[81] F.W. Williams, D. Kennedy, M.S. Anderson, and R.Butler. VICONOPT - program for exact vibration and buckling analysis or design of prismatic plate assemblies. *AIAA Journal*, 29(11):1927–1928, 1991.

[82] Y. Xiong, C. Poon, P.V. Straznicky, and H. Vietinghoff. A prediction method for the compressive strength of impact damaged composite laminates. *Composite Structures*, 30(4):357–367, 1995.

[83] C.B. York. Characterization of nonsymmetric forms of fully orthotropic laminates. *Journal of Aircraft*, 46(4):1114–1125, 2009.

[84] C.B. York and P.M. Weaver. Balanced and symmetric laminates - new perspectives on an old design rule. In *Proceedings of the 51st AIAA/ASME/ASCE/AHS/ASC Structures, Structural Dynamics and Materials Conference*, Orlando FL, 2010.

[85] J. Zhou and T. He. On the analysis of the end-notched flexure specimen for measuring mode ii fracture toughness of composite materials. *Composites Science and Technology*, 50(2):209–213, 1994.